Inkjet Printing for High Throughput Screening Arrays

Thesis submitted in accordance with the requirements of

The University of Liverpool

for the degree of

Doctor of Philosophy

by Eduardo Bonilla Bustillo

December, 2018

UNIVERSITY OF LIVERPOOL

Abstract

This thesis describes the novel ink development and manufacturing process of cell screening arrays, for analysing the effects of surface chemistry and topography on stem cell behaviour. Inkjet printing was used for the deposition of both cell repellent and 'cell active' inks on glass cover slips. Two new inks were developed: a polyethylene glycol (PEG)-based formulation, to contain cell populations to a specific location and a range of aminopropyl-triethoxysilane (APTES) in isopropanol inks that enable cell activity to identify cell response to the modified substrate.

Three main approaches were followed to develop the cell repellent PEG-based formulations: physical binding of PEG on the glass substrates, chemical binding of PEG chains to glass substrates, and the use of a UV curable formulation to be deposited on glass. A novel UV curable PEG-based formulation with a silane component was developed, allowing the selective silanisation of the glass substrate where the PEG is needed to bind on the substrate. The printed UV curable PEG-based coatings were assessed in terms of cell repellence.

A range of five APTES inks in an isopropanol carrier was developed, to amino-silanise a glass substrate via inkjet printing. The concentration of APTES dissolved in the carrier was defined by the results shown in the literature to drive stem cell differentiation toward bone cells. The APTES modified glass substrates via inkjet printing were characterised using a variety of techniques (contact angle measurements, FTIR and AFM), to ensure that amino-silanisation had occurred.

The manufacturing of functional cell screening arrays comprised of a cell repellent ink formulation and five 'cell active' inks was achieved by the use of inkjet printing. The printed cell screening arrays were successfully tested in terms of resistance to the cell culture environment for over 28 days, and an initial cell response analysis to the APTES modified substrate is presented.

Acknowledgments

Firstly, I want to thank my supervisors, Dr. Kate Black and Dr. Jude Curran for their unconditional support, trust and encouragement. From day one Kate showed me complete support and guided me through this adventure, not only on an academic level, but also on a personal one when I needed it most. Jude was very supportive and welcoming from the beginning, her positivity and trust on my work helped me continue through difficult times, and her guidance and supervision helped me appreciate the work I've done and to trust myself. I consider myself lucky to have been mentored by them.

Secondly, I want to thank CONACyT and the Mexican Government for their financial support throughout my formation in the University of Liverpool. Without their funding none of this would be possible. Thank you very much for allowing a boy to pursue his dream of becoming a scientist.

A special thank you to Dr. Rui Chen who was a constant through my research and who supported me from the beginning, guiding me with experiments and his materials knowledge, whit out his support I would have been lost.

I would also like to thank the friends in Liverpool and Mexico, and family that I made in my time in Liverpool, especially to David and Pati. Your continuous support throughout this journey has no match and I cannot think of better people to share this adventure with.

Finally, to my parents Eduardo and Aurora and my sister Ximena, thank you for your unconditional and immeasurable support on anything I decide to do.

Contents

List of Figures

List of tables

List of Equations

Chapter 1

Introduction

1.1. Context of research

To obtain effective control of material induced biological responses (i.e. protein selection/adsorption and subsequent cell attachment), stimuli must be controlled and presented to the biological environment (i.e. protein solution or cell suspension) at the sub-micron level[1,2]. A limited range of dynamic surface chemistries which have a proven effect, on protein adsorption and stem cell responses have been developed[1,2]. However, to date, cell pattern processes have been labour intensive and time consuming[3–7]. Inkjet printing however could provide a viable alternative as a high-throughput material fabrication technique, due to the digital and high-speed nature of the technique. This project explores the possibility of employing inkjet printing as a manufacturing technique for screening arrays and defining the optimal material properties (surface chemistry and topography) that can be used to optimise targeted cell function in vitro. Surface chemistry and topography properties have been

incorporated into cell screening arrays production using inkjet printing as the manufacturing tool.

Inkjet printing is a technology that could have a high impact in the field of tissue engineering. The use of digitally driven processes for the manufacture of high throughput screening arrays has been on the increase in recent year[8,9]. Among many cell patterning techniques, inkjet printing offers a user-friendly approach and scalability for possible mass manufacture thanks to its ability to transfer developmental materials into industrial printers[3,9]. Inkjet printing allows the use of different ink formulations simultaneously as used in graphics inkjet printing using different colour inks[9–11]. In this project, the use of surface chemistry and the use of "off the shelf" chemical groups that can drive stem cell differentiation will be explored to develop bio-inks suitable for inkjet printing and to explore cost-effective and reproducible alternatives to bio-fabricated devices in tissue engineering and regenerative medicine.

1.2. Project aim and objectives

The aim of this research was to assess the use of inkjet printing technology as an alternative manufacturing technique for the production of high-throughput screening arrays.

Conventional methods of modifying substrates employ peptides or proteins which are labour intensive and expensive processes. The approach outlined in this thesis is to use silane based inks, which are cheap and often used for surface modifications, which will obviate the need for supplementing the cell growth environment with growth factors

and cytokines to induce cell differentiation by controlling initial protein and cell adsorption thanks to the silane modified substrates[1,12].

Screening arrays with different surface chemistries have been assessed in terms of cell adhesion and cell population viability.

Figure 1 shows the preliminary layout of the cell screening arrays to be produced.

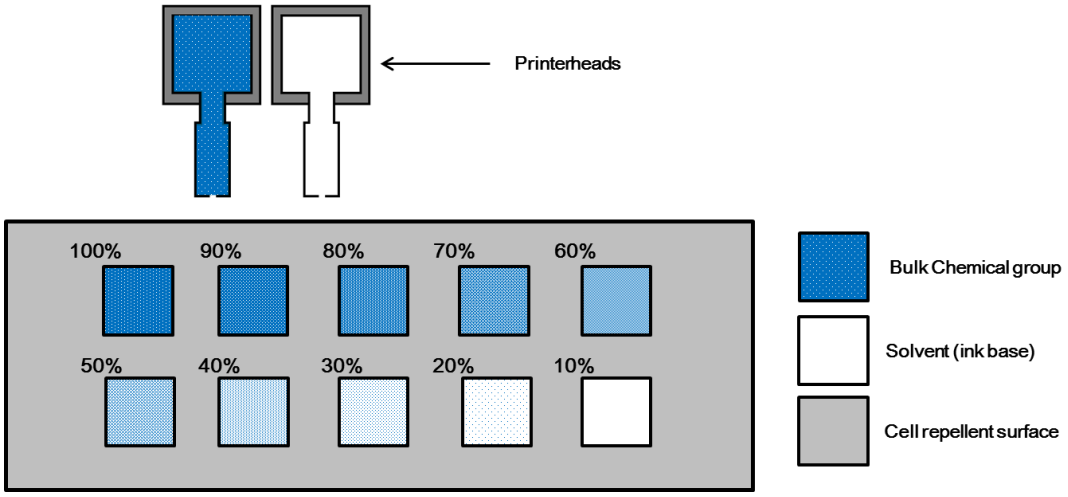

Figure 1 Cell screening array design for stem cell characterisation where the grey area represents a cell repellent surface and the coloured areas represent windows where stem cells can adhere on a glass slide.

The main objectives of the project were:

- Develop an inkjet printable formulation that act as a cell repellent coating to contain cell populations to specific areas.
- Develop an inkjet printable set of silane based formulations to selectively modify the surface chemistry and topography of a substrate where cells can adhere and maintain viability.

- Characterise the surface of the silane based modified areas.
- Design and manufacture cell screening arrays that can maintain cell populations segregated to specific surface modified areas.
- Assess the cell response of a contained cell population on a modified substrate with the silane based formulations.

1.3. Thesis structure

Chapter 2 investigates the material design for tissue engineering and bio-fabrication. The manufacturing process of inkjet printing and how it can be used for the fabrication of cell screening arrays is also explored. An overview of how cell screening arrays have been manufactured by other groups and different approaches for surface passivation are discussed. Finally, the use of specific surface chemistries used to drive stem cell differentiation is reviewed.

Chapter 3 describes the materials, methods and analytical techniques used throughout the research. The process followed for the cleaning of the samples is described as well as the fabrication of the different formulations and surface treatments. The analytical techniques used for the analysis and characterisation of the materials and samples are also presented. The protocols used for cell culturing and cell testing are also described.

In Chapter 4, the development of a novel surface passivation ink formulation and printing process is reported. A polyethylene glycol (PEG) based is developed and optimised for the inkjet printing of continuous coatings on glass cover slips. The PEG based ink acts as a cell repellent coating for the containment of cell populations. Cell

adhesion analyses were conducted to prove the repellent characteristics of the inkjet printed coating.

Chapter 5 investigates the use of amino-propyl(triethoxy)silane (APTES) ink formulations for the surface modification of glass cover slips. APTES inks are used to modify the surface chemistry and topography of the glass cover slip. Surface characterisation techniques are used to ensure that a chemical and topographical change is made in the areas where the silane inks are printed. Cell adhesion experiments were analysed to show that cells can adhere and maintain viability on the silane modified glass cover slips.

Chapter 6 discusses the manufacture of cell screening arrays using the inks developed in Chapter 4 and Chapter 5. The optimisation of the manufacturing process is discussed for the printing of both the PEG based ink and the silane inks. Cell adhesion experiments are presented and the effect of the inks is assessed in terms of cell adhesion and behaviour.

Finally, in Chapter 7 a summary of the main outcomes of this thesis and their applicability to tissue engineering applications is presented. Chapter 7 also discusses potential future research that can be carried out thanks to the results of the research presented. Areas for further development include using the developed cell screening arrays for stem cell differentiation analysis; the development of new inks to drive stem cell differentiation; the inclusion of the optimised surface chemistries into three dimensional scaffolds to produce scaffolds that can drive stem cell differentiation in order to produce living implants.

Chapter 2

Literature review

This thesis investigates inkjet printing as a manufacturing method for cell screening arrays. Cell screening arrays can be used for a variety of purposes such as microbial detection and identification, drug resistance analysis, drug development and stem cell differentiation analysis. The key areas presented in this review are: inkjet printing and the characteristics of inkjet inks, material design for tissue engineering, cell screening arrays, surface passivation and stem cell control through surface modifications.

Cell screening arrays can be manufactured by different technologies; this thesis focuses on their production using inkjet printing. Inkjet printing is an additive manufacturing technology that can be used to produce two dimensional patterns and three dimensional structures. In this review, investigation into the inkjet printing technology and the fabrication of inkjet inks is presented. A review of different technologies that are used to produce cell screening arrays is considered. A discussion on surface modification for stem cell differentiation is also presented. Inkjet printing of cell screening arrays and its benefits is discussed.

2.1. Material design for tissue engineering applications

Biofabrication is the production of living and non-living products using living cells, bio-molecules and bio-materials. It is important to mention that the biofabrication of living structures with defined surface functionality needs the effort and collaboration of experts in the physical, life and engineering sciences. These kinds of projects need the implication of all these areas making them complex and interdisciplinary[13,14].

One of the most desirable goals of biofabrication is being able to engineer and fabricate living human tissues for implantation and regeneration of damaged tissues in-vivo, after this is achieved the fabrication of larger and more complex products such as living organs suitable for implantation is also desired. The use of inkjet printing technologies can help design and produce scalable and cost-effective production processes for the fabrication of living structures.

Tissue engineering can be approached in different ways but there are three 'classical' approaches that are used: the first is the use of an instructive environment to guide and recruit host cells to regenerate the tissue; the second is the delivery of repair cells or factors into the affected area; and the third approach is the cultivation of cells on bio-materials scaffolds in a culture system under well-defined condition designed to engineer the wanted tissue[14]. It is thought that the controlled deposition of bio-materials on substrates in the form of micro-patterns will have the ability to produce functional, reactive materials with high performance under regular ambient conditions[13,15].

The engineering of such materials has the potential of revolutionizing the bio-medical industry and improving the development of products for tissue engineering as well as allowing research groups to better understand the behaviour of cells and bio-molecules when in contact with specific designed substrates. The precise positioning of bio-materials, polymers, proteins, hydrogels and cells is of great interest in the field of tissue engineering. Different techniques can be used for this purpose some of which will be briefly described in this section.

2.1.1. Micro-contact printing

This is a direct contact technology that has proven to be useful for printing bio-materials. Some of the materials printed with this technique include polymers or lipids into culture flasks or tissue culture polystyrene (TCPS) and the printing of long-chain alkanethiols on gold substrates for the fabrication of bio-sensors[16].

Before the printing of the bio-materials a master of the patterns to be printed is produced, usually by photolithography[16,17]. Once the master is defined a stamp of polydimethylsiloxane is made. When the stamp is ready to use it is usually submerged in an ink with the bio-materials that will be immobilised on the substrate, the ink is allowed to dry for a period of time, specific to the ink, and then is stamped onto the substrate[17]. This technique allows the creation of patterns with nano-scale resolution.

2.1.2. Electron beam radiation

Electron beam radiation (e-beam) is a technology considered a soft lithography that incorporates a metal mask that can resist the irradiation. This technique has been used to investigate the adhesive nature of a variety of cells[18].

The results of micro-patterning with e-beam technology allow the investigation and documentation of the adhesive properties of the cells and it can also identify the primary binding sites[18]. Both cell adhesive and cell repellent materials can be patterned using this technique. With the use of e-beam radiation different factors that control cell adhesion such as the polarity of the patterned substrate can be varied in order to produce different results[13].

2.1.3. Non-contact printing

The contact printing techniques can produce high resolution patterns at low costs, but the patterns frequently show unstable patterns and stamp fatigue, in some cases nano-patterned substrates have shown post-printing degradation[19]. Non-contact printing processes are straight forward techniques thanks to their computer graphical interface.

Images, graphic files and structures can be converted to bitmap images (or a series of them in case of three dimensional models) that can then be introduced as a series of X and Y coordinates showing where the drops or material needs to be deposited[20]. The production and quality of patterned coatings is dictated by the properties of the ink solution used to deposit the materials but is also dependant to the substrate and the characteristics for specific non-contact techniques.

2.1.4. E-Jet printing

This type of drop-on-demand technique uses an electric field to micro-pattern small droplets of ink onto a conductive surface[21]. Electro-hydrodynamic jet (e-jet) printing was created as a response to avoid the exposure of inks to high temperatures like in the case of thermal inkjet printing[21].

High resolution prints have been achieved with this technology and a range of organic and inorganic inks have been used on a variety of substrate allowing the formation of features of approximately 10um[21]. The reach of this technology is still limited due to the charge associated with the deposited drops.

2.1.5. Solid free form printing

Solid free-form (SFF) printing is one of the tools that have been used for designing and fabricating scaffolds for tissue engineering thanks to its ability to produce very complex geometries and three-dimensional (3D) structures by the use of layer-by-layer deposition[14]. This technique uses a liquid monomer or sintered powder as an ink that is photo-polymerised for printing.

2.1.6. Drop-on-demand printing

Drop on demand printing is also known as inkjet printing and it is a very straight forward technique thanks to user-friendly interface[22]. The need for fast printing, high resolution patterns and small volumes of material to be deposited on the substrate

have made drop-on-demand printing a desired technology in the bio-medical field to engineer surfaces and fabricate scaffolds[4,5]. Drop-on-demand inkjet printers evolved from the standard graphic desktop printers. Drop-on-demand inkjet printing process will is described in depth in Section 2.6.

2.2. Surface passivation

Surface passivation in the biomedical field refers to make a surface or a device resistant to bio-adhesion, and is also referred to as anti-fouling surfaces[23–25]. Surface passivated surfaces are of great importance to a wide range of areas, ranging from coatings designed for ship hulls[26], biomedical implants[27], biosensors[28] and cell screening arrays[29].

For a surface to be considered passivated it has to remain undetected by cells and proteins in a biological environment[23,24]. Many biomedical devices do not perform as expected due to an inadequate passivating performance of the materials used for their manufacture[30]. The accumulation of biological materials and biomolecules on the surface of the materials leads to a non-optimal performance when exposed to biological environments, both in vitro and in vivo[31,32].

Different bio-adhesion manifestations are derived of a rapid adsorption of proteins to the surface of the materials[33,34]. For this reason, the prevention of protein adsorption is the main objective when developing surface passivated surfaces[23–25], It is of great importance to consider that in many surface passivating reports it is not always stated to what extent a surface has been passivated. Some surfaces may be reported as

passivated where cell adhesion and protein adsorption has only been reduced and not avoided[23,30].

Nature presents its fair share of anti-fouling surfaces, but is important to emphasise that these natural surfaces mainly reduce the interaction with living organisms and bacteria, instead of avoiding interaction with biomaterials, cells and proteins[25]. Marine organisms, such as sharks, mussels and crabs, are known to present natural antifouling surfaces[35–37].

The manufacturing strategies for the production of bio-adhesion resistant surfaces can be divided in two main groups: physical strategies and physico-chemical strategies[23,25]. Physical strategies focus on the modification of the surface topography and can also be referred to as contact guidance techniques[25,38]. By modifying the surface micro-topography, a change in wettability will be observed, as well as a change in the surface roughness, modifying the way that cells and their adherence mechanisms interact with the surfaces[39–43].

In physico-chemical techniques the surface chemistry of the surfaces plays an important role since it is a major factor in the adsorption of proteins and cell adhesion[25,44,45]. The change in surface energy can drive the interaction of water and water-based environments and their dispersion on substrates also affecting protein adsorption[44]. Polyethylene glycol has been largely studied for its high resistance to cell adhesion when optimised[29,46,47]. In the section below an overview of PEG and its surface passivating characteristics are reviewed.

2.2.1. PEG for surface passivation

The most effective polymer for manufacturing protein and cell resistant surfaces has proven to be PEG thanks to its molecular conformation in aqueous solution[48–50]. The use of PEG to produce surfaces that resist protein and cell adhesion has proven to be successful, both as a surface coating[51–53] and as the main structural material. PEG has also shown to resist patlet adhesion, in vitro and in vivo, leading to the reduction of tissue damage, cytotoxic effects and thrombus formation[47,54].

PEG attaches to surfaces with not a major effect on their chemistry[31,47,51]. Surfaces, molecules and particles coated with PEG often gain the favourable characteristics of PEG. Another advantage of PEG is that it is soluble in water and most organic solvents[48,49], making it an ideal material for the fabrication of biomedical devices[31,55–57] and implant coatings[27,58,59].

It is thought that the protein resistant capabilities of PEG are caused by a steric stabilisation effect[39,48]. The steric effect is that caused by the fact that atoms occupy space[52,60–62]. The arrangement of atoms and molecules comes with a use of energy[52,63]. The electrons that are closer the atoms repel each other, changing the way that molecules and biomolecules react to each other[60,61,64]. When there is a balance of the forces between the electrons the energy is at equilibrium, not allowing other atoms/molecules to interact with the stabilised material[48,60,62]. PEG has proven to achieve this steric stable effect so when a protein gets close to a PEG coated surface, the energy available in the surface of the polymer segments is not enough for the proteins to interact with the surface[61,64,65]. Due to its ability to remain "undetected" by proteins and biomolecules PEG is often used to 'camouflage' drugs, implants and medical devices[47,51].

PEGylation of proteins has proven to be an effective way of reducing their bioactivity[65–67]. PEG wraps around the protein via hydrophobic interaction and then forms hydrogen bonds with surrounding water molecules present in the aqueous environment[65]. The steric effect of PEG can achieve the loss in the bioactivity of the coated proteins by shielding the bioactive domain (substrate or receptor binding domain)[68–70].

The mass of the PEG molecule used can play an important role in its behaviour and the consequent bioactivity it can have on the protein or the substrate[71,72]. Manjula et al. found that when coating haemoglobin with PEG, the coating coverage is not proportional to the chain length because the PEG chain can fold loosely on the surface of haemoglobin[73]. However, Yang et al. modelled a PEG-insulin system and predicted that PEG chain length has an effect on possible bioactivity, showing that the steric shielding effect improves with larger PEG molecular weights[74]. Studies carried by Qimeng et al. corroborate that the steric shielding effect of PEG on coated proteins is dependent on the PEG mass[62].

Qimeng et al. have confirmed that the native conformation of the proteins is not affected by the PEG coating or PEGylation of the molecule. In contrast, it is shown that the bioactivity, molecular symmetry and hydrodynamic volume of the PEGylated molecules are dependent on the PEG chain length[62].

Studies have shown that PEG molecular weight plays an important role in the porosity, permeability and protein interaction when manufacturing PEG membranes[75] and PEG-DA monoliths[76]. The fabrication of PEG membranes discussed by Chakrabarty et al[75] shows an increase in porosity, pores size and, by consequence, the permeability of the PEG membranes when larger molecular weights of PEG are used, impacting the antifouling properties of the PEG surface. When

manufacturing PEG-DA monoliths the lower the molecular weight of the PEG-DA used presents a higher density network of crosslinked monomers, which not only impacts the passivation properties of the PEG-DA but also improves mechanical stability and reproducibility of the PEG-DA structures[76].

PEG has proven to be a material that has very low rate of cell adhesion[29,46,47,77–79]. These use of these chemicals reduce the adsorption of proteins to which cell attach such as collagen and fibronectin from the culture media, the cell patterning is then achieved by the use of surfaces composed of cell-repellent and cell-adhesive regions. One of the major problems with using conventional protein/cell-repellent chemicals is that the formed cell patterns are temporary and break within several days because of increased desorption from the surfaces and gradual adsorption of cell-adhesive proteins[80,81]. For this reason a cell repellent coating will be produced for this project that can withstand these conditions and will allow the cells to differentiate in the desired specific areas.

As mentioned in this section, PEG not only has proven to be an effective surface passivating material, but thanks to its physico-chemical characteristics, such as the fact that it is soluble in water and other organic solvents, it has the potential to be used to coat substrates by the use of a wide range of technologies.

2.3. Stem cell control/differentiation

Mesenchymal stem cells (MSC) are a fundamental key in the field of tissue engineering thanks to their potential as an unlimited source of autologous multi-potent cells that can be cultured and then differentiated for the production of tissue-

engineered products in vitro for in vivo applications. There are studies showing that controlling the level of cell adhesion on a surface could offer a way to influence the differentiation process when MSCs are cultured in contact with the modified surfaces[1,2,12,80–82].

It is important to consider that the materials designed to provide the cell culture environment for the MSCs must provide cell selection properties to improve the performance of the cell population, or alternatively control initial adhesive events that subsequently result in autocrine control by the release of specific growth factors from the adhering cell population. Research has proved that cells respond to stimuli at the nano-scale for this reason materials should be developed that provide definition and control from this scale and upwards[1,2,12,81]. This project will focus on the surface modification at the micrometre scale using inkjet heads that range from the 20µm to 80µm diameter drops.

In the areas of study of regenerative medicine and cell biology substantial research has been focused on using minimally invasive methods to produce a specific cellular response. A way of achieving this is by controlling the direct contact and interaction between the MSC and a well-defined material and surface chemistry[81].

Control over the stem cell phenotype and function is required so the cells will characterise changing their form and function to realise their potential, producing efficient reproducible living tissue formation and cellular function in the appropriate environment at all points in the scaffold. It is important to understand that the control of the cells adhesion to the surface will drive the differentiation of the cells, this being reflected by the different morphologies presented by the cells one they have been differentiated for example into osteoblasts (bone cells) or chondrocytes (cartilage

cells). Differentiation capacity would greatly increase the utility of expansion culture substrates[1,2,12,83,84].

Many biomedical devices such as microarrays, drug delivery systems, biosensors, and scaffolds for tissue engineering have been recently developed for the study and manipulation of biomolecules, and they have proven to be valuable experimental tools for solving many biologically based problems. Microarray technology in particular has become a crucial tool for large-scale and high-throughput biological experiments, as it enables fast, easy, and parallel detection of thousands of addressable elements in a single experiment under identical conditions, the use of this microarray technology combined with the MSC differentiation by using specific surface chemistries will be investigated for this project[80].

2.3.1. Surface modification for stem cell differentiation

The capacity of controlling cellular response and induce stem cell differentiation using surface modifications to the substrate has great academic and commercial benefits. The use of these surface modifications could lead to the fabrication of scaffolds with different chemistry that controls the phenotype of the attached MSC making an advance in the field of tissue engineering and lead to more efficient and personalised implants[1,83].

Experiments show that the direct contact of MSCs with defined chemical groups that have been accurately arranged and physically defined as part of their immobilisation to a material substrate, can be used as the controlling tool to interact with cells in order to define their phenotype and function. The control and definition is directly

related to the cell adhesion which in turn controls specific cell signalling pathways and ultimate function[2].

By inducing material-controlled differentiation a revolution in the fabrication of current tissue-engineering scaffolds could start, enhancing the performance by reducing the incubation times (both in vitro and in vivo) required to obtain viable functional tissues that will enhance the status quo of many conceptual biomaterials and scaffolds. This technology could prove to be fundamental research resulting in the formulation of a new era of more efficient and effective tissue-engineering scaffolds[2,12,83].

Using both glass and polymer as the material substrate $-CH_3$ groups have shown enhancement of the MSC phenotype, –OH and –COOH groups have directed stem cells to a cartilaginous tissue phenotype and $-NH_2$ groups directed the stem cells to an osteogenic phenotype[1,2,12,81,83].

Studies show that –OH chemistry can provide the optimal chemistry for chondrogenic stem cells characterisation while $-NH_2$ chemistry can provide the conditions for bone formation and possibly neurogenesis due to cellular elongation. These functional chemistries provide proof that cell differentiation can be controlled and driven using substrate definition by defined micro-patterns through the use of specific chemically modified surfaces which can be selected for different cell phenotypes and functions for in vitro and in vivo studies. Modifications using silane chemistry was used to successfully produce surfaces presenting $-CH_3$, the presented $-CH_3$ radicals were controlled by changing the chain length and the binding of the chain to the substrate, The $-CH_3$ functionality has proven in previous experiments to enhance the MSC phenotype with nano-scale modifications to the surface as well as using the bulk

chemical group, this project will focus on micro-metre modifications to achieve these results[1,2,12,81,83].

2.4. Cell patterning

Cell patterning is used to control the geometric organization of cells on a defined substrate. This control can be aimed for single cell studies or the analysis of behaviour for cell populations[85]. Cell patterning can lead to better control and understanding of cellular behaviour that can later be applied to biomedical systems, tissue engineering devices, organs-on-chips devices[86–88]. Cell patterning and cell manipulation are widely used to obtain information on cell behaviour and activity in the areas of drug testing, microfluidic device design and manufacturing, to better understand biochemical processes and to collect data of the behaviour of biomolecules, bacteria, proteins and other biologically active agents[89–92].

A number of cell patterning approaches can be used to explore and understand behaviours from single cells to cell populations. When a single cell and cell population behaviours are studied together a better understanding of cellular biology and tissue engineering can be achieved[85,93–95].

Different scales of cell patterning can be achieved and engineered which will provide controlled special architectures for the systems (either single cells or cell populations/tissues) which can provide different information on cell behaviour[87,96].

Micropatterns usually have a resolution of 5 to 40µm and are aimed for single cell analysis and allow the observation of how geometrical constraints affect single cell

phenotype and behaviour[96,97]. A paramount consideration when producing single cell patterning devices is that the cell active or adhesive areas have to be smaller than the optimal spreading area of the cell; this constraint will force cells to maximise their spreading by modifying their cytoskeletal orientation which results in a shape change that replicates that of the patterned area[96,98,99]. The size of the areas patterned for single cell analysis allows the manufacture of high throughput arrays to analyse several cells in a single experiment allowing quantitative analysis of the cell behaviour[96,97].

Micropatterns can also be used to analyse multi-cellular populations seeded in specific areas ranging from 50 to 500µm producing cellular micro-sheets[100]. When analysing cellular micro-sheets the geometry of the sheet is controlled, however individual cells are allowed to grow naturally without modifying their phenotype in the same way as it is done in single-cell studies[96,97]. The dimensions and shape of the pattern can induce changes in the shapes of the cells present in the micropattern due to geometric constraints; for example, if the designed patterns are narrow, the cells growing in the area are likely to align parallel in order to accommodate more cells in the specified area[101,102].

Patterning allows the study of larger scale cell populations, usually ranging from 500µm to millimetres, allowing observing how larger cell populations behave to specific modifications to the substrate areas where cells are to adhere[96,103–105]. This macroscopic approach focuses on the control of cell population growth to specific locations, the response of the population to different topographical patterns and surface chemistries and it provides a better representation of cell and tissue behaviour in-vivo[85,87,97]. Cell patterning and micropatterning can also be referred to as cell screening arrays as long as more than one cell or cell population are being analysed in

the same experiment, however, in this thesis, only the macroscale patterning will be explored. A more specific description of cell patterning requirements and techniques are explained in Section 2.5.

2.5. Cell screening arrays

For the creation of new engineered bio-surfaces two main requirements must be met: maintain the functionality of the bio-ink that is intended to be immobilised on the surface (i.e. proteins, chemical groups, cell suspension) and to generate accurate and repeatable patterns at micrometre levels on the substrates. Standardisation is one of the cornerstones of modern engineering and has become a requirement for the fabrication and manufacturing of products. Standardisation refers to having a set of parameters and specifications defined for the product and its fabrication process to allow repeatability making the process more cost effective, this repeatability is another great advantage of using inkjet printing by integrating computer aided design (CAD) and engineering tools[8,11].

A cell screening array is usually a two dimensional arrangement of specific biological samples (i.e. DNA or proteins) or biomaterials (such as PEG), deposited in an arranged way on a substrate (usually glass slides or glass cover slips)[106,107] where then cells are seeded to analyse their interaction with the deposited materials.

Cell screening arrays use conventional methods for cell investigation with high-throughput screening capabilities[108–110]. Cell screening arrays can be used for the development of new biomaterials, drug testing and in vitro toxicology tests[16,106,111].

The fabrication of cell screening arrays is inherently a fluid dispensing process where biological or fluid biomaterials are deposited in a defined position on a substrate[112–114].

The fabrication techniques for cell screening arrays follow the same main objective: the uniform deposition of materials while avoiding contamination and biomolecular damage of the materials being deposited[106,107,111]. Screening arrays fabrication technologies can be divided in two main categories: contact and non-contact printing technologies[106,107]. In contact technologies, the device that is depositing the biomaterial or biological sample comes in physical contact with the substrate. In non-contact technologies there is no physical contact between the dispensing device and the sample substrate.

2.5.1. Contact techniques

Contact fabrication methods can fabricate arrays of materials or biological samples (such as DNA and proteins) by directly depositing on a substrate by means of direct physical contact. The main contact fabrication methods are pin printing, nano-tip printing and micro stamping[106,107].

2.5.1.1. Pin printing

Pin printing fabrication is very common technique used for the manufacturing of microarrays. This technology allows an accurate deposition of materials in specific locations on a substrate[115,116]. In pin printing technology, pins are carried by a pin carrier head from the ink or material formulation container to the substrate[106], as

shown in Figure 2. The solution is held to the pins by surface tension and capillary forces[117,118]. The pins can move vertically in the pin head when they make contact with the solid substrate. Pin heads usually contain arrangements of 16, 64 and 96 pins per head[117].

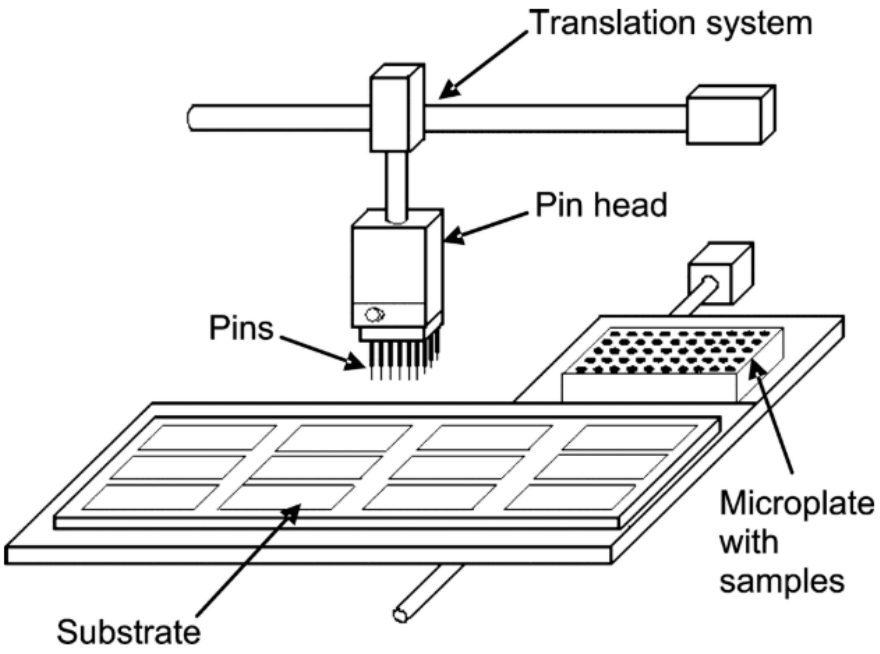

Figure 2 Schematic illustrating a microarray pin printing system[106].

The pins for pin printing can be either solid or split pins. Solid pins are, as described by their name, made of a solid piece of material. Solid pins are dipped in the material solution container where the solution is adhered to the tip of the pin by capillary forces[119]. Split pins on the other hand, are not a solid piece of material but usually have a slit in the tip to allow the collection of larger amounts of material solution, allowing the fabrication of denser arrays when compared to solid pins[118,119]. Figure 3 shows the diagram of a solid and a split tip and their interaction with the material

solution. The material solutions need to be tailored depending to which type of pins are to be used since the surface tension and viscosity can affect the deposition of materials to the substrate.

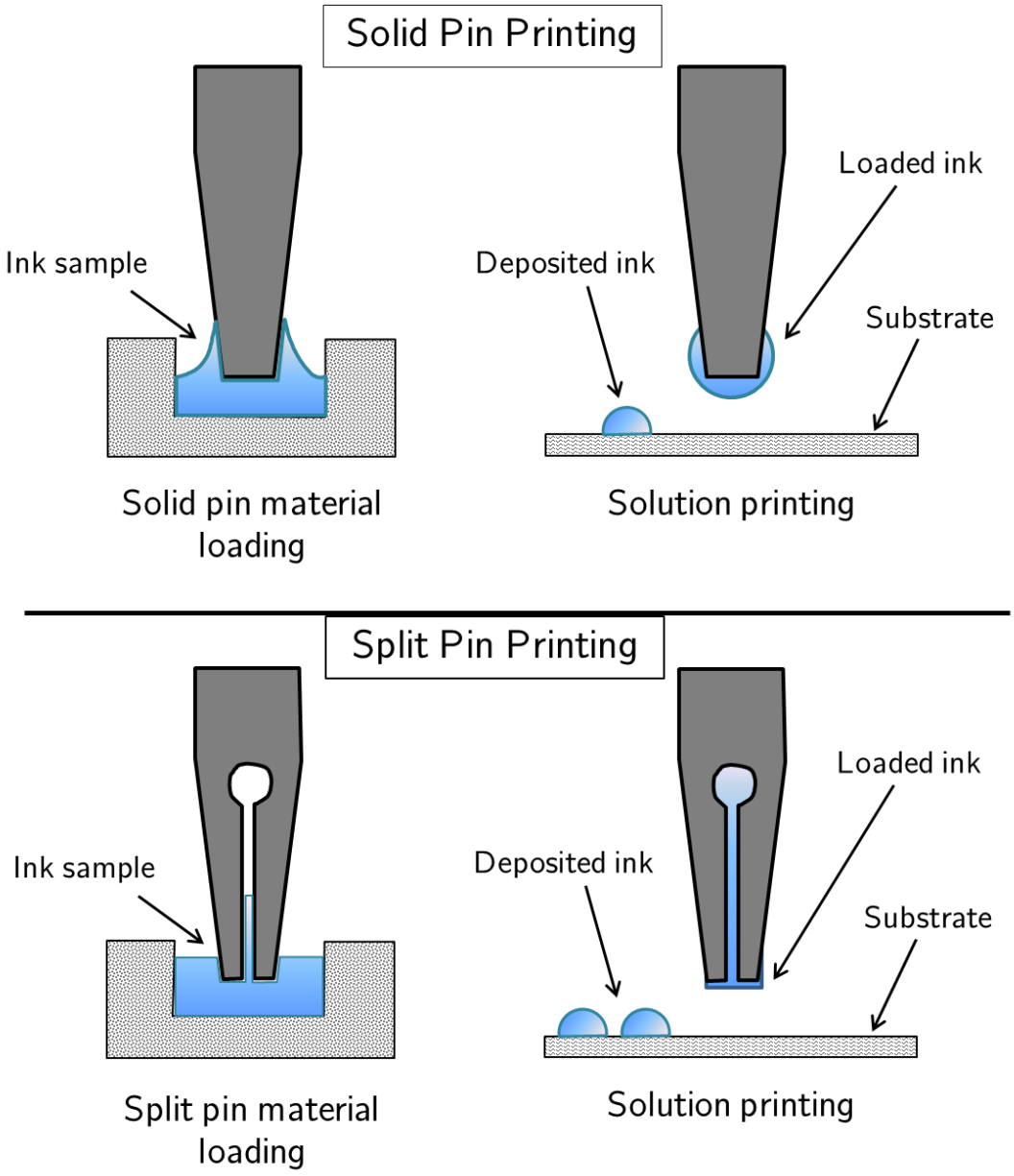

Figure 3 Schematic illustrating the material loading and solution printing through a solid pin printing and split pin printing process.

2.5.1.2. Stamping/microstamping

The stamping/microstamping technology is an alternative that allows parallel printing of hundreds of spots or predefined areas, allowing a high-throughput array manufacturing[106,107]. In stamping/microstamping first a stamp or mould is made, this stamp is then inked or dipped into the material solution and then transferred to the substrate via physical contact[120]. The stamping/microstamping process is shown if Figure 4.

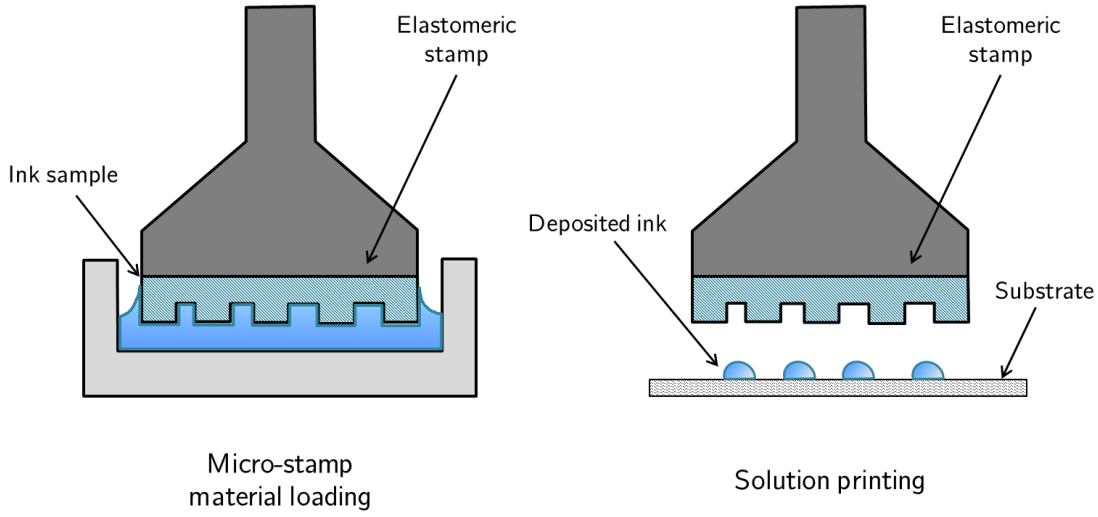

Figure 4 Schematic illustrating the material loading and solution printing through a microstamping process.

The stamps are usually made of elastomeric polymers such as PDMS in order to obtain good contact without damaging the substrates[120,121]. The mould masters are usually manufactured using photolithography to define a pattern on the stamp. The use of master moulds allows the production of reproducible batches of disposable stamps[121]. The use of disposable stamps reduces the risk of contamination in the

samples, cross-contamination and reduces the time by not having to clean pre-used stamps[107,121].

Elastomeric polymers like PDMS are by nature hydrophobic, which means that the material solution to be deposited on the substrate is most likely not going to adhere to the stamp, for this reason the stamps are treated with ozone plasma in order to make them hydrophilic and allow the stamp to carry the solution[122]. Once the stamp has been plasma treated it is dipped into the solution container and then taken to the sample where it is pressed against the substrate. Microstamping has the potential to produce high resolution arrays with spacing between features of 100nm[123,124].

2.5.1.3. Nano-tip printing

Nano-tip printing allows the fabrication of arrays with higher spot density, allowing the fabrication of very complex arrays of dots in the range of nanometres[125]. Nano-tip printing technologies are based on the principle of atomic force microscopy (AFM) where nano-tip either adds material to a substrate or where the tip removes material from a substrate[106,107].

Dip-pen nanolithography (DPN) is a technology that allows the binding of molecules to a substrate in a very precise way[125,126]. In DPN a material solution is carried to a substrate via an AFM-like tip that will transfer the material solution to the sample by creating nano-patterns[126]. The material solutions usually used with DPN are composed by proteins but other biomolecules can be used[81,125]. The substrates used for DPN are usually blocked by molecules that do not bind with biomolecules or cells, allowing a very specific adhesion of proteins and cells[81,125,126].

2.5.2. Non-contact techniques

In non-contact printing techniques the manufacturing device does not come in contact with the substrate to be modified, this gives the advantage of reducing contamination of the samples when producing screening arrays[106]. Non-contact methods have the potential of increasing cell screening arrays throughput since some of them allow parallel deposition of solutions allowing different arrays to be produced simultaneously[106,107].

2.5.2.1. Photochemistry printing

The photochemistry microarray manufacturing method is based on the chemical treatment of a sample and then its exposure to UV lights through photomasks. There are two main methods of photochemistry printing: photolithography[113,127,128] and direct photochemical patterning. Photo chemistry fabrication technologies are mostly used to manufacture DNA arrays, although cell screening arrays can also be produced[128–130].

In photolithography, a photoresist layer is deposited on the substrate (usually by spin or dip coating) and then it is exposed, through a mask, to UV light. The sample is then submerged in a solvent in order to remove the un-cured photoresist material still present on the substrate. Molecules that promote adhesion-resistance of proteins and/or cells are bound to the untreated substrate via wet chemistry[113,129,130].

Direct photochemical patterning is very similar to photolithography, with the exception that a photoresist treatment is not needed. The substrate is directly coated

with photochemical molecules and then exposed to UV light through the photomask where the molecules exposed to the UV light are either activated or deactivated to bind the desired biomolecules, proteins or cells[128,131].

Photochemistry printing technologies have the disadvantage of a high risk of biomolecules/proteins degradation due to the exposure to solvents and UV light[132].

2.5.2.2. Laser writing

The laser ablation technology has been used to manufacture cell screening arrays and protein microarrays[132,133]. For this technology a sample that has been previously coated with a biologically inert coating, a laser is then scanned to selectively remove the coating material allowing the micro-patterning of the substrate to modify its topography. The laser processed sample can then be exposed to a biological solution so different combinations of topography and chemistries can be assessed[133,134].

2.5.2.3. Inkjet printing

Inkjet printing is a non-contact fabrication technology that dispenses droplets of a ink formulation on a substrate through a printer head nozzle[135,136]. Inkjet printing is ab attractive technology since it can reduce the cost of fabrication while maintaining material waste to the minimum, and it can deposit small droplets of the ink formulation with reproducible volumes,[7,136]

One of the major drawbacks of inkjet printing is that the ink has to be jetted through a very small nozzle (in the range of micrometres) which forces the droplets to high shear forces when ejected. This high shear forces can denature or degrade certain biomaterials and can affect cell viability when printing living cells[7,137].

The inkjet printing technology is explained in depth in the following section.

2.6. Inkjet printing

Inkjet printing technology has developed into a technique which plays a prominent role in the graphical printing industry and in many new industrial and research applications thanks to its ability to transfer a computer-generated image and its translation to an equally digital output.

Inkjet printing is an important technology in colour document production[138,139]. In the decade of 1970, Hertz of the Lund University of Technology developed inkjet techniques that allowed grey-scale printing by changing the number of ink droplets deposited per pixel[140,141]. In 1977, Applicon introduced colour inkjet printing, based on the printing principles developed by Hertz. His methods were used by Iris Graphics and Stork to print high-quality colour images in the prepress colour hardcopy market[142,143]. The Iris Graphics proofer was able to deposit up to 32 ink droplets on a single dot at a resolution of 300dpi[143].

The inkjet printing ejection technology was initially developed in the for printing text, by the 1980-1990s its market had expanded to that of domestic devices that could print colour images with very good resolution[144]. The jump to digital printing happened in the 2000's and its commercialisation drove the technology to be utilised in new fields such as the printing of electronics and bioprinting[4,11,20,145–147].

Digital inkjet printing has quickly become one of the preferred technologies for bio-surface functionalization because of its non-contact process, reducing cross-contamination between samples[7,15,136]. This technology allows reproducing images or, in recent years, three dimensional models onto a substrate by jetting drops in the pico-litre scale by receiving the information from computers[20,147]. Inkjet printers can jet drops continuously or on demand, drop-on-demand (DOD) printers jet the drops at specific locations when required, making this process very accurate[4,11].

The continuous inkjet printing (CIJ) process works by jetting a constant stream of individual electrically charged droplets that can be directed to the substrate by an electric field, when the droplets are not required to be directed to the substrate they are collected and redirected back to the ink container for their reuse[148–150]. Figure 5 shows a schematic of a continuous inkjet printing system showing how droplets are either directed to the substrate or to the drop collector.

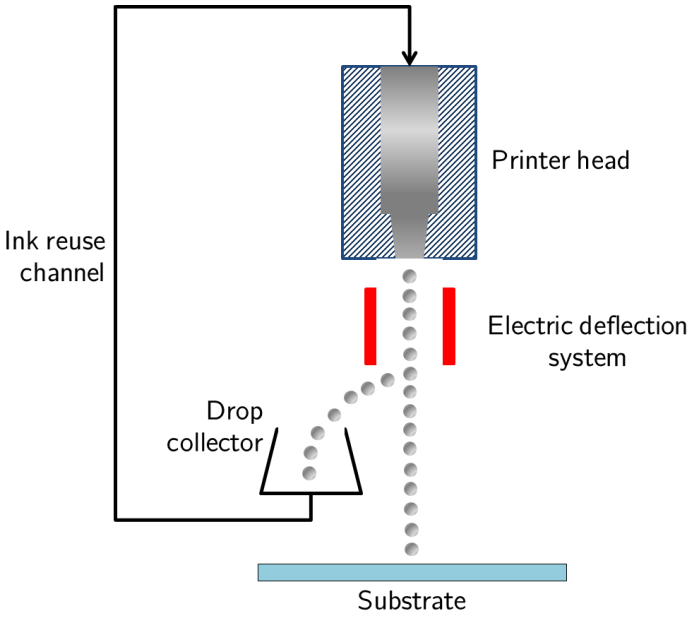

Figure 5 Schematic illustrating the continuous inkjet printing process.

One of the advantages of CIJ is that due to its high drop frequency and high velocity, it allows high speed printing[149,151]. One of the major disadvantages of continuous printing is that the ink formulations need to be electrically charged so the droplet direction can be controlled[150,152,153]. Continuous inkjet printing is generally used for high speed graphical purposes, such as text printing.

Drop on demand printing, contrary to continuous printing, only generates ink droplets at specified substrate locations, making this process very accurate[149,154,155]. Drop on demand printing is widely used for the development of new materials and ink formulations for inkjet printing and has been used for a wide range of purposes, from printing conductive inks to bioprinting[5,123,156]. Major advantages of DOD printers over continuous inkjet printing include the fact that there is no need for complicated hardware responsible of break-off synch, electrodes for charging and deflection of the droplets, guttering and recirculation of unwanted ink[138]. In the decade of 1940 the Radio Corporation of America started planting the seeds for DOD printing working on a project for a graphic writing mechanism; however, it was never developed into a commercial product[138].

At present, thermal inkjet printing (TIJ) and piezoelectric inkjet printing (PIJ) have become the two most important technologies when it comes to graphic printing.

In thermal inkjet printing, the temperature of the ink is raised drastically by the use of a heat resistor producing a vapour bubble in the ink chamber. The vapour bubble produces an increase of pressure in the ink chamber, forcing the ink to be jetted in the form of a droplet[11,20,149]. One of the major drawbacks of using thermal inkjet printing is the limitation of materials that can be printed, since the ink formulations need to

be heated, in order to achieve the pressure change, and this has the potential of degrading any functional materials present in the inks[55,136,145,150,157]. Figure 6 shows a schematic of a thermal printer head.

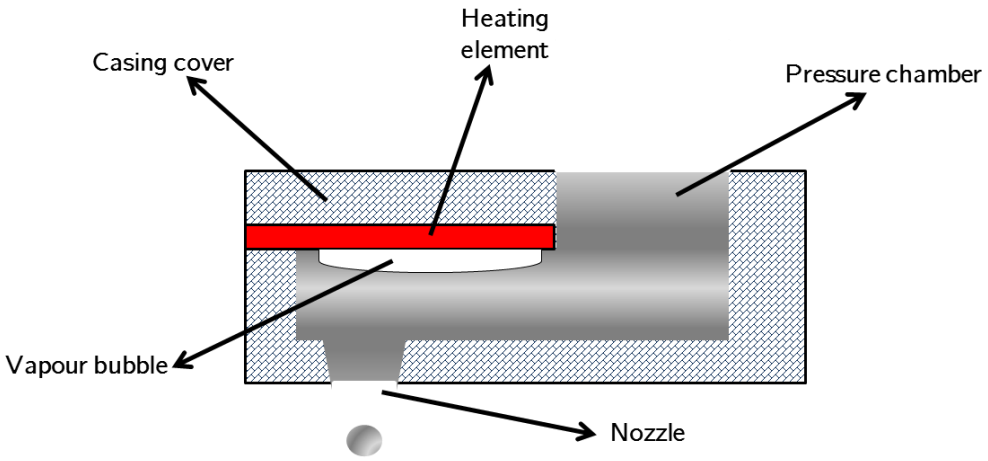

Figure 6 Structure of a thermal inkjet head

The piezoelectric element in the piezoelectric inkjet head (Figure 7 shows the components of a piezoelectric inkjet head) can be controlled by two methods. The first method is known as the pull-push method and the second is known as push-pull method[158]. The pull-push method is the most common since its present in all commercial piezoelectric inkjet printers, in this method the piezoelectric element in stand-by with an applied voltage and no drops are being ejected[158]. This stand-by state bends the piezoelectric element towards the pressure chamber while no pressure is being generated to counteract this[151].

When the computer sends the signal for jetting a drop the voltage in the piezoelectric element becomes zero causing the piezoelectric element to return to a no-bend state causing negative pressure to be generated inside the pressure chamber because of its

increase of volume[151,159]. The negative pressure is then reflected causing a wave of positive pressure to propagate to the tip of the nozzle causing the drop to be ejected. In the push-pull method no voltage is applied to the piezoelectric element of the printer head when is in standby mode and when the signal for drop jetting is received a voltage is applied to the piezoelectric element pushing it towards the pressure chamber causing an increase of pressure that leads to the drop formation[20,159,160]. The pull-push method can use about half of the drop volume compared to the push-pull method making it more desirable for printers where higher resolution is important[158]. Most of the inkjet test devices used for research use the pull-push drop jetting method, but there have been studies that employ both methods for bio-printing and biofabrication[3,7,11].

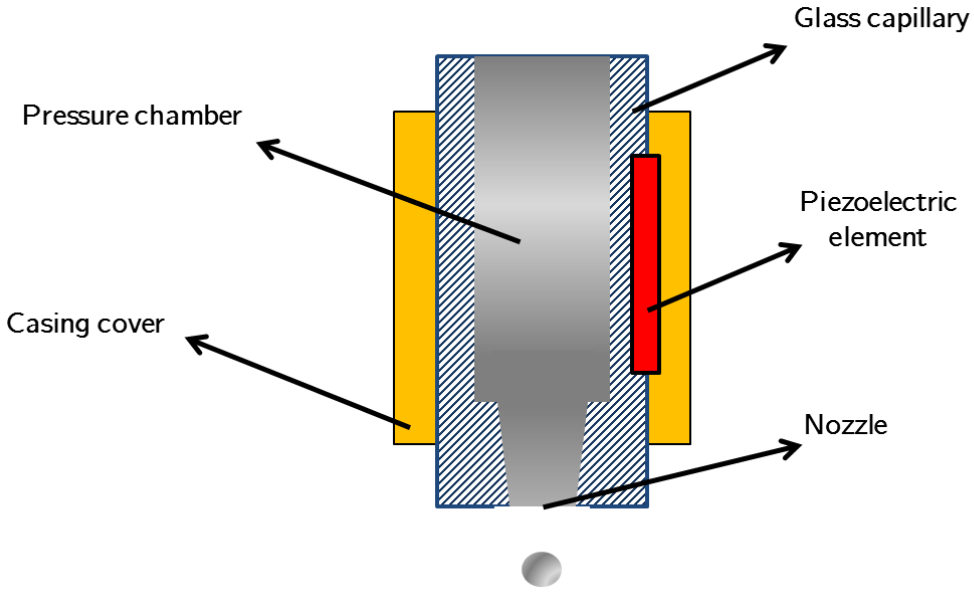

Figure 7 Structure of a piezoelectric inkjet head

In recent years other applications apart from printing onto paper have emerged[138,161–163]. In the display market, inkjet printing has been used to manufacture flat panel

displays, liquid crystal displays and colour filters[164–166]. In electronics, inkjet printing has been used to manufacture conductive trails by the use of conductive inks, both on rigid and flexible substrates[138]. Electrical components and circuits such as wearable electronics, tags, batteries, fuel cells and solar cells have also been manufactured via inkjet printing technologies[167,168].

Jetting of UV curable polymers has become a key technique of producing micro-lenses in a cost effective way, which can be used in devices ranging from fibre optic collimators to biomedical devices[169–171]. Inkjet printing can also be used as a tool for research purposes, as it will be used during this project. The capability of depositing very small amounts of liquid is very useful for the development of new substrates and coatings[172,173]. The biomedical research using inkjet printing is also expanding at a fast rate where dispensing DNA, proteins and biomolecules are required to further the research[174–176]. Inkjet printing has also been used to explore the possibility of fabricating living tissue[11,40,177,178].

Inkjet printing is a non-contact process that can be used for printing biomaterials[13,15,106,178,179]. Inkjet printing avoids the drawbacks such as time, waste of materials and cost of other printing methods like screen printing and lithography[7,16,29,136,180]. Inkjet printing present several advantages like repeatability, low waste of materials, cost efficiency, scalability, high speed and most importantly a wide variety of materials that can be used and developed for this technology[181,182]. These advantages make inkjet printing an optimal manufacturing method of cell screening arrays. In the last couple of years there has been a growing interest in the use of systems for precisely controlling cell-material interactions[3,179,183].

The University of Liverpool has a MicroFab JetLab 4 piezoelectric inkjet printer with 4 different positions for inkjet heads, for this reason the piezoelectric jetting technology will be the one used for this project. Since inkjet printing depends on the formation of droplets and their deposition on a specific area of the substrate, the formation of droplets is paramount. Certain rheological properties and ink characteristics need to be considered when developing new ink formulations.

2.7. Characteristics of inkjet inks

The fabrication of inkjet inks can be a challenging task due to the complexity of inks and the requirements the inks have to meet.

There are physic-mechanical properties that are particular to the different printing devices. For example each printer head has a unique range of viscosity and surface tension that allows the appropriate jetting of the ink[144,152]. These device specific characteristics must be considered when formulating a new ink.

Most of the times inks are made of different components and each component can affect the behaviour of the ink[11,152]. For this reason the person, or team, in charge of the formulation of the inks must consider all the possible effects that the components could have on the ink, from the storage and shelf life, storage in the cartridge, jetting to the deposition and performance on the substrate and the effects the ink could have to the environment and health[18,144].

2.7.1. Ink preparation and physic-mechanical properties

Inks are used to place functional molecules onto a substrate by the controlled deposition of small volumes of material. These functional molecules can be dyes (as used for graphic printing), bio-materials, polymers, conductive inks and a wide variety of other materials[150,152].

All inks share the fact that, when jetted, the whole ink should be liquid. For this reason, inks can be seen as composed of a vehicle and functional molecules[144,150,152]. The vehicle or carrier can be composed of liquids such as water, organic solvents, solvents; and additives which add a specific function to the ink such as photo-initiators (for curable inks), defoamers, and colorants[144,152,184].

The final function of the ink and inkjet printing technology to be used will define which components and carrier will be used for the fabrication of the ink. Inks can then be divided according to the carrier they use: water-based inks, solvent based inks and reactive inks.

Once the ink has been prepared it must meet the following parameters:

2.7.1.1. Ink stability

An ink where the properties remain constant over a desired period of time is considered a stable ink[144,150]. Many inks change after a period of time depending on the components that form the ink, for example when UV curable inks start polymerising in their containers. Instability is caused by the interaction of the ink components. Solution based inks can also become unstable due to the precipitation of the particles, phase separation and even the interaction with the container they are

stored in[144,150,185]. Precipitation and phase change can occur due to the effect of gravity and changes in temperature[144,150,152]. Aggregation and sedimentation are the main stability problems occurring in colloidal or suspension based inks[150]. Aggregation occurs mainly due to the natural instability of dispersion systems. Small particles such as pigments and nano-particles, can aggregate due to the van der Waals effect[144,179]. This is one of the major issues when formulating inks for graphic purposes.

Stability tests have to be conducted during the shelf life of the ink to ensure that the ink formulation is still functional. Changes in viscosity can suggest that the ink is degrading[150].

2.7.1.2. Viscosity

The viscosity of a fluid is the measure of its resistance to deformation or flow and it is determined by the friction between the molecules of the fluid. The performance of an ink during the jetting stage and the interaction of the substrate are very important and are given in a great measure by the viscosity of the ink[144]. The viscosity can be affected by the solvent (carrier) composition and the added components of the ink[150,152,185]. An ink viscosity is also affected by temperature, generally when the temperature increases the viscosity tends to decrease due to the increase of the thermal motion of the fluid's molecules, meaning that it is easier for the molecules to overcome their attractive interactions allowing them to move more freely, therefore decreasing the viscosity[150,186]. For this reason is important to consider the temperature at which the ink will be printed in order to measure the viscosity of the ink at said temperature. Like ink stability, the viscosity can change with time, for example in UV

curable inks when polymerisation starts the viscosity increases which can lead to the not jetting of the ink and blockages in the system[180,185].

The required viscosity of the ink will be given by the printer head and by the type of inkjet printing process to be used; usually viscosities below 20cP are desired for piezo-electric inkjet printing[155].

2.7.1.3. Surface Tension

The formation and jetting of drops and their interaction with the substrate is given primarily by the viscosity and the surface tension[187]. Surface tension is the elastic propensity of a fluid to acquire the least surface area possible. For a liquid, when external influences, such as gravity and aero-dynamical forces, are discarded its lower surface area is given by adopting a spherical form[186].

The surface tension is also driven by the equipment and printer head being used and it can be modified by the use of surfactants and additives to the ink. For example, adding propanol to water can decrease largely the surface tension[150,186].

Generally, most commercial inks have values in the order of tens of mN/m, with water having a surface tension of 72.5mN/m at 20 degrees Celsius and other organic solvents having surface tensions in the range of 20-40mN/m[144]. It is important to consider that when the surface tension is given by the composition of the liquid base, it is more likely to stay the same over time and it can be measured under equilibrium conditions[144,150,155]. If the surface tension is controlled by surfactants is important to also consider the dynamic surface tension, not just the static surface tension. The

resultant surface tension of the ink is dependent on the formulation of the ink, its components and how they interact and behave in the carrier[144,150,155].

2.7.1.4. pH

In some water based inks the pH of the solution is important and it could have a direct effect on the solubility of the components, and when pigments are used, it could also affect the dispersion of the dye particles[150]. For this reason some inks are formulated with the use of buffers to control this property and to make the solution less prone to the small variations in the ink components and the solvent or carrier quality.

2.7.1.5. Dielectric properties and conductivity

In continuous inkjet printing these characteristics are very important, so the jetted droplets can be deflected by the generated electrical field. The conductivity of the ink must be very well controlled so the ink can be used under the process conditions and the non-required droplets can be collected[150].

2.7.1.6. Foaming and defoamers

The presence of bubbles in the inks is a common problem in the formulation if inks[144,150]. In inks containing polymers and surfactants bubbles or foaming can be

usually observed. The use of molecules that break foam (or defoamers) is the most common solution for this issue. Defoamers usually work by reducing the surface tension in localised areas to very low values (amyl alcohol) to reduce the foam[150].

All the properties mentioned must be considered when formulating an inkjet ink and as mentioned, the printer head and the process to be used drive some of the characteristics. Once the ink has been formulated it is ready to be tested for jetting and surface interaction.

2.7.2. Printability of inks

Four dimensionless numbers can be used to define the importance of the rheological properties of an ink (viscosity, surface tension and density) when investigating the printability and droplet formation of a formulation. These dimensionless numbers are the Reynolds number (Re), Weber number (We), the Ohnesorge number (Oh) and the printability factor Z[153,155,188–190].

The relationship between the viscosity and inertial forces of a moving fluid, in this case an ink formulation[155,189–191], is defined by the Reynolds number. The Reynolds number is defined by:

$$Re = \frac{\rho V d}{\mu}$$

Where ρ is the fluid density, V is the velocity of the fluid, d is the drop diameter and μ is the viscosity of the ink formulation.

The Weber number is given by the relation of the ratio between the fluid's inertia and its surface tension[155,189,190]. The Weber number is defined as follows:

$$We = \frac{\rho V^2 d}{\sigma}$$

Where σ represent the surface tension of the formulation. The Ohnesorge number is not dependent on the velocity of the fluid, but it shows the relation between the viscosity, the density, the surface tension and the size of the droplet[155,189,190]. The Ohnesorge number is defined as follows:

$$Oh = \frac{\sqrt{We}}{Re} = \frac{\mu}{\sqrt{\sigma \rho d}}$$

Having calculated the Ohnesorge number, the printability factor Z can be calculated as follows:

$$Z = \frac{1}{Oh}$$

When the printability factor complies with the relation $1 \leq Z \leq 14$, a formulation is consider printable and can be translated to an inkjet printer[155,189–191]. It is paramount to consider the dimensionless number described in this section when formulating inkjet inks.

2.8. Summary

In this literature review, the material design characteristics and manufacturing processes have been described, focusing on surface passivation techniques. Literature has shown that PEG has proven to be a material that has very low rate of cell adhesion. These use of these chemicals reduce the adsorption of proteins to which cell attach such as collagen and fibronectin from the culture media, the cell patterning is then achieved by the use of surfaces composed of cell-repellent and cell-adhesive regions. For this reason a cell repellent coating will be produced for this project that can withstand these conditions and will allow the cells to differentiate in the desired specific areas.

Stem cell control and differentiation through surface modification has also been reviewed. The results reviewed in the literature show the potential of using inkjet printing technology for the modification of glass substrates surfaces in terms of topography and chemical composition.

Many biomedical devices such as screening arrays, drug delivery systems, biosensors, and scaffolds for tissue engineering have been recently developed for the study and manipulation of biomolecules, and they have proven to be valuable experimental tools for solving many biologically based problems. Screening array technologies in particular have become a tool for large-scale and high-throughput biological experiments, as it enables fast, easy, and parallel detection of a variety of addressable elements in a single experiment under identical conditions.

The inkjet printing process is reviewed and described as the selected manufacturing technique for the fabrication of cell screening arrays to be produced by using a PEG-

based cell repellent coating and a set of 'cell active' inks that allow the surface topography and chemistry modification.

Chapter 3

Experimental methods

In this study, a multi-technique experimental approach has been adopted to provide a range of information on the rheology and printability of the inks and the cell response to the printed cell screening arrays.

3.1. Cleaning of glass cover slips

The printing experiments for the development of the cell repellent and silane based formulations; and the manufacturing of the cell screening arrays were carried out on glass cover slips.

Glass cover slips needed to be cleaned to remove any organic materials/residues and to introduce –OH groups to the surface. The glass cover slips were cleaned as follows:

The glass cover slips were rinsed with ultra-pure water three times and then sonicated in the ultra-pure water bath for five minutes. The ultra-pure water was replaced and the cover slips were rinsed a further three times before sonicating them in acetone for

20 minutes. The cover slips were then rinsed with ultra-pure water three times to remove the acetone. The cover slips were submerged in a 3:1 piranha solution, three parts of sulphuric acid (Sigma-Aldrich) to one part of hydrogen peroxide solution (Sigma-Aldrich), for 60 minutes. The glass cover slips were removed from the piranha solution and then rinsed a further three times with ultra-pure water. The piranha cleaned glass cover slips were then rinsed three times using isopropanol and dried under nitrogen at room temperature.

3.2. Surface treatments and ink formulations

3.2.1. Amino-silanisation of the piranha cleaned glass cover-slips

To introduce the amine groups on to the surfaces, glass slides were submerged in methanol while preparing the amino-silanization solution, 100ml of methanol, five millilitres of acetic acid and three millilitres of (3-Aminopropyl)triethoxysilane (APTES, Sigma-Aldrich)) were mixed. The samples were incubated for 20 to 30 minutes in the amino-silanization solution. The glass slides were rinsed four times with methanol and three times with isopropanol. The amino-silanised glass cover slips were then dried with nitrogen at room temperature.

3.2.2. Ozone plasma treatment of glass cover slips

Ozone plasma treatment on glass has proved to leave –OH groups on the surface of the glass, making the substrate more hydrophilic and allowing it to bind to chemicals such as silane. As such glass cover slips were plasma treated using an EMITECH K1050X plasma machine. The glass cover slips were treated with oxygen @100 watts for 2.5 minutes.

3.2.3. Water-based PEG formulation

A solution of 10% Polyethylene glycol (PEG) was prepared with pure water.10 g of PEG MW: 18,500 (Sigma-Aldrich) were dissolved in 100 ml of pure water. After the PEG flakes dissolved the glass cover slips were submerged in tubes with the 10% PEG solution and left submerged for five mins. The solution was then removed from the tubes and the samples were washed with pure water four times to remove any excess PEG solution and were left to dry in the ambient.

3.2.4. Silane-based PEG formulation

2 ml of 90% [Methoxy(polyethylenoxy)propyl] trimethoxysilane (Sigma-Aldrich, UK), were diluted in a solution of 95ml 2-propanol and 5 ml of acetic acid.

The solution was mixed and then the glass cover slips were submerged in a 2% PEG-silane solution for two hours. The 2% PEG-silane solution was removed from the tubes and the samples were washed four times with isopropanol and four times with methanol.

3.2.5. Ultraviolet light curing PEG-DA formulation

Three PEGs with different molecular numbers (PEG-DA 250, PEG-DA 400 and PEG-DA 700, Sigma Aldrich) were used. These PEGs were in liquid form and then mixed with a photo-initiator powder [2,2 Dimethoxy-2-phenylacetophenon, 99% (DMPA), Sigma Aldrich] to allow the formation of a thin layer coating when cured under UV light. 10 mg of the DMPA, which acts as a photo-initiator, was dissolved in 1 ml of the corresponding PEG-DA (1% w/v of photo initiator to PEG-DA). Different percentages of photo-initiator to PEG-DA were explored and prepared for this research, varying from 1% to 9% w/v of photo-initiator to PEG-DA.

3.2.6. Ultraviolet light curing PEG-DA + TMSP-MA formulation

A solution of 10% of 3-(Trimethoxysilyl)propyl methacrylate 98% (TMSP-MA, Sigma Aldrich) in PEG-DA 250 was prepared by dissolving 100µL of TMSP-MA in 1mL of PEG-DA 250. Additionally 150mg of the photo-initiator (DMPA) were dissolved in the PEG-DA + TMSP-MA solution.

3.2.7. Amino-silane formulations

Amino-silane inks were prepared by mixing APTES [(3-Aminopropyl)triethoxysilane, 99%, Sigma-Aldrich] in isopropanol at different v/v ratios. Throughout this research, silane formulations are referred to as 1%, 3%, 5%, 7% and 9% APTES inks depending on the percentage of APTES present on the isopropanol solution.

3.3. Deposition techniques

3.3.1. Inkjet printing MicroFab4

Inkjet printing is an additive manufacturing technique where droplets of small volumes of ink are deposited onto a substrate. It is a non-contact deposition technique that has become a powerful tool to functionalise surfaces.

For this project, a MicroFab JetLab 4 piezoelectric printer (Figure 8) fitted with an 80um nozzle was used. The MicroFab JetLab 4 printer uses a drop-on-demand process. A single droplet of ink will be jetted only when required at a specific location, reducing the waste of materials. Since the inkjet printer used for the project is a piezoelectric printer a wave-form must be defined for each ink formulation in order to produce individual droplets when required.

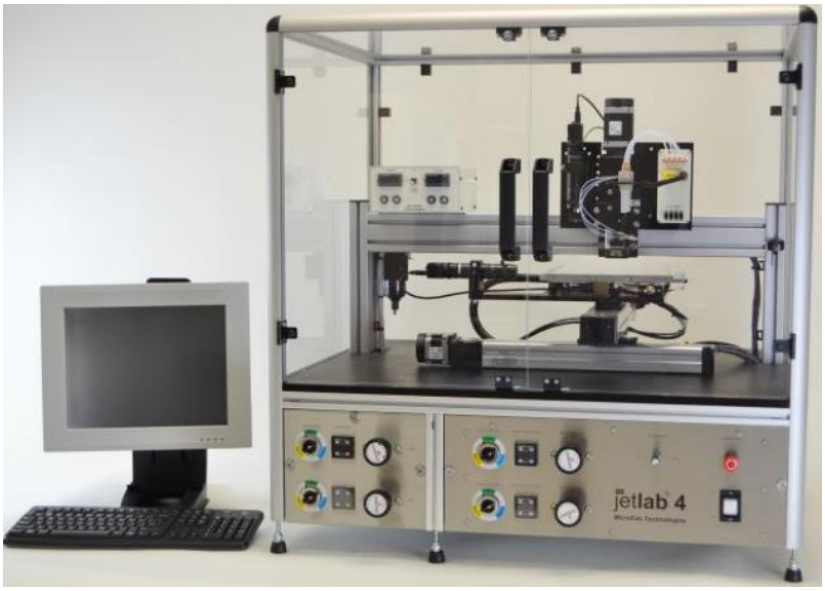

Figure 8 MicroFab JetLab 4 inkjet printer used of the printing experiments presented in this thesis.

The wave-form controls when and how much voltage is applied to the piezoelectric component in the printer head. The piezoelectric component flexes depending on the voltage applied, generating a change of pressure in the ink chamber. This pressure differential pushes the liquid out of the nozzle and when optimal it jets a single drop of ink.

Each ink formulation requires a different wave form based on the composition of the ink and its rheological properties. Different inks will have specific rheological properties such as viscosity and density, therefore the energy required for the piezoelectric component to generate an optimal change of pressure in the ink chamber to break the fluid into individual droplets is different. Wave forms used in this study are shown in Table 1.

3.3.2. Spin coating

Spin coating is a process used to manufacture thin coatings on flat surfaces. The material to be used as a coating is deposited on the centre of the desired substrate. The sample is then rotated at high speed which allows the coating material to be spread homogeneously in all directions by centrifuge force.

Different thicknesses can be achieved at various rotation speeds. The higher the speed, the less thick the coating will be.

400µl of the PEG-DA solution were placed on the sample covering the whole surface. The glass cover slip was placed in the spin coating machine making sure that the vacuum is on. The sample was coated using a Laurell Model WS-400B-6NPP/LITE spin coating machine @1000rpm for one minute. Once the spin coating cycle was over the coated samples were placed under UV light for 2 minutes to cure.

Table 1 Wave forms used for inkjet printing of ink formulations

Ink formulation	Rise Time	Dwell Time	Fall Time	Echo Time	Rise Time	Dwell Voltage	Echo Voltage
PEG-DA UV curable ink formulation	20 µs	20 µs	20 µs	40 µs	20 µs	50 V	-50 V
PEG-DA + TMSP-MA UV curable ink formulation	30 µs	20 µs	30 µs	40 µs	30 µs	65 V	-65 V
1% APTES in isopropanol ink formulation	10 µs	10 µs	10 µs	20 µs	10 µs	25 V	-25 V
3% APTES in isopropanol ink formulation	10 µs	10 µs	10 µs	20 µs	10 µs	25 V	-25 V
5% APTES in isopropanol ink formulation	10 µs	10 µs	10 µs	20 µs	10 µs	25 V	-25 V
7% APTES in isopropanol ink formulation	10 µs	10 µs	10 µs	20 µs	10 µs	30 V	-30 V
9% APTES in isopropanol ink formulation	10 µs	10 µs	10 µs	20 µs	10 µs	30 V	-30 V

3.4. Analytical techniques

3.4.1. Surface tension measurements

Surface tension is defined by the cohesive forces among the molecules of a liquid in contact with a gas. The intermolecular force at the surface of the liquid is greater, due to its interaction with the gas molecules, than the intramolecular force within the liquid and creates a 'net effect' at the surface of the liquid, acting as it if was covered with an elastic membrane.

Surface tension is an important property to be considered when working with inkjet printing since it impacts the behaviour of the inks when deposited on the substrate, but it also allows a better understanding of the printability of a formulation and the ease to produce individual droplets when jetted through a nozzle.

The surface tension of all ink formulations was measured using a Kruss DSA100 Tensiometer. At least three measurements were carried per formulation and the presented surface tensions presented in this work are an average of each set of measurements.

3.4.2. Viscosity measurements

The viscosity of a fluid can be described as the resistance to flow or to gradually deform. Viscosity is an important factor to consider when developing ink formulations

since it affects both the jettability of a solution and its behaviour when deposited on a substrate.

When the viscosity of a fluid changes when exposed to different shear forces it is considered a non-Newtonian fluid; if the viscosity remains constant it is considered Newtonian.

The PEG-DA UV curable formulations developed for this research had the potential of being non-Newtonian fluids due to the inclusion of the photo-initiator, for this reason the viscosity measurements were carried out using an Anton Parr MCR302 controlled stress rheometer at 20 °C

For the silane formulations the viscosity was measured using a RheoSense microVISC TC viscometer, Figure 9 shows the operation schematic of the viscometer. The silane formulations are isopropanol based, which evaporates at low temperatures and high rates, the microVISC TC viscometer carries out its measurements in a controlled micro-chamber where evaporation of the solvents is not an issue.

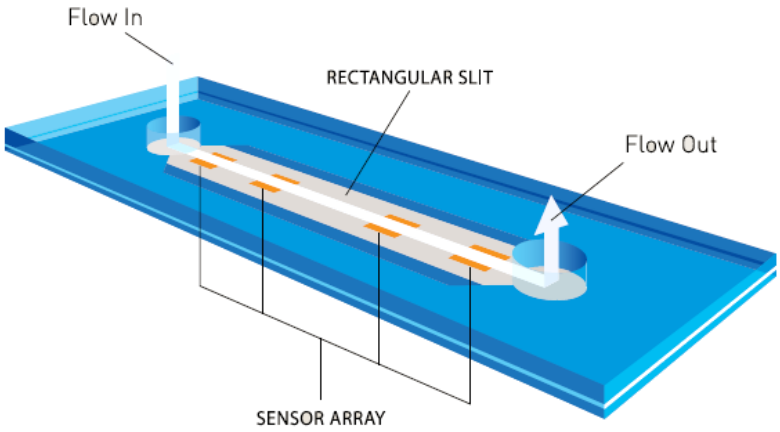

Figure 9 Schematic showing the operating set-up of a microVISC TC viscometer.

At least three measurements were carried out per formulation and the presented viscosity values are an average of each set of measurements.

3.4.3. Density measurements

The density of a substance is measured as the mass of said substance per unit of volume. Density of a fluid, in this case an ink formulation, can have a defining effect on the printability of the ink.

Density measurements were carried on all the developed ink formulations by weighting 1ml of the formulation on a Fisherbrand PS-60 analytical balance. At least three measurements were carried out per formulation and the presented density values are an average of each set of measurements.

3.4.4. Contact angle measurements

When a system between a solid, a drop of liquid and a gas is in equilibrium the contact angle between the liquid-vapour interfaces to the solid substrate can be measured.

The contact angle determines the wettability of a substrate by a liquid, and is dependant of the surface tension of the liquid, therefore is an important property to know when working with inkjet printing in order to better understand the interaction of the jetted ink when deposited on the desired substrate. Contact angles of the

different formulations used for inkjet printing were Attension ThetaLite optical tensiometer (Biolin Scientific, Västra Frölunda, Sweden). The sessile drop method was used and contact angles were taken at 17 frames per second for 10 s. Data was collected using OneAttension software (Biolin Scientific, Västra Frölunda, Sweden). At least three measurements were carried per formulation and the presented contact angles are an average of each set of measurements.

3.4.5. Digital single-lens reflex imaging

Digital single-lens reflex (DSLR) cameras combine the optics of a single-lens reflex camera with a digital imaging sensor instead of a photographic film. Lenses can be changed onto DSLR cameras depending on the type of photograph needed.

A Canon70D DSLR camera was used with a Canon Macro EF 100mm lens to take the photographs of printed samples. The camera was mounted on a gage that ensured the samples were always going to be at a 180mm distance from the lens which proved to be ideal to image the printed samples.

3.4.6. Optical microscopy

Optical microscopy is a technique used to view the magnification of a sample through the use of a lens with visible light. Optical microscopy allowed checking cells when in culture.

A ZEISS Axio Vert A.1 microscope was used to capture micrographs of cells in culture and of cells seeded onto samples. All optical microscopy micrographs were obtained using this microscope in transmission mode and a lens of x10 magnification was used unless otherwise specified.

3.4.7. Fluorescent microscopy

Fluorescent microscopy has the same functioning principles as optical microscopy with the difference that it not only uses transmitted light, but different lights of specific wavelengths can be used to excite fluorescent markers previously added to the samples to analyse. These fluorescent markers are excited by the specific wavelengths of light selected and allow the imaging of specific areas of interest in biological samples such as stress fibres in the cells.

A ZEISS Apotome.2 microscope was used to capture micrographs of cells seeded on printed samples and stained with fluorescent markers. All fluorescent microscopy micrographs were obtained using this microscope with a lens of x10 magnification used unless otherwise specified.

3.4.8. Atomic Force Microscopy (AFM)

Atomic force microscopy is a high-resolution type of scanning probe microscopy using a probe fitted in a piezoelectric element that registers the change in energy on the tip of the probe when in contact with the surface of a sample. The tip is at the end of a

cantilever that is placed parallel to the sample surface. The tip, which is typically made of silicon or silicon nitride, is brought into contact with the surface, which leads to an interaction force between the tip and the surface. As this force varies, deflections are produced in the cantilever. Before the operation, a laser spot is positioned on top of the cantilever at an angle allowing it to be reflected into the photodetector. The deflections of the cantilever are measured by these reflections into the photodiode, to produce a three-dimensional topographical image at the micro-/nanoscale allowing a resolution in the order of a fraction of nanometres.

There are three modes of operation for AFM: tapping, contact and non-contact. In this research, the tapping mode was used. In this mode the tip oscillates over the surface, and only touches it for a very small amount of time, reducing the issue of lateral force damage and drag across the surface. The topography is imaged by adding the short-range repulsive and long-range attractive forces together to get an average force response curve.

AFM was used to observe and analyse the surface topography of printed samples. A Burker Multimode 8 system was used. Figure 10 shows the operation schematic of the AFM system used for sample analysis. Samples were imaged in air using a silicon RTESPA-150A tip operating at a scan rate of 0.9Hz. The scan images were flattened with a third order correction to enhance the image. Scans of 5µm x 5µm were taken and the roughness of the surface (both Ra and Rq) was measured using NanoScope Analysis 1.7 software, where Ra is the arithmetic average of the absolute values of the peaks and valleys over the whole length of the sample. Rq is the root mean square average of the profile height deviations from the mean over the whole length of the sample. Data was determined from at least three replicates of each sample type.

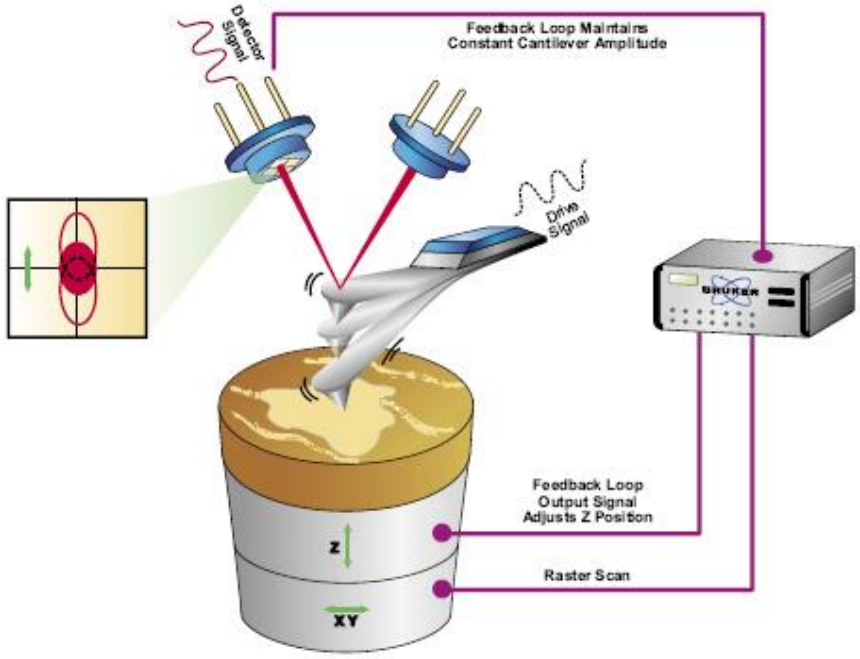

Figure 10 Schematic of the Burker Multimode 8 system used for AFM measurements of samples.

3.4.9. Fourier-Transform Infrared spectroscopy (FTIR)

Fourier transform infrared spectroscopy is a method that presents a spectrum of the absorption of light at different wavelengths. Depending on the composition of the sample analysed the molecules present on the sample vibrate to specific wavelengths allowing the identification or characterisation of a samples composition. The vibration of specific molecules is represented by peaks present in a spectrum. By identifying the peaks appearing in a spectrum it can be defined the chemical composition of a sample, making FTIR a powerful technique for surface characterisation.

The infrared (IR) region of the light spectrum is split into three sub-regions and ranges in wavelength from approximately 0.78 – 1000 µm, however, wavelengths between 2.5 – 15 µm are most useful for IR spectroscopy.

Higher energy radiation types such as x-ray, ultraviolet and near-infrared deal with electronic transitions, whilst the lower energy of IR radiation is only concerned with rotational and vibrational energy transitions. An absolute necessity in IR active compounds is that the molecules exert net change in the dipole moment as they vibrate or rotate. This arises when the elemental components are different in electronegativity making the charge unevenly dispersed. When such molecules vibrate and rotate the fluctuation in dipole moment is observed. The electrical field of the IR radiation interacts with these fluctuations. When the frequency of the radiation and vibrational frequency of the molecule match, the radiation can be absorbed, which leads to a change in the amplitude of molecular vibration.

In these studies FTIR spectra were obtained at room temperature in the spectral range between 3200 cm-1 and 1400 cm-1, using a PerkinElmer Frontier FTIR Spectrometer (Perkin Elmer, UK). The spectra were obtained with 64 scans at a resolution of 4 cm-1 and data was collected using PerkinElmer Spectrum v10.4 software.

3.5. Cell testing

3.5.1. Cell culturing of fibroblasts (L929)

Cells were cultured in a humidified 37°C/5% CO2/95% air (v/v) environment in Dulbecco's modified Eagle's medium (DMEM; Sigma-Aldrich) containing 10% (v/v) Fetal Bovine Serum (FBS, Sigma-Aldrich) and 1% (v/v) penicillin/streptomycin (Sigma-Aldrich),

3.5.2. Cell culturing of human mesenchymal stem cells (hMSC)

Cells were cultured in a humidified 37°C/5% CO2/95% air (v/v) environment in Dulbecco's modified Eagle's medium (DMEM; Sigma-Aldrich) containing 10% (v/v) Fetal Bovine Serum (FBS, Sigma-Aldrich) and 1% (v/v) penicillin/streptomycin (Sigma-Aldrich),

3.5.3. Cell counting and cell seeding

The media in which cells were grown was removed from the flask. The surface were the cells grow was washed with phosphate buffered silane (PBS, Sigma-Aldrich). Once the PBS was removed the relevant amount of trypsin (Sigma-Aldrich) solution for the

flask volume was added (the trypsin solution was prepared by dissolving 2 ml of trypsin in 18ml of PBS).

Cells were incubated for 5 mins with the trypsin solution. Once the cells detached from the flask surface, media was added in the same volume as the trypsin (i.e. 5ml of trypsin added, add 5ml of media). The cell suspension was then homogenised and transferred to conical tubes for centrifuge. The solution was centrifuged at 1500rpm for 5 minutes. Excess media was removed from the conical tube leaving only the cell pellet in the tube and 5 ml of new media was added, and the concentration of cells was investigated.

For counting the cells the haemocytometer was cleaned with 70% ethanol, then 200µL of the homogenised cell suspension was pipetted in the haemocytometer. The cells were counted in the five areas of the haemocytometer shown in Figure 11. The average of counted cells in the five different areas corresponds to the amount of cells $x10^3$ that are present in 100µL of the suspension.

After the cell count, the cell concentration was adjusted to the desired cell density per 100µL by adding the corresponding volume of cell culture media to dilute the cell suspension.

The PEGylated samples were washed with PBS. Once the PBS was removed 100µl of the cell suspension were pipetted on the passivated surface. After being incubated for 1 hr, the samples were covered in media and incubated overnight.

After this protocol was completed, the samples were checked in the microscope to review if there cells were attached to the surface.

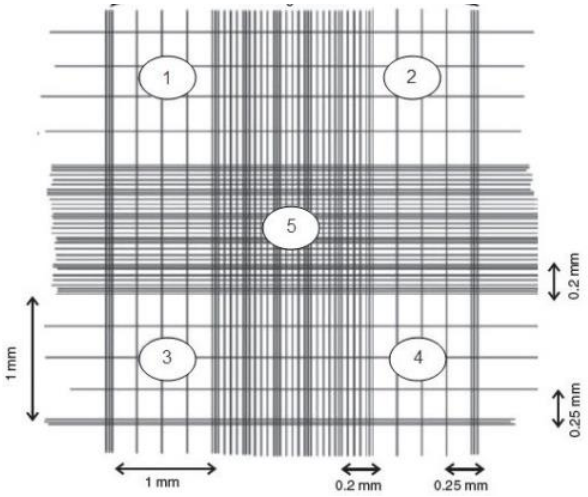

Figure 11 Cell counting areas in the haemocytometer

3.5.4. Cell fixing

Media was removed from the well plates or petri dishes and the samples were washed with PBS. Once the PBS was removed, the cells were fixed using a fixing agent (4% formaldehyde + 2% sucrose + 94% water). The samples were left covered with the fixing agent for 20 minutes. The excess of fixing agent was then removed and the samples were stored in PBS.

3.5.5. Cell staining/dying

For staining the cells for fluorescent microscopy 10ml of PBS were mixed with 100µl of Triton X-100. The samples were covered with this solution and refrigerated for 5 minutes.

The Oregon Green dye was prepared by mixing 975µl of PBS with 25µl of Oregon Green dye.

The Triton X-100 solution was removed from the samples and they were washed with PBS to remove the Triton X-100 solution, 100µl of the dye solution were pipetted onto the surface with the fixed cells on the samples. The samples were covered from light and refrigerated for 30min. The dye was removed from the samples and the samples were stored in refrigeration.

After this protocol was completed the samples were analysed using fluorescence microscopy.

Chapter 4

Surface Passivation

Overview

The development of a surface passivating coating suitable for inkjet printing and the optimisation of its printing process is investigated in this chapter. Four different approaches for manufacturing PEG-based coatings are assessed in terms of cell repellent capabilities. The translation of the surface passivating coating developed into an inkjet printable ink formulation is analysed in terms of rheological properties. The resulting printed coatings are assessed on the capability of containing cell populations to specific areas.

4.1. Background and rationale

An effective way of creating microarrays is by patterning protein or cell-repellent chemicals such as polyethylene-glycol (PEG) and its derivatives. PEG has proven to be a material that has a low rate of protein and cell adhesion[29,46,47,77–79]. The use of these chemicals reduces the adsorption of proteins to which cells attach to, such as collagen and fibronectin from the culture media. Cell screening arrays can be achieved by the use of surfaces composed of cell-repellent and cell-adhesive regions. One of the major problems with using conventional protein/cell-repellent chemicals is that the produced cell patterns are temporary as they can degrade within days because of increased desorption from the surfaces and gradual adsorption of cell-adhesive proteins[80,81]. Therefore a cell repellent coating will be produced for this project that can withstand cell culture conditions.

The following sections present the results of a series of experiments carried out to investigate the use of PEG based formulations as cell repellent coatings. Printing trials and the subsequent analysis of cell viability on the printed PEG surfaces are presented and discussed.

4.2. Optimisation of PEG formulations for surface passivation

In order to produce cell screening arrays, it is paramount to contain cell populations in a defined area for their analysis. Cell populations have to be surrounded by an area

where cells cannot adhere or proliferate. Optimised PEG has proven to resist cell adhesion and PEG based formulations such as hydrogels have been successfully inkjet printed[56,192]. For these reasons PEG has been selected as the base for the ink formulations to explore in order to produce printed cell repellent surfaces.

The experiments presented in this section explore three different PEG based ink formulations deposited on glass cover slips, in order to analyse cell adhesion and viability when seeded on PEG treated substrates. All glass cover slips were cleaned using a piranha solution process (described in the experimental chapter), before being exposed to the different PEG based treatments.

4.2.1. Physical binding of PEG to glass substrates

The deposition of a PEG water based solution was explored due to the nature of its simple fabrication (dissolving PEG flakes in water). The glass cover slips were dip coated in a 10% PEG (w/v) in water solution prepared as described in the experimental chapter. The decision to dip coat the samples was made in order to prove the cell repellence capabilities of this potential surface passivation method before translating it to inkjet printing. The idea of physically binding the PEG to the substrate, is to have the PEG chains covering the surface of the glass slides, blocking the interaction of the cells with the glass cover slips and stopping cell adhesion.

Figure 12 illustrates the PEG deposition process and the PEG to glass cover slip interaction.

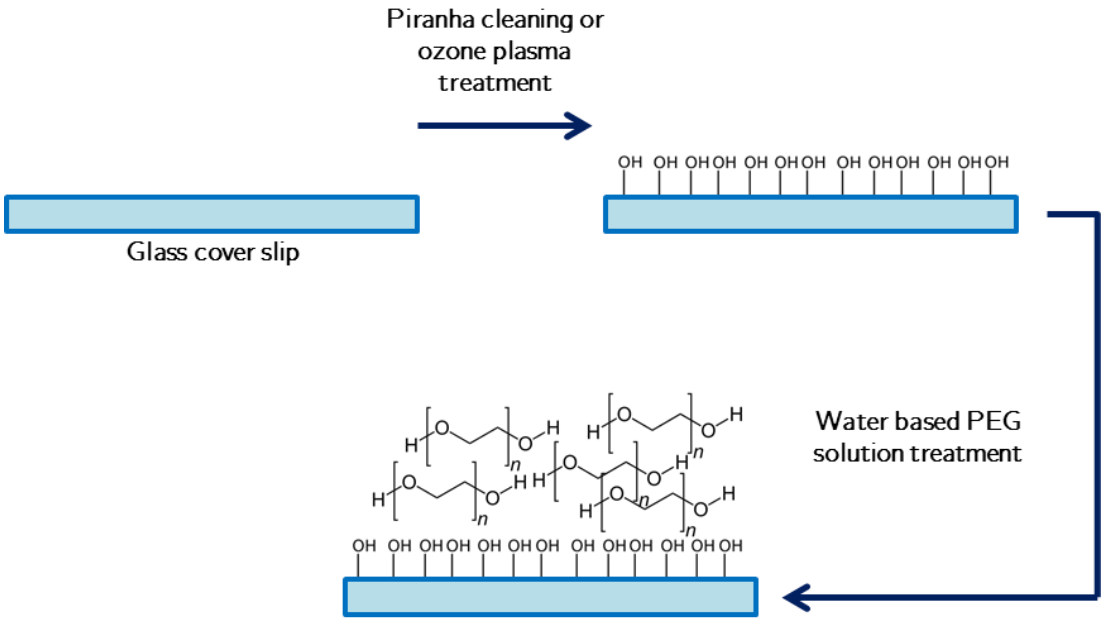

Figure 12 Water based PEG solution interaction with a piranha etched glass cover slip

As can be seen from Figure 12 the PEG molecules are only deposited on top of the substrate, covering the surface of the glass cover slips. In order to assess the efficiency of this cell repellent coating, 10,000 L929 fibroblasts were seeded and cultured on top of the PEG treated surfaces for 5 days, following the cell seeding and cell culture protocols described in the experimental chapter.

Figure 13 shows that cells adhered and proliferated over a period of 5 days when seeded on the water-based PEG coated samples. The surface passivation potential of the double physical binding of PEG to glass substrates process was assessed by seeding 10,000 L929 fibroblast cells and culture them for 5 days.

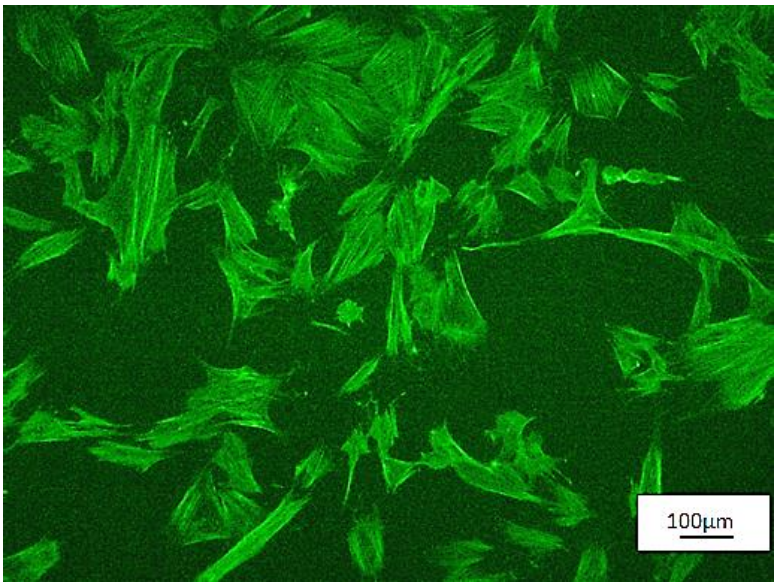

Figure 13 Cell attachment on a water based PEG coated sample seeded with 10,000 L929 fibroblasts and cultured for 5 days. Cells dyed with FITC (Oregon green fluorescent dye).

This experiment was repeated three times and all water-based PEG treated samples did not prevent cell adhesion. The fact that cells adhere and proliferate on the treated glass cover slips discards this PEG formulation as an effective cell repellent coating. The main reason for this coating failing to repel cells is the fact that the PEG molecules are lying on the substrate and are not fully bonded to the substrate. The PEG is also water soluble so when the coatings are subjected to cell culture media, the

PEG molecules are washed off the substrate. This means that an alternative treatment is required which will fully bind to the substrate.

4.2.2. Chemical binding of PEG to glass substrates

The PEG physical deposition approach demonstrated to not being suitable for the manufacturing of cell repellent coatings on glass slides. The fact that the PEG used is soluble in water proved a limitation when exposed to the cell culture environment. In order to ensure that the PEG chains remain adhered to the glass cover slips, the use of a PEG chain with a silane component was considered as a suitable alternative.

The chemical binding of a PEG molecule chain to the piranha cleaned glass cover slips was explored in order to assess its ability to inhibit cell adhesion. By using [Methoxy(polyethylenoxy)propyl] trimethoxysilane, a PEG chain can be chemically bonded to a glass substrate since it has a silane component at one end of the molecule as seen in Figure 14.

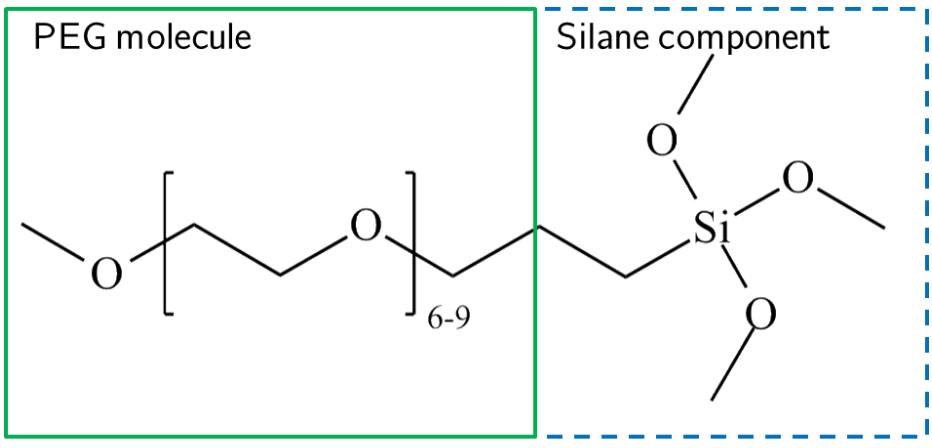

Figure 14 [Methoxy(polyethylenoxy)propyl] trimethoxysilane molecule (Gelest, UK)

A 2% solution of this PEG-silane component was prepared, as described in Chapter 3, and used as a surface passivation treatment. Studies have shown that within 2% and 3% of silanisation solutions, optimal homogeneous distribution of silane adherence to an –OH populated substrate is produced.

The glass substrates were cleaned with piranha solution prior to the PEG-silanisation process and this allows the surface to be populated with –OH groups prior to the dip coating of the samples. The decision of dip coat the samples was made in order to prove the cell repellence capabilities of this potential surface passivation method before translating it to inkjet printing. The silane component of the molecule will react with the –OH groups populating the glass substrate as shown in Figure 15, allowing a chemical bond between the PEG chain and the glass substrate.

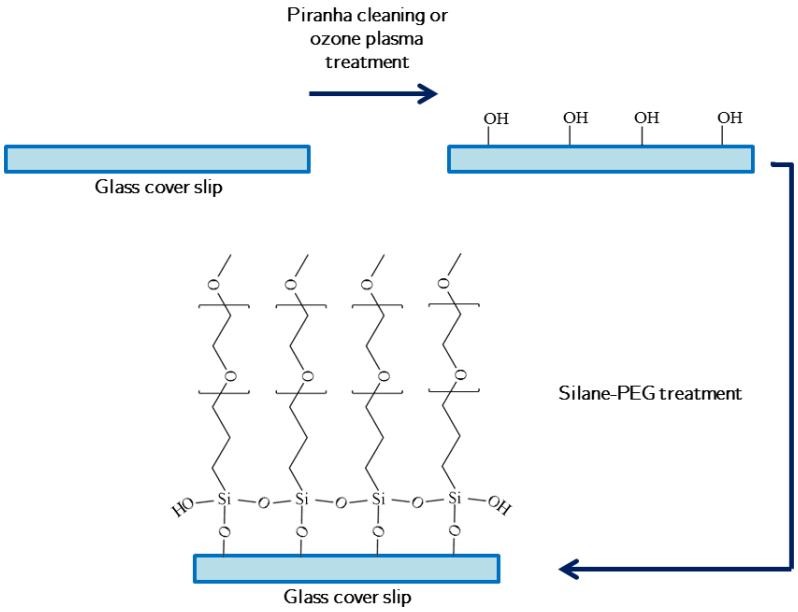

Figure 15 Silane-PEG molecules interaction with a piranha cleaned glass cover slip

The fact that the silane is now chemically attached to the –OH groups mean that the PEG chains should not be washed-off during the cell culture process.

The cell repellence was assessed for this potential surface passivation treatment by seeding 10,000 L929 fibroblast cells onto the silane-PEG treated surfaces and cultured for 5 days. Samples were then dyed using Oregon Green FITC fluorescent dye. However as can be seen from Figure 16 cells adhered and proliferated over a period of 5 days when seeded on the silane-PEG treated samples. The experiment was repeated a further three times but cells adhered and proliferated each time.

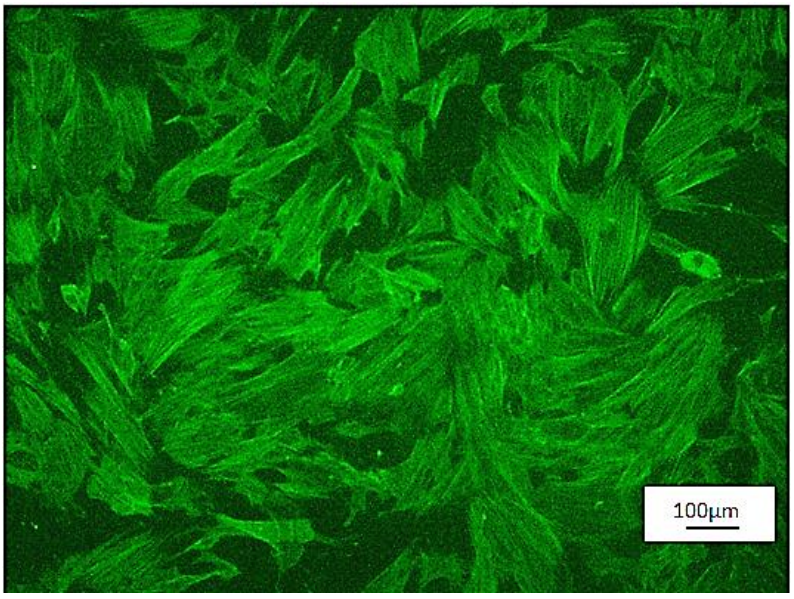

Figure 16 Cell attachment on a silane-PEG treated sample seeded with 10,000 L929 fibroblasts and cultured for 5 days. Cells dyed with FITC (Oregon green fluorescent dye).

The hypothesis is that the PEG coverage is not dense enough to block all cell interaction with the surface. The silane component of the formulation are reacting and attaching within each other as seen in Figure 15 but there is no binding between the PEG chains. The breaks between PEG coverage allows the cells to interact with the chemically modified glass coverslip instead of forcing the cell interaction to only the

PEG chain in the molecule. The fact that cells adhere and proliferate on the treated glass cover slips, discards this PEG formulation as an effective cell repellent coating. In order to increase the density of the PEG on the surface the crosslinking of PEG chains deposited on the substrates was explored as described in Section 4.2.3.

4.2.3. Ultraviolet curing PEG binding to glass substrates

The use of Ultraviolet (UV) light has previously been shown to cross link PEG-based hydrogels[57,192]. It is thought that UV may be able to cross-link the PEG-based formulations in this research and therefore improve the PEG coverage across the glass substrates. As previously discussed, it is the lack of continuous PEG coverage on the glass surfaces is allowing cells to adhere, grow and proliferate. In order to create a continuous coverage of PEG molecules, the use of a UV curing PEG based formulation is investigated in the following section. This approach is considered viable as the PEG chains should crosslink with each other when excited by a photo-initiator.

In order for the PEG to have the ability to be cross linked, a double bond that can be opened by a photo-initiator when excited, needs to be present in the PEG molecule. The inclusion of a di-acrylate 'ending' on each side of the PEG molecule is ideal for this purpose. The PEG-DA base molecular structure is shown in Figure 17. A series of PEG-DA (polyethylene glycol – di-acrylate) monomers with varying chain lengths can be commercially found in liquid form (Sigma Aldrich, UK).

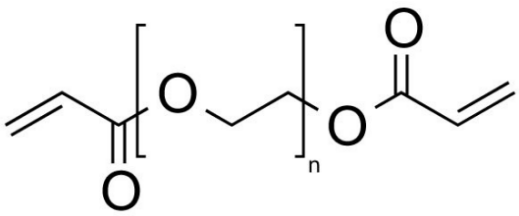

Figure 17 PEG-DA molecular structure.

Commercially available PEG-DA monomers of chain lengths 250, 400 and 700 where assessed in the following sections, as passivation treatments. The photo-initiator, DMPA (2,2 Dimetoxy-2-phenylacetophenon) was also added to enable a crosslinking reaction. This photo-iniator has previously been used to crosslink PEG molecules[29,57,182].

Figure 18 shows the crosslinking of the PEG-DA molecules when DMPA is present and exposed to UV light

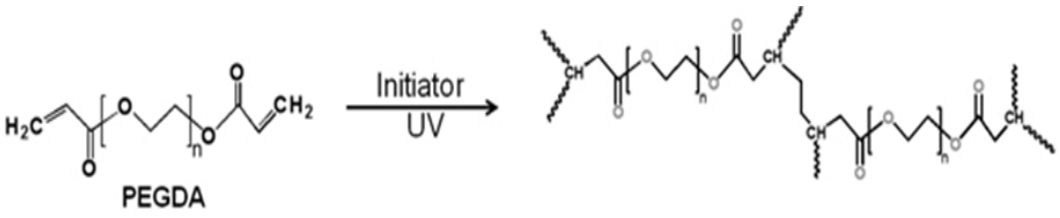

Figure 18 PEG-DA crosslinking when DMPA is present under UV light.

Prior to the PEG-DA treatment, the glass substrates have been piranha cleaned and amino-silanised as described in the experimental chapter and a schematic of this reaction is presented in Figure 19.

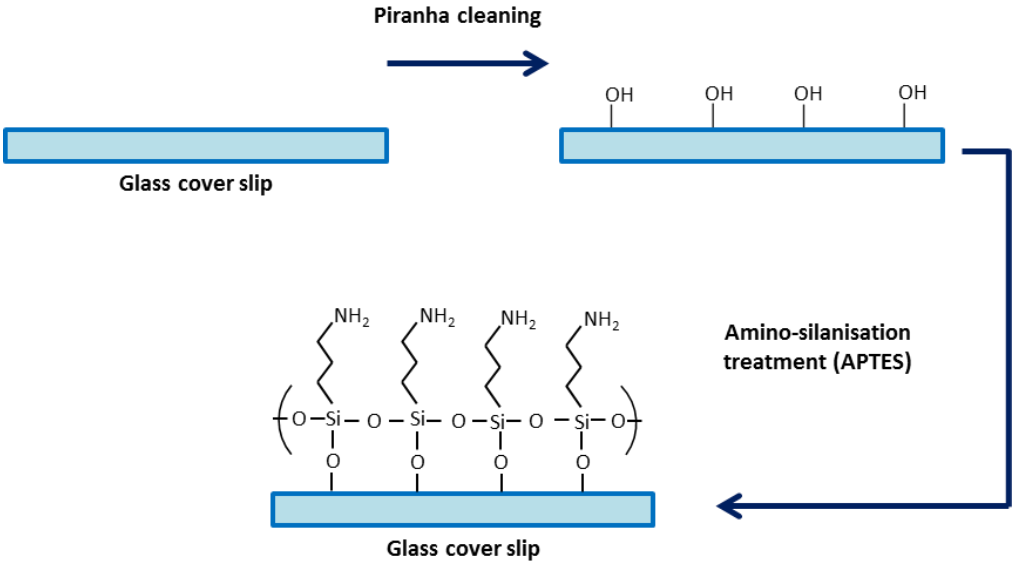

Figure 19 Amino-silanisation of a piranha cleaned glass cover slip using APTES.

The cross-linking of the PEG-DA molecules was carried out on an amino-silanised glass cover slips. The amino-silanisation enables anchorage points for the PEG vertically and then when UV cured the PEG cross-links horizontally as seen in Figure 20. Hypotetically this process ensures a continuous coverage of PEG which hasn't been achieved for the previously described PEG coatings

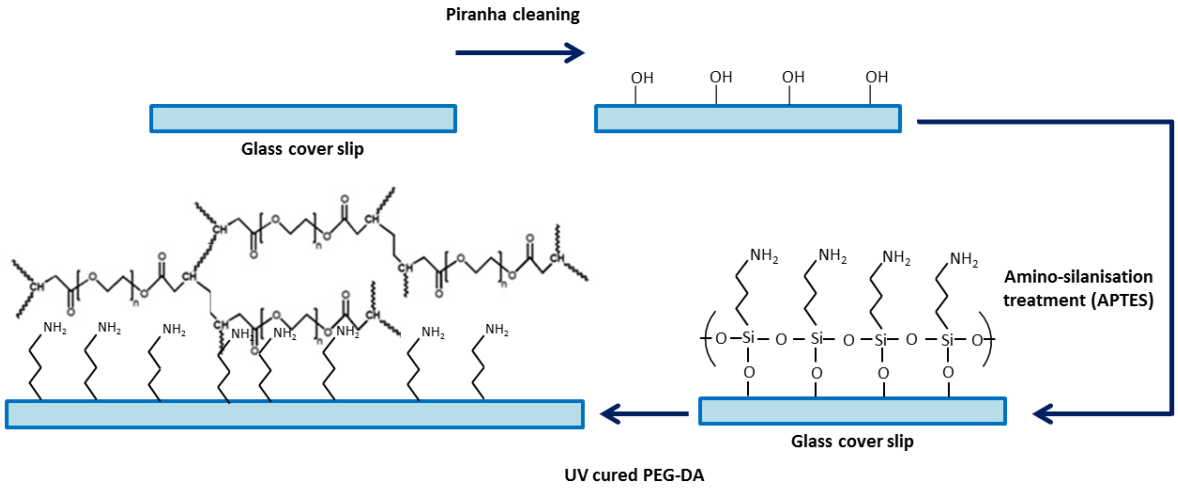

Figure 20 PED-DA UV cured formulation anchored by the amino-silanisation of the piranha cleaned glass cover slip.

The PEG-DA based UV curable formulations were initially spin coated on amino-silanised glass cover slips in order to assess their potential cell repellent capabilities and the ability to form a homogeneous coating before translating them to inkjet printing. They were then exposed to UV light (wavelength of 365nm max.) for 5 minutes in order to achieve the curing and immobilisation of the PEG-DA coating[193].

Each PEG-DA UV curable formulation was spin coated onto three glass slides each and the experiment was repeated five times. Cell repellence was assessed for this

surface passivation potential treatment by seeding 10,000 L929 fibroblast cells and cultured for 5 days. As can be seen from Figure 21 no cells adhere to the PEG-DA 250 and 400 coatings. However cells do stick to the 700 coating. The control sample shows the adhesion and proliferation of a L929 population of cells that were seeded on a non-treated glass coverslip.

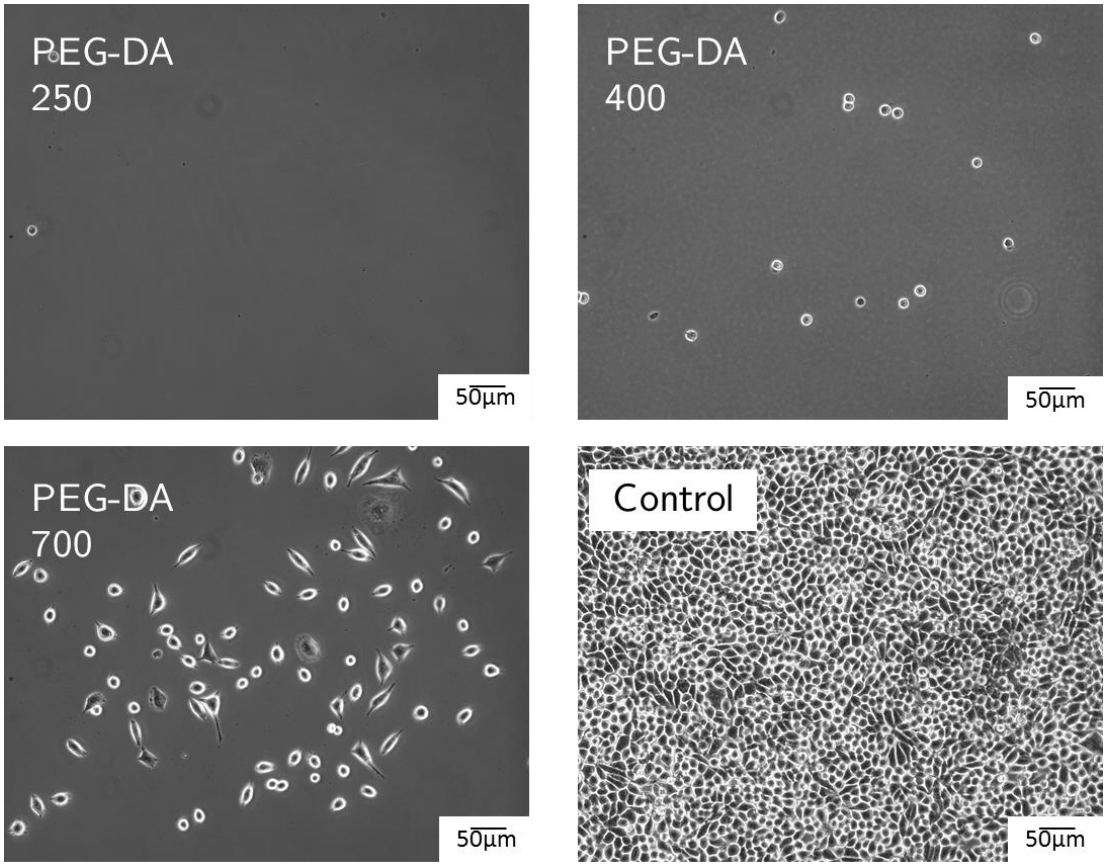

Figure 21 UV cured PEG-DA based treated surfaces and untreated glass cover slip (control) seeded with 10,000 L929 fibroblasts and cultured for 5 days.

The fact that cells did not adhere to the PEG-DA 250 and 400 UV cured samples corroborates the surface passivation capabilities of PEG. However, with cells adhering and mainting viability when seeded on the PEG-DA 700 UV cured samples poses the question of why cells can adhere (in lower densities than those adhered on the control samples) on PEG-DA UV cured samples. Literature has shown that when manufacturing PEG membranes[75] and PEG-DA monoliths[76], the molecular weight of the PEG chain plays an important role on the porosity, permeability and protein interaction.

The fabrication of PEG membranes discussed by Chakrabarty et al[75] shows an increase in porosity, pores size and, by consequence, permeability of the PEG membranes when larger molecular weights of PEG are used.

When manufacturing PEG-DA monoliths the lower the molecular weight of the PEG-DA used presents a higher density network of crosslinked monomers, which not only impacts the passivation properties of the PEG-DA but also improves mechanical stability and reproducibility of the PEG-DA structures[76].

The increase of molecular weight on PEG-DA UV cured coatings presented in this section has confirmed that the cell repellent capabilities of PEG are improved at lower molecular weights (PEG-DA 250 and 400), and it opens the possibility of having more stable coatings when the lower molecular weight is used (PEG-DA 250).

4.3. Inkjet printing of PEG-DA UV curable formulation

In order to have an inkjet printable cell repellent formulation, it is paramount that individual droplets can be jetted from the printing nozzle. Literature has shown that a dimensionless number defined as Z can predict if a formulation is printable in regards of its rheological properties and the diameter of the nozzle by which the formulation is to be jetted[153,155,188].

The rheological properties to be considered for the formulations are the viscosity, density, and surface tension as well as the diameter of the nozzle by which the ink will be jetted. These properties are used to calculate the Ohnesorge number (Oh) which is a dimensionless number that relates the viscous forces to the inertial and surface tension forces[153,155,189].

The Ohnesorge number is calculated using Equation 1 where the viscosity of the ink is represented by μ; ρ represents the density and σ the surface tension. D represents the diameter of the nozzle to be used.

Equation 1 Calculation of Ohnesorge number

$$\frac{\mu}{\sqrt{\rho\sigma D}} = Oh$$

The printability of an ink, represented by Z, is given by Equation 2, it is important to consider that for an ink to be printable the following relation needs to be met: $1 \leq Z \leq 14$[155,189–191].

Equation 2 Calculation for printability factor

$$Z = \frac{1}{Oh}$$

The use of a PEG-DA 250 based UV curable formulation has been selected for inkjet printing studies, since it meets the cell repellence characteristics needed in order to contain cell populations. The rheological properties also show that it has a printability factor of 3.6 as shown in Table 2. The other PEG-DA based UV curable formulation which showed promising cell repellent properties was the PEG-DA 400. However due to its higher viscosity it lies out of the printing range, as its Z value is 0.69 and does not comply with the $1 \leq Z \leq 14$ relation.

Table 2 Rheological properties of PEG-DA 250 and PEG-DA 400 based UV curable formulation

Formulation	Viscosity (Ns/m^2)	Density (Kg/m^3)	S. Tension (N/m)	Nozzle Dia (m)	Oh	Z
1% PEG 250	0.01685	1150	0.04018	0.00008	0.277	3.60
1% PEG 400	0.085	1200	0.03659	0.00008	1.434	0.69

The parameters presented in Table 2 are of importance when it comes to manufacturability of the screening arrays as stable inks need to be developed for a repeatable and reliable process. Viscosity is a good indicator as to whether an ink is suitable for printing. Theory shows that inks with viscosities lower than 20cPa are most likely to be printed[155].

Viscosity measurements were carried out and as can be seen from Figure 22 the viscosity for the PEG-DA 250 UV curable formulation with 1% (w/v) photo-initiator is 16.85cPa. This number plus the Z number calculated in Table 2, confirms that the developed PEG-DA 250 based formulation should be able to be printed using inkjet printing.

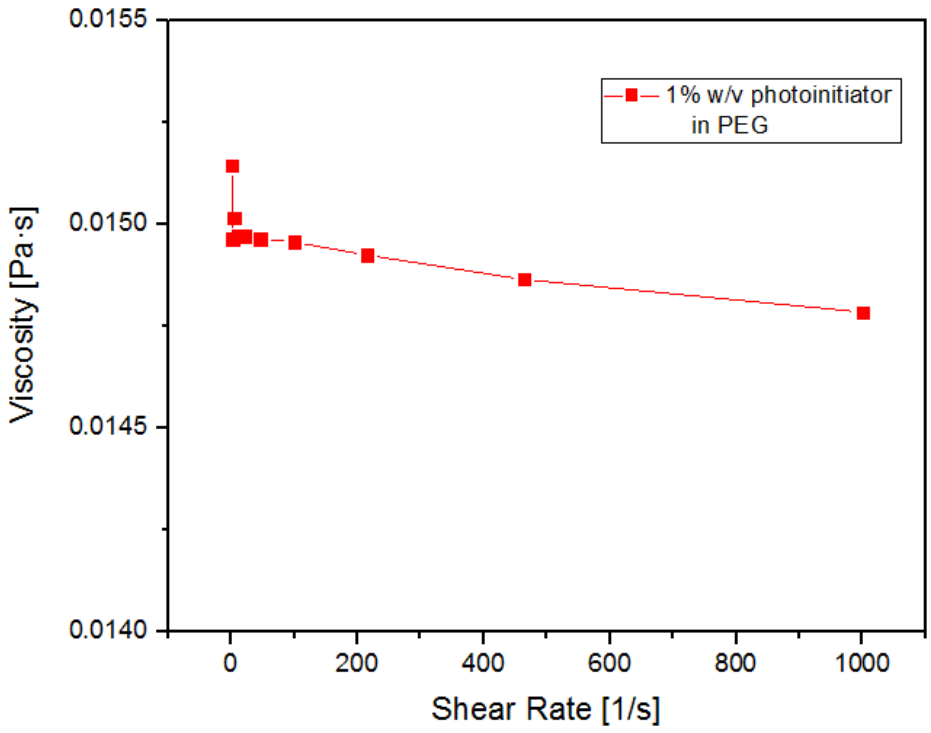

Figure 22 Viscosity of a 1% (w/v) photo-initiator in PEG-DA 250 UV curable formulation

A wave-form is required for the PEG-DA 250 based UV curable formulation to be jetted in the MicroFab JetLab4. The wave-form is given by the voltage at which the piezoelectric element of the printer head will be exposed to and a set of times, that can vary depending on the different ink formulations used (rise time, dwell time, fall time and echo time). The optimal wave-form for the PEG-DA250 UV curable formulation is shown in

Table 3 and Figure 23.

Table 3 Voltage and time values set for the production of a single droplet when printing with a 80um printer-head nozzle

Rise time	20µs
Dwell time	20µs
Fall time	20µs
Echo time	40µs
Rise time	20µs
Dwell voltage	+50 V
Echo voltage	-50 V

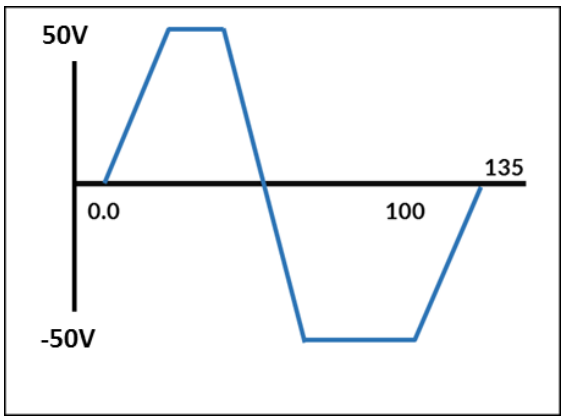

Figure 23 Wave-from for droplet production of the PEG-DA 250 based UV curable formulation through am 80um nozzle

4.3.1. Track optimization for PEG-DA 250 UV curable ink

Using the waveform produced in Section 4.5 a series of track optimisation studies for the PEG-DA 250 ink were carried out in order to achieve stable continuous tracks. A series of tracks were printed using four different step sizes (0.05, 0.10, 0.15 and 0.20 mm), the step size being the spacing between deposited droplets and by varying the print velocity (0.05-3.0 mm/s), which is the velocity at which the substrate moves in relation to the printer head. Other factors which have proven to affect print line stability is the viscosity of the ink and its interaction with the substrate[136,144].

Figure 24 shows that when comparing the tracks printed using different step sizes and different velocities, printing at lower velocities (0.05mm/s) show more consistent lines in comparison to tracks printed at higher velocities (3mm/s). In addition printed tracks with smaller step sizes produce less stable tracks.

When droplets are deposited at step sizes smaller than the drop diameter (in this case 80µm), the drops do not always merge into a stable line but instead can join into

larger beads or breaks into larger drops on the substrate, as seen in Figure 24 This phenomena has been previously seen in the literature for example by Schiaffino & Sonin (1997)[194].

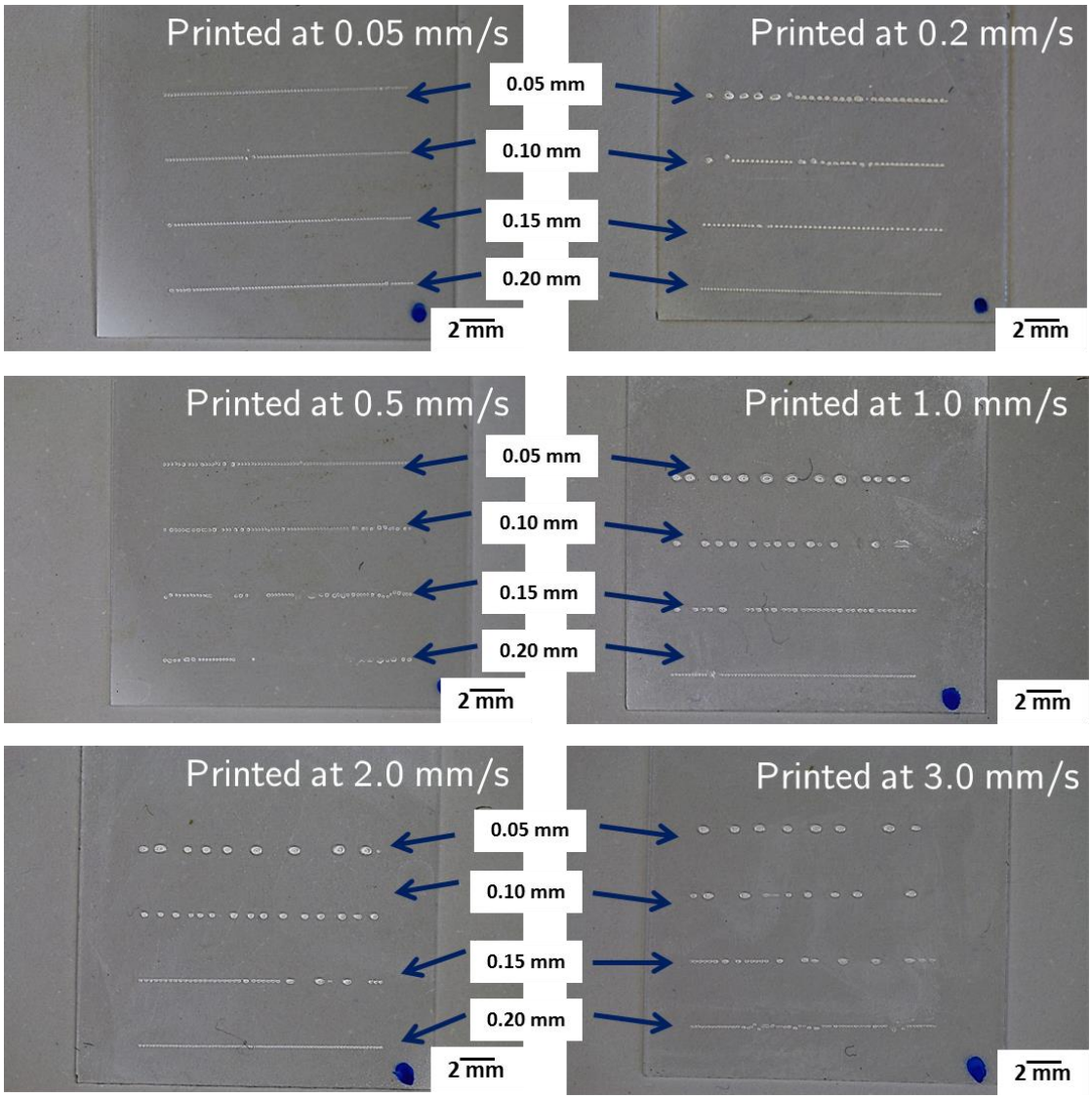

Figure 24 Tracks of the 1% photo-initiator (w/v) PEG-DA 250 based UV curable formulation printed with different step sizes and at velocities ranging from 0.05mm/s to 3.0mm/s.

In order to see if step size could be optimised further, step sizes ranging from 0.15mm to 0.25mm, in increases of 0.01mm were assessed. All tracks for this set of experiments were printed at optimum velocity of 0.2mm/s.

In Figure 25, it can be observed that the most consistent tracks are the printed with a 0.20mm step size. Tracks printed with 0.15mm and 0.25mm step sizes show that the individual droplets have merged to form large, isolated beads, while tracks printed with a 0.20mm step size show that droplets are almost touching each other, making a more consistent straight line.

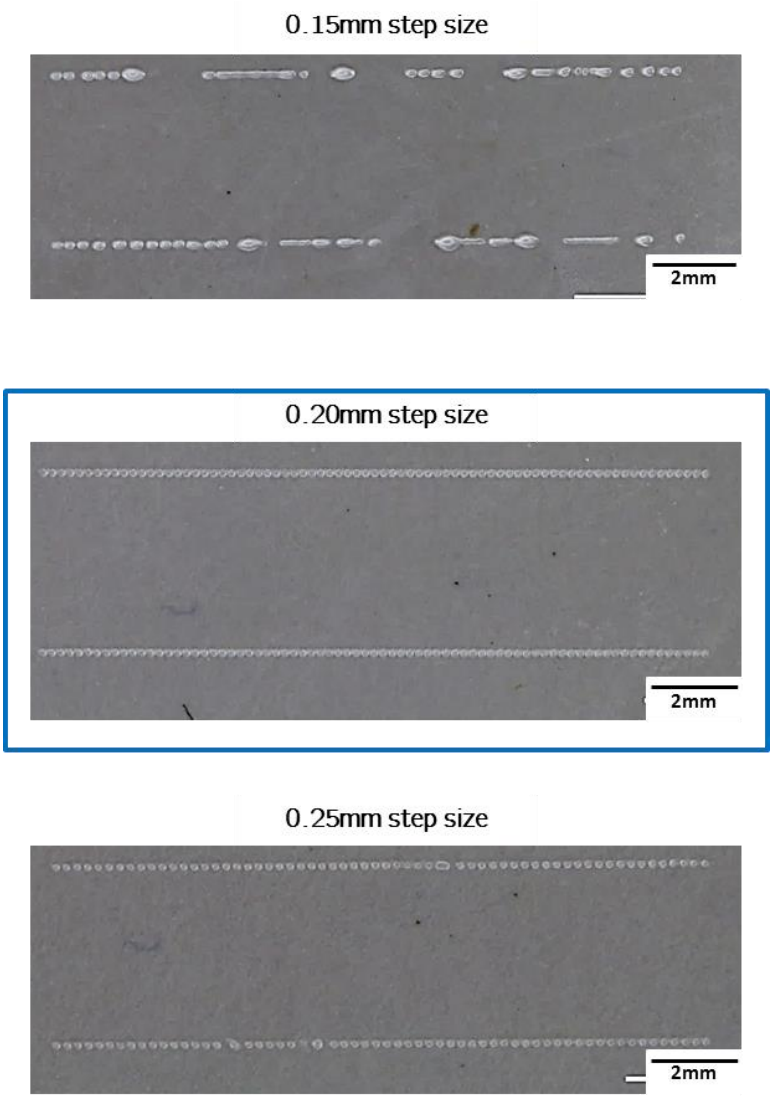

Figure 25 Tracks of the 1% photo-initiator (w/v) PEG-DA 250 based UV curable formulation printed with 0.15mm, 0.20mm and 0.25mm step sizes and at velocities of 0.2mm/s, highlighting the iteration with the most consistent tracks.

In order to manufacture the cell screening arrays for analysing stem cell differentiation, it is important to be able to contain cell populations to specific areas. The 1% photo-initiator (w/v) PEG-DA based UV curable formulation developed in Section 4.4 is used to define these areas. The PEG-DA UV curable solution has proven to be cell repellent so a pattern developed for the containment of cell populations has been developed.

The pattern consists of a squared area of the printed cell repellent formulation where a window in the middle of this square has been left clear of the cell repellent ink in order to allow the adherence and proliferation of cells as seen in Figure 26.

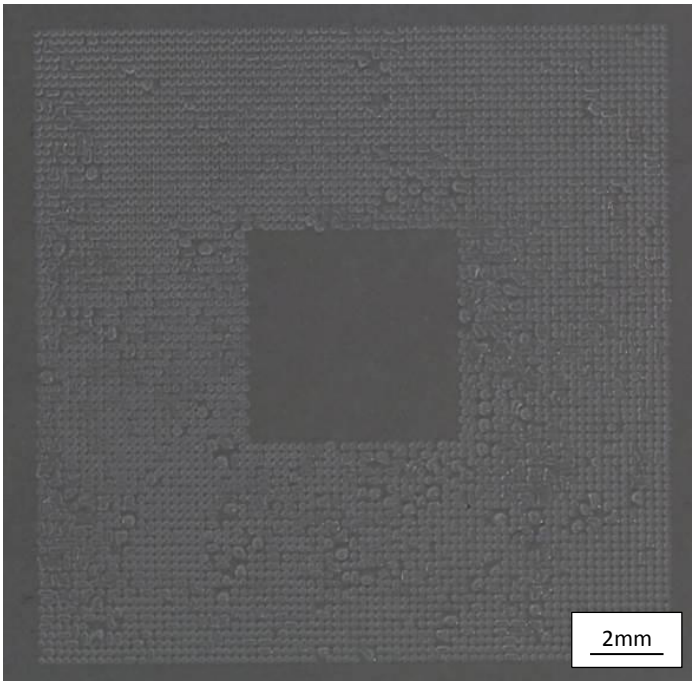

Figure 26 Printed pattern with the 1% photo-initiator (w/v) PEG-Da based UV curable ink showing a square of cell repellent coating with an untreated window to allow cell adhesion and proliferation.

The pattern presented in Figure 26 has been printed using the parameters that were defined as the optimal after the track optimisation experiments (0.20mm step size and a printing velocity of 0.2mm/s).

A clear definition of the pattern can be observed in Figure 26 where a square within the cell repellent ink has been left blank for the cells to directly interact with the glass cover slip. The printed pattern does not present a continuous coating but a series of small beads placed in the glass cover slip as expected from the previous track optimisation experiments.

Glass cover slips with the printed pattern were exposed to the sterilisation process they need to withstand and to the cell culture environment.

The sterilisation process consists of washing the glass slides with 70% ethanol three times and then rinsing them three times with phosphate buffer silane (PBS), an inert solution, to wash away the 70% ethanol from the samples.

After being sterilised with 70% ethanol, the printed samples were submerged in cell culture media and incubated in a controlled environment at 37 degrees with 5% CO2. Micrographs were taken of the printed samples before being sterilised and exposed to the cell culture environment and 24 hours after being placed in the incubator.

When the PEG-DA UV curable ink with a 1% w/v ratio of photo-initiator printed samples were exposed to the sterilisation process and 24 hours in cell culture media it can be noted that the drop size in the print reduced in approximately 28.30% as shown in Figure 27.

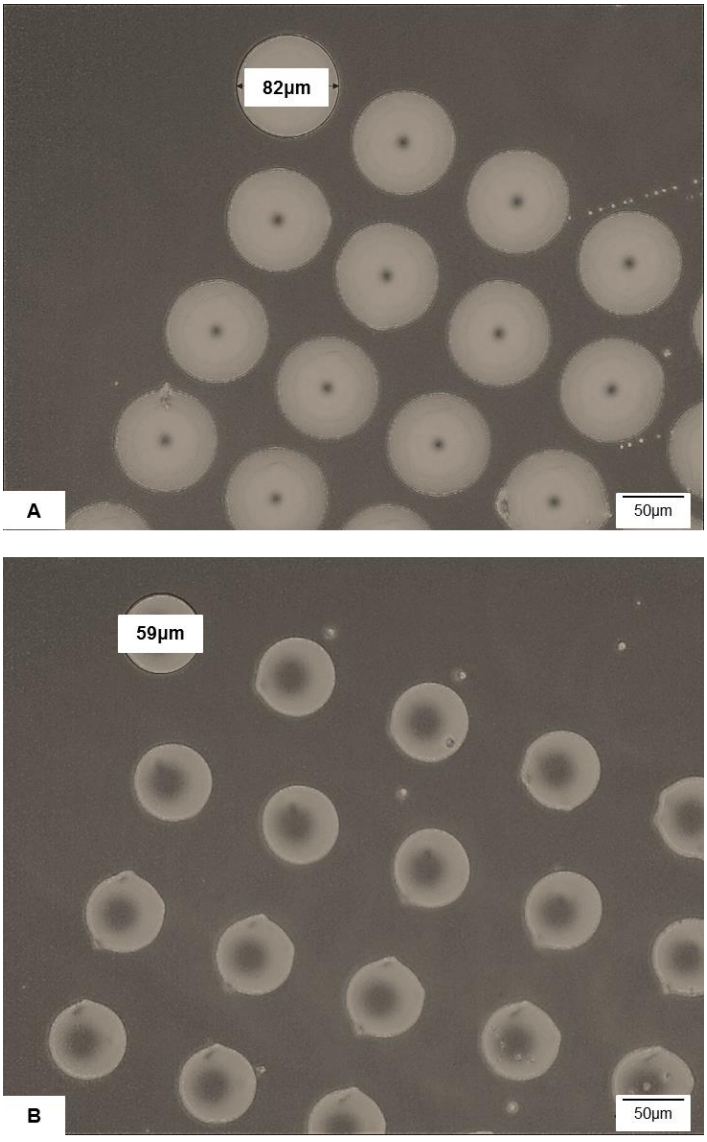

Figure 27 Micrographs showing the reduction in size of printed 1% photo-initiator (w/v) PEG-DA based UV curable ink before and after sterilisation and exposure to cell culture environment for 24 hours.

This reduction in size shows that the PEG-DA UV curable ink droplets are being washed away in the sterilisation and cell culture process due to lack of curation of the PEG-DA ink. The printed PEG-DA reduction in size is not observed in previous experiments with larger volume areas in drop tests of PEG-DA ink being cured. In order to ensure curing of the PEG-DA inks experiments increasing the percentage of photo-initiator in the ink were conducted.

In the literature it is stated that the use of LED lamps (like the one used for the experiments here presented) to cure UV curable inks can present some problems, such as inks not fully curing. The not appropriate curing to the ink using LED lamps is caused by the low energy and single wavelength emitted by the LEDs.

In order to achieve complete curing of the printed inks the percentage of photo-initiator is increased in intervals of 2% from 1% to 9% to ensure that there will be more free radicals to be excited and start the polymerisation during the curing process[180,185].

4.3.2. Increase of photo-initiator in PEG-DA inks

Inks with an increasing percentage of photo-initiator by 2% in a w/v ratio (inks with 3%, 5%, 7% and 9% w/v) were prepared and inkjet on the piranha cleaned and amino-silanised glass cover slips. Samples were then UV cured for further cell repellence experiments and to analyse bead reduction of the inkjet printed UV cured PEG-DA formulations.

With the increase in photo-initiator the rheological properties of the PEG-DA formulation are modified. The viscosity, surface tension and density are expected to change.

Table 4 shows the rheological properties of the five different formulations where the Ohnesorge number and the printability facto Z are calculated using Equation 1 and Equation 2 respectively.

Table 4 Rheological properties of the five iterations of PEG-DA UV curable formulations with different ratios of photo-initiator.

	Viscosity (Ns/m^2)	Density (Kg/m^3)	S. Tension (N/m)	Nozzle Dia. (m)	Oh	Z
1% Ph-i	0.01685	1150	0.04018	0.00008	0.277	3.60
3% Ph-i	0.01726	1157	0.04149	0.00008	0.278	3.59
5% Ph-i	0.01798	1180	0.04267	0.00008	0.283	3.52
7% Ph-i	0.01851	1220	0.06174	0.00008	0.238	4.19
9% Ph-i	0.01916	1260	0.06683	0.00008	0.233	4.28

Surface energy, wettability of the ink and printing velocity are other factors to be considered and are analysed via a track optimisation process[155,190].The viscosity of an ink is a determining factor in producing stable lines and coatings and as described in the literature when the viscosity of a formulation is higher than 20cPa is harder to be inkjet printed. For this reason no formulation of the PEG-DA 250 UV curable ink was prepared with a ratio larger than 9% w/v of photo initiator since the 9% photo-initiator in PEG-DA formulation is just below the 20cPa limit for inkjet printing.

Figure 28 shows a UV cured 5mm x 5mm square pattern printed with the 3%, 5%, 7% and 9% photo-initiator ratios in the PEG-DA UV curable formulation. In Figure 28 it can be observed that the rheological properties of the formulations impacted on the potential of producing continuous homogeneous PEG-DA UV curable coatings.

The increase in the photo-initiator ratio in the PEG-DA solution shows to have ability to improve the coating formation for the PEG-DA UV curable formulations. As shown in Figure 28, while in the 3% and 5% photo-initiator w/v ratio prints individual PEG-DA UV cured beads can be observed, in the 7% and 9% photo-initiator w/v ratio prints the formation of continuous lines (7% photo initiator w/v ratio) and continuous PEG-DA UV cured coatings (9% photo-initiator w/v ratio) can be observed.

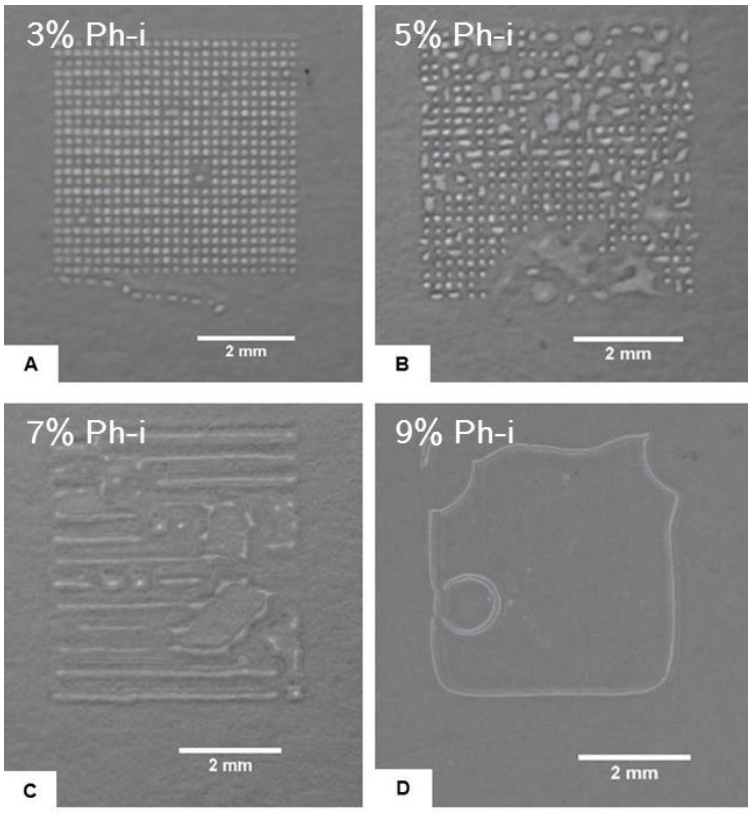

Figure 28 A) 5mm x 5mm square printed with 3% w/v photo-initiator. B) 5mm square printed with 5% w/v photo-initiator. C) 5mm square printed with 7% w/v photo-initiator. D) 5mm square printed with 9% w/v photo-initiator.

In order to have an optimal printing of the PEG-DA UV curable formulation with a 9% w/v ratio of photo-initiator a set of experiments of track optimisation for the PEG-DA formulation were made and are described in Section 4.3.3.

4.3.3. Track optimisation for PEG-DA UV curable ink with increased photo-initiator

Track optimisation printing experiments were conducted using the PEG-DA UV curable formulation with a 9% w/v ratio of photo-initiator. Step sizes ranging from 0.05mm to 0.20mm in increases of 0.05mm were printed. Printing velocities from 0.05mm per second to 3.0mm per second were evaluated in order to find the optimal printing parameters for the ink onto the silanised glass cover slip that has been defined as substrate. When comparing the tracks printed at different step sizes and printed at different velocities it can be observed that printing at lower speed produces more consistent lines as shown in Figure 29.

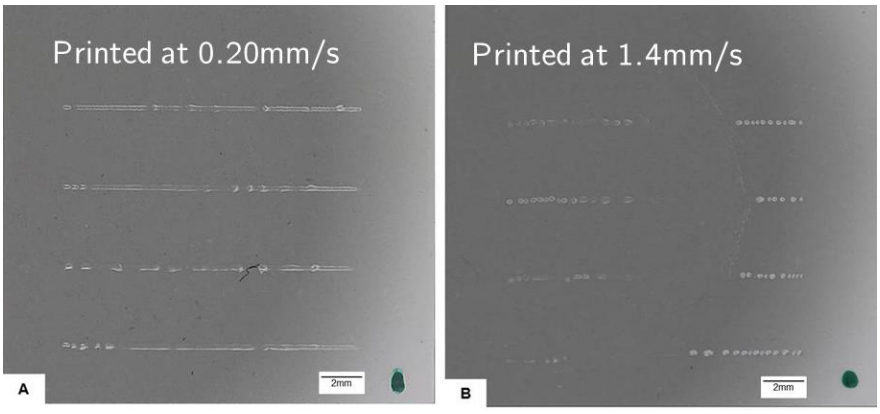

Figure 29 A) 4 tracks with a 0.20mm step size printed at 0.20mm/s. B) 4 tracks printed with a 0.20mm step size at 1.4mm/s

Once the optimal parameters for printing with the new ink have been identified (0.2mm step size with a drop ejection frequency of 250Hz at a 0.2mm/s velocity) a series of patterns were printed to assess the PEG-DA UV cured coating formation and the performance of the ink when exposed to the sterilisation process and the cell culture environment.

4.3.4. Printing of patterns of PEG-DA UV curable ink with 9% w/v ratio of photo-initiator

In order to produce a homogeneous PEG-DA UV cured coating, different patterns are developed in order to better define the optimal printing parameters with the 9% photo-initiator w/v in PEG-DA ink. The designed patterns are also intended to help better understanding the ink behaviour on the substrate and optimise the printing of the ink.

The pattern shown in Figure 30 has been developed to analyse the formation of a PEG-DA UV curable coating at different widths. The areas in white are where the PEG-DA ink is printed.

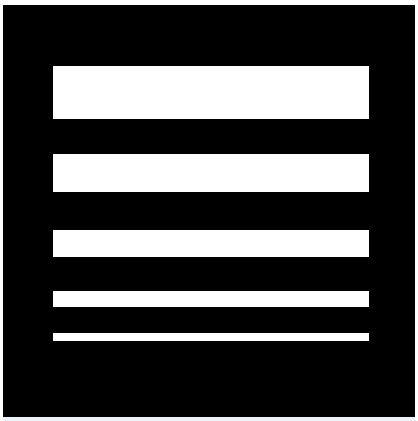

Figure 30 Pattern developed to analyse line width and coating formation.

Figure 31 shows that with the designed pattern tracks with different widths produce areas of continuous coatings when inkjet printed using the PEG-DA UV curable ink with 9% w/v ratio of photo-initiator. However stable homogeneous coatings were not achieved.

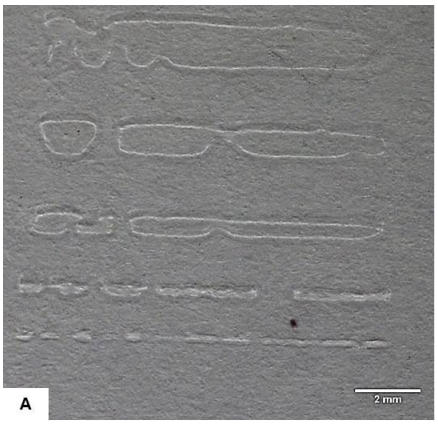

Figure 31 PEG-DA UV curable ink printed pattern for widt 2mm ıg formation analysis.

Track optimisation experiments produced before this point focused in line formation, not film formation. All experiments were being evaluated in the 'x' axis, therefore single droplet lines were produced. A series of scripts were developed to print tracks with different spacing between them to assess if a different step size in the 'y' axis improves the printing of the ink and allows film formation of the PEG-DA UV curable ink.

In Figure 32 it can be observed that the spacing in between the printed tracks does have an effect on the formation of a continuous coating. As presented by Figure 32 B the 'y' axis step size that showed a more consistent and better defined coating is that of 0.20mm.

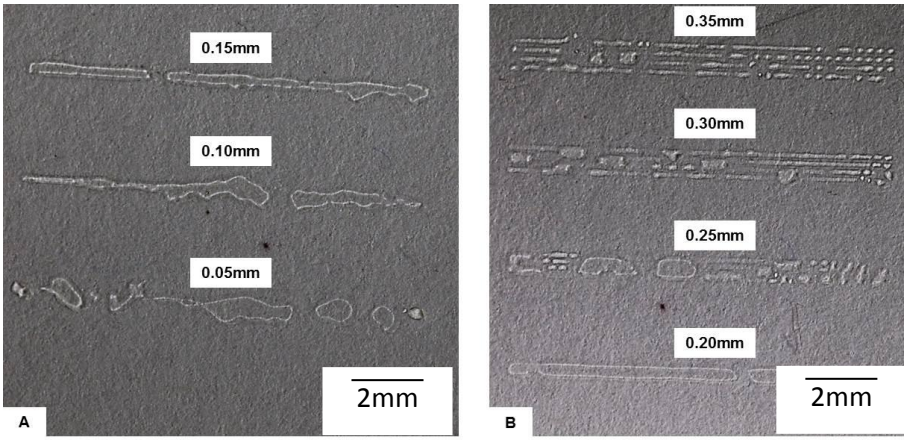

Figure 32 PEG-DA UV curable ink printed patterns to analyse the optimal spacing between tracks for the formation of homogeneous coatings.

After defining the optimal spacing between lines (step size on 'y' axis) a different set of patterns are developed to review the film formation and for later cell adhesion testing.

The patterns shown in Figure 33 have been developed to analyse the formation of a PEG-DA UV curable continuous coatings, where white areas represent where PEG-DA is being deposited via inkjet printing.

Figure 33 Patterns developed to analyse cell adhesion and coating formation of the PEG-DA UV curable ink.

The printed samples, of the patterns shown in Figure 34 A), present breaks and patchy areas after the PEG-DA ink is cured. In Figure 34 B) the broken coating is more noticeable due to the larger print area.

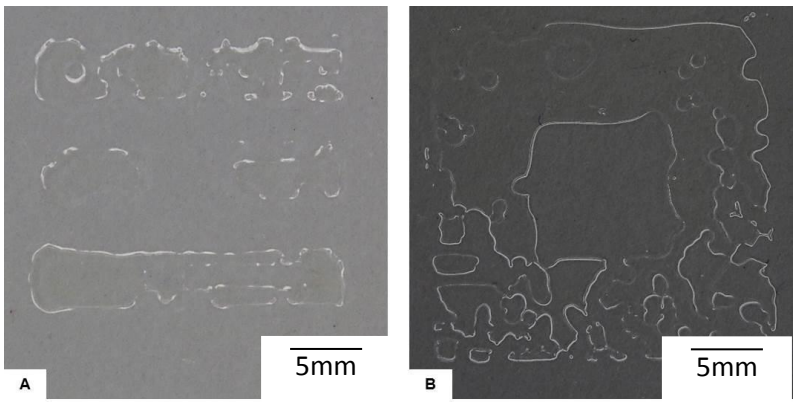

Figure 34 Printed patterns for analysis of coating formation and cell adhesion tests. A) I pattern B) Square in square pattern.

With non-continuous cell repellent coatings, cell populations cannot be contained to specific locations as required for the manufacturing of cell screening arrays as described in Chapter 1. In order to produce stable PEG-DA based cell repellent coatings the interaction between the ink formulation and the substrate has to be modified, the pertinent modifications are explored in Section 4.5.

4.4. Cell adhesion tests on printed samples

In order to confirm the cell repellent properties of the PEG-DA inks, a series of cell adhesion experiments are conducted. The cell adhesion experiments are made to ensure that cells do not adhere and proliferate on PED-DA ink covered areas, but they thrive in the areas where PEG-DA has not been deposited.

4.4.1. Printed patterns with 1% w/v photo-initiator

The samples printed with the PEG-DA UV curable ink with 1% w/v photo-initiator ratio are seeded with 10,000 cells in order to evaluate if the printed PEG-DA UV curable ink works as a cell repellent surface. As seen in Figure 35 areas where cells adhered are not covered with the PEG ink. Drops of the UV cured PEG-DA ink are avoided by cells, showing the cell repellent feature desired from the PEG-DA inks.

In order of being able to contain a population of cells to specific locations is important to have a continuous coating. As seen in Figure 35 the cells still grow in between the UV cured droplets of PEG-DA ink. With the cell seeding experiments it can be confirmed that an inkjet printed PEG-DA UV cured pattern does have an effect on where cells adhere. The cell repellent properties of PEG can be exploited by selectively depositing the ink via inkjet printing.

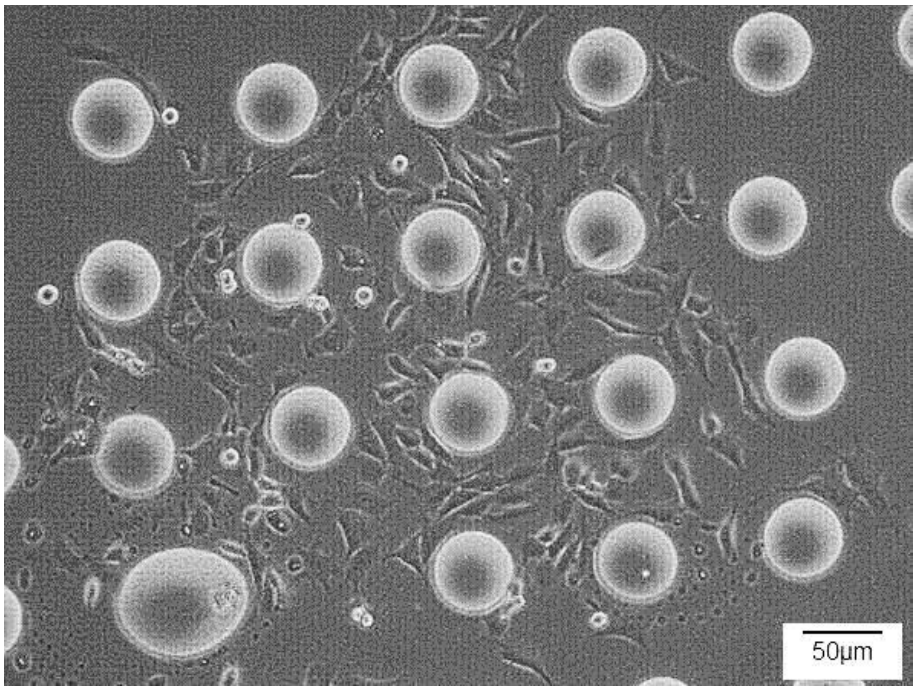

Figure 35 PEG-DA UV curable ink with 1% w/v of photo-initiator pattern showing cell adhesion in between the cured PEG-DA beads after 24 hrs in cell culture with 10,000 cells seeded on the sample.

4.4.2. Printed patterns with 9% w/v photo-initiator

The samples printed with the PEG-DA UV curable ink with 9% w/v photo-initiator ratio are seeded with 10,000 cells in order to evaluate if the printed PEG-DA UV curable ink works as a cell repellent surface, samples with this number of cells presented little cell attachment as shown in Figure 36, for this reason the number of seeded cells is later increased to 50,000 cells.

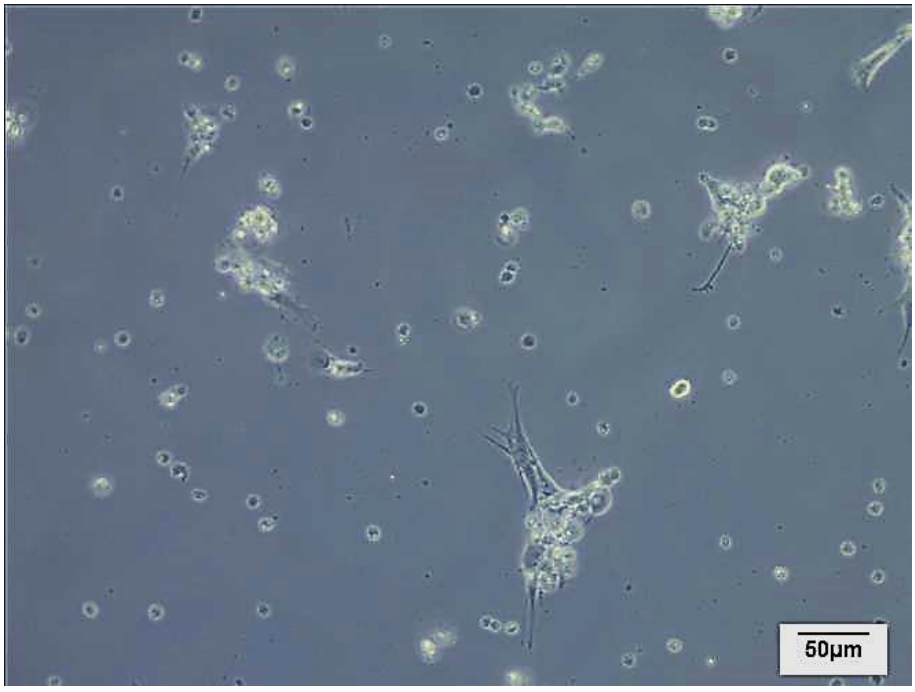

Figure 36 Control sample with 10,000 cells seeded showing cell adhesion on the substrate after 24 hrs in cell culture. The control sample consists of a piranha cleaned and then amino-silanised glass cover slip.

Figure 37 shows the interaction of the cells when cultured on the 9% w/v photo-initiator ratio in the PEG-DA UV curable ink. The number of seeded cells for this sample was of 10,000.

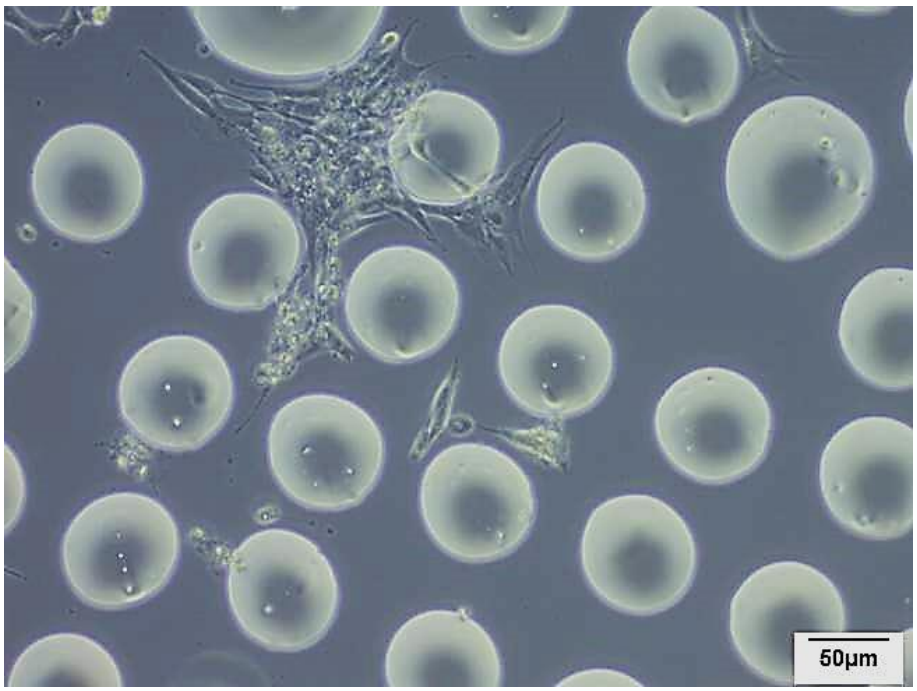

Figure 37 Printed PEG-DA UV ink with 9% w/v photo-initiator ratio showing cell adhesion in between the cured PEG-DA beads after 24 hrs in cell culture, seeded with 10,000 cells.

The behaviour of the cells around the PEG-DA UV curable ink (with 9% w/v photo-initiator ratio) printed droplets is very similar to what is observed with the PEG-DA ink with 1% w/v photo-initiator ratio. The cell repellence properties of the PEG-DA UV curable ink have not been affected by the increase of photo initiator.

With this information it can be hypothesised that when a continuous coating of the printed PEG-DA UV curable ink is present on the substrate cells should not attach to that specific area. In order to confirm this hypothesis, cells were seeded in samples

with continuous PEG-DA UV curable ink coatings. In these cell adhesion tests the number of seeded cells was increased to 50,000 cells due to the low cell density present in the past experiments when seeding 10,000 cells per sample.

Figure 38 shows the cell population after 24 hours of a control sample where 50,000 cells suspended in 1ml of cell culture media were seeded onto a control glass cover slip.

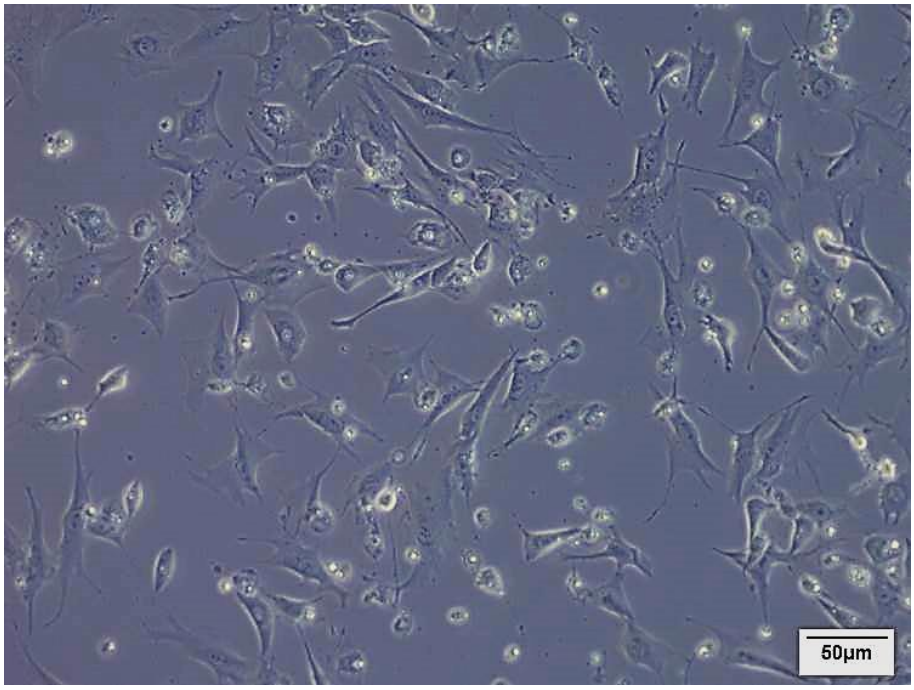

Figure 38 Control sample with 50,000 cells seeded showing cell adhesion in between the cured PEG-DA beads after 24 hrs in cell culture. The control sample consists of a piranha cleaned and then amino-silanised glass cover slip.

When a PEG-DA printed coating is present in the substrate the cells do not attach to the PEG-DA UV cured ink cover surface. Figure 39 shows that cells do not adhere to the PEG-DA covered surface, the spots that can be seen in Figure 39 are non-viable cells.

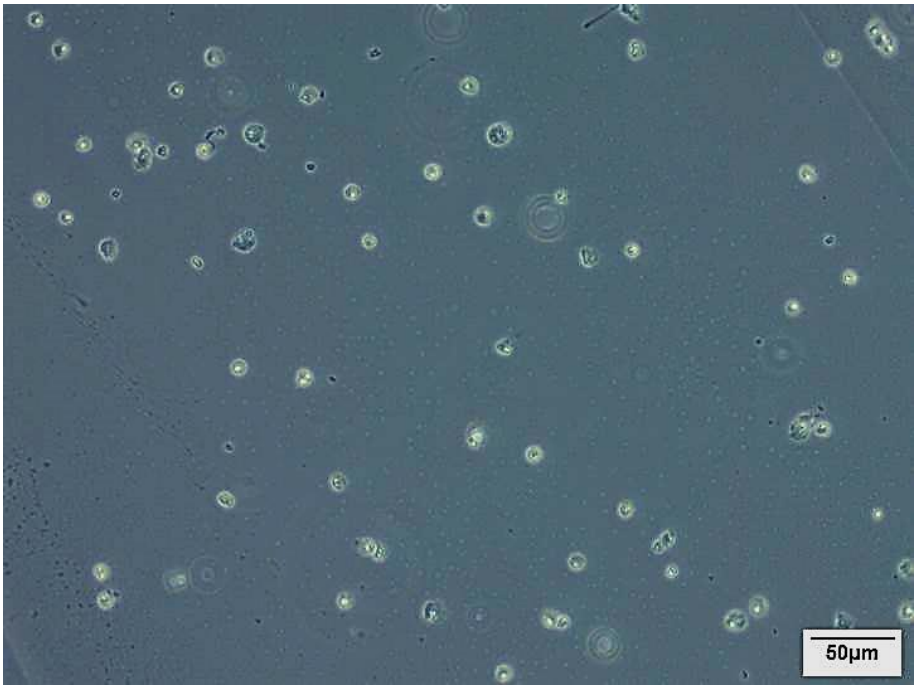

Figure 39 Continuous coating of printed PEG-DA UV curable ink 9% w/v photo-initiator ratio showing no cell adhesion in between the cured PEG-DA beads after 24hrs in cell culture .

In Figure 40 the barrier between a PEG-DA UV cured ink and a non-PEGylated surface is highlighted by the dashed red line. Cells are attached to the area of the substrate where the PEG-DA ink is not present while where there is PEG-DA, cells do not adhere.

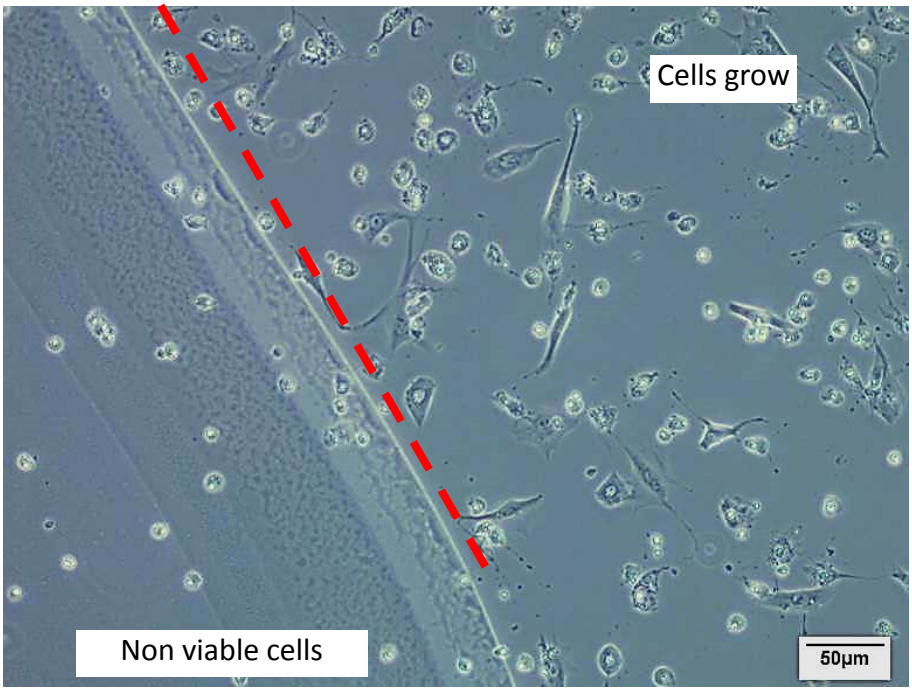

Figure 40 Edge of printed PEG-DA coating showing cell adhesion in the non-PEGylated surface and cell repellence in the PEG-DA coated surface.

Figure 41 shows an area of the sample where the substrate was not covered by the PED-DA UV curable ink surrounded by a red dashed line. The area presented is completely surrounded by PEG-DA UV cured ink; the non-PEGylated area shows cell attachment while the surrounding area does not. The round area in Figure 41 shows that a cell population can be contained when completely surrounded by PEG-DA UV cured ink deposited via inkjet printing which is a very important confirmation for the manufacturing of the cell screening chips mentioned in the aims of the project.

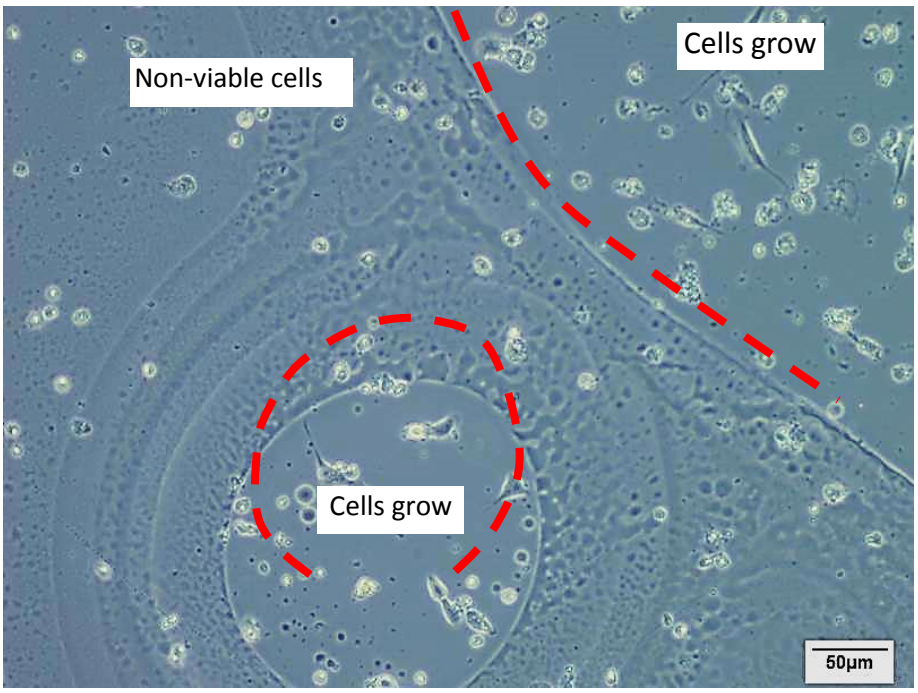

Figure 41 PEG-DA UV cured surface with a small non PEGylated area where cells adhered.

4.5. Printing of continuous PEG ink coatings

One of the major challenges of surface modifications for biological applications is to ensure that the precision and integrity of the inks remain while being deposited and

produce repeatable prints[11,179]. In order to further analyse the contained cell populations, production of continuous coatings is paramount.

As shown in Figure 26 the printed samples present a series of individual beads instead of a continuous coating of printed PEG-DA UV curable formulation. In order to produce homogeneous coatings of printed PEG it is necessary to increase the wettability of the ink on the substrate[150,155,190].

The wettability of an ink when deposited on a substrate is an important condition when printing inks to produce stable continuous films or lines. The final spread of the droplet of ink defines a diameter that controls the final resolution of the print. The resolution or minimum feature size of a printed pattern is controlled by the dimensions of its footprint which is given by the diameter of the deposited drop[190], the inks formulation rheological properties and it's wettability can affect the print resolution, which for inkjet printing is in the range of micrometres[155,190]. For lower contact angles the spread or wettability of the ink will be larger thus allowing the deposited droplets to coalesce allowing a drop to drop interaction producing a larger bead of ink that under the optimal parameters can produce an homogeneous continuous coating[155]. Two main possibilities are explored: making the substrate more hydrophilic and increase the wettability of the ink (reducing its contact angle).

4.5.1. Substrate modification to increase wettability

To produce a hydrophilic substrate the pre-cleaned glass coverslips (silanised coverslips) were exposed for 2 minutes to ozone plasma. The exposure to ozone plasma increased the hyrophilicity of the substrate as shown in Figure 42.

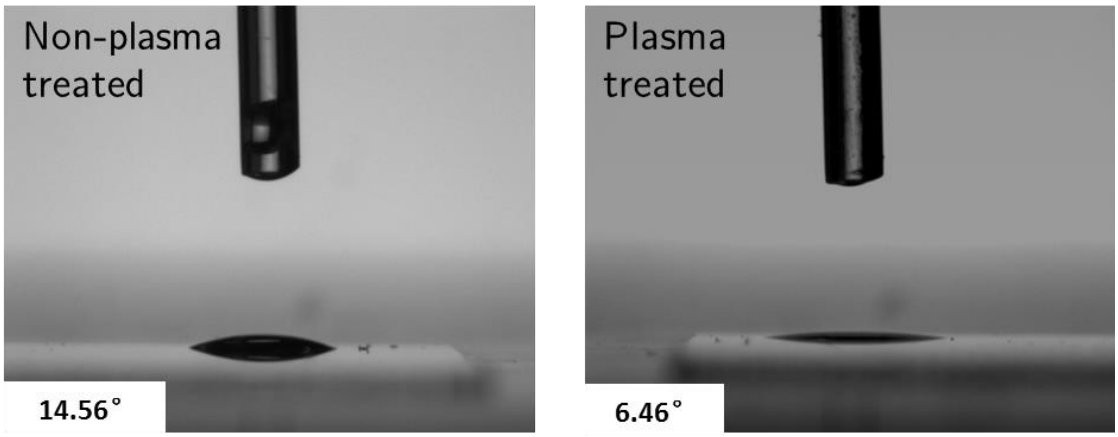

Figure 42 Increase of hydrophilicity of silanised glass slide reflected in contact angle of PEG-DA UV curable ink on non-plasma treated and plasma treated substrates.

Track optimisation experiments were conducted and, as shown in Figure 43, continuous and homogenous lines were printed at different velocities, ranging from 0.2mmps to 10mmps.

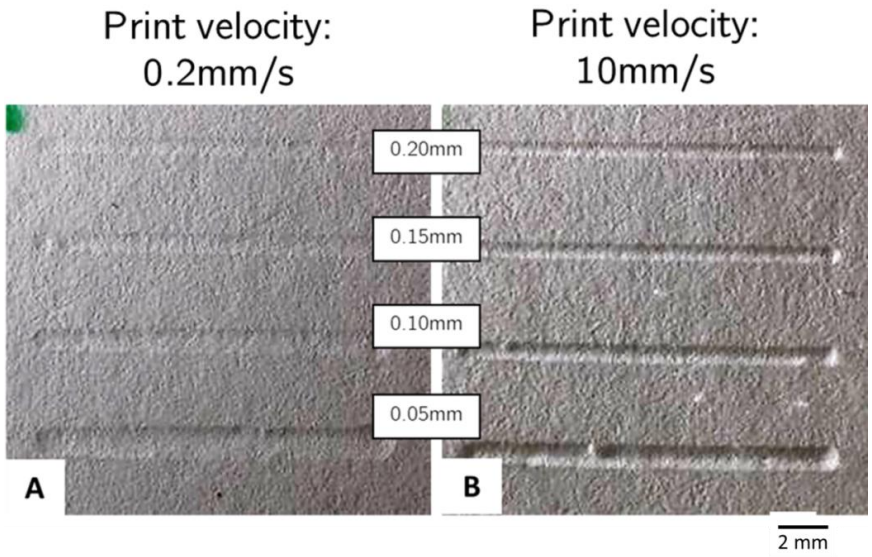

Figure 43 Track optimisation on plasma treated substrate A) sample printed at 0.2mmps B) sample printed at 10mmps

The increase of wettability, reflected on the decrease of the contact angle of the PEG ink on the substrate from 14.56 to 6.46 as shown in Figure 42, allows printing at higher velocities producing a continuous PEG coating on the substrate, as reflected in Figure 43.

When printing the square on square pattern a continuous coating is produced but, as shown in Figure 44, the quality of the pattern is not optimal as there are no sharp edges and the pattern of a square within a square is distorted. The lack of resolution is caused due to the accumulation of liquid ink during the printing process. The excess ink overflows the edges of the script, producing a distorted pattern.

The moving liquid in the inkjet printed lines or films can generate a pressure difference at the receding line that can be strong enough to create a large bulge, causing the contact angle in the ridge to be smaller than the advancing contact angle and edges of the printed image will be lost, resulting in a low quality print[189,190]. This depends on the printing velocities and the liquid volume deposited on such substrate[155].

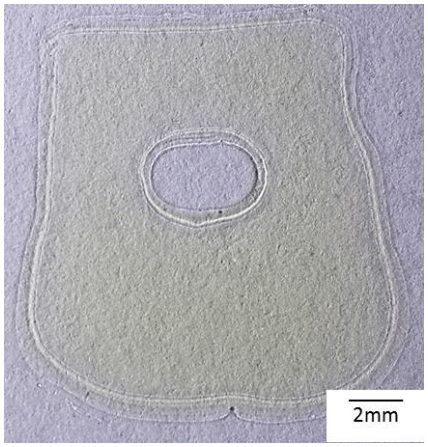

Figure 44 Sample printed on plasma treated substrate. The sample was printed at 10mmps using a 0.05mm step size.

In order to improve the quality of the printed patterns, the step size is increased. The increase in step size reflects directly on the amount of ink deposited in the substrate, the smaller the step size is the larger volume area of ink is deposited. By increasing the step size from 0.05mm to 0.10mm the amount of ink deposited is reduced by 50% since only half of the droplets are being deposited on the substrate.

Figure 45 shows a printed sample with an improved print feature, reflecting more accurately square in square pattern.

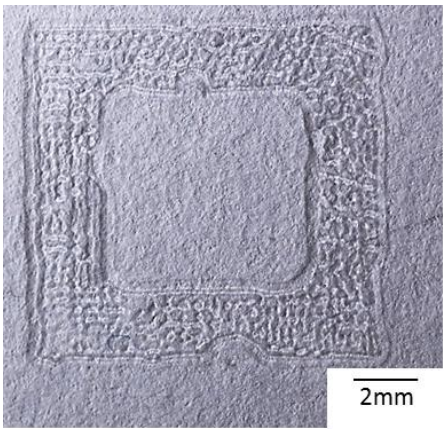

Figure 45 Sample printed on plasma treated substrate. The sample was printed at 10mmps using a 0.10mm step size.

The printed samples are then exposed to the cell culture environment (incubation at 36 degrees Celsius and 5% CO_2). For this, the samples are washed with methanol to remove any excess PEG from the print. The samples are sterilised using 70% ethanol. Once sterile, the prints are submerged in cell culture media for 24 hours to assess if the printed patterns can withstand the cell culture process.

Figure 46 shows that the printed patterns detached from the substrate after being exposed to the cell culture environment.

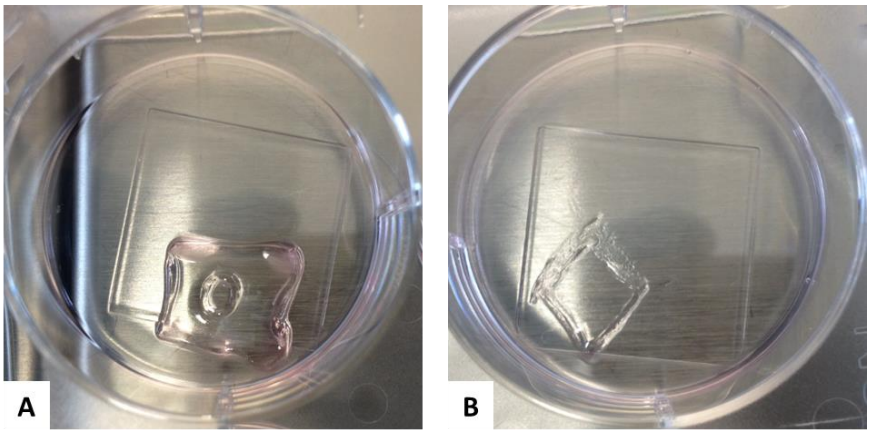

Figure 46 Detached PEG printed patterns A) sample printed using 0.05mm step size B) sample printed using 0.10mm step size

As explained in Section 4.2.3, glass cover slips are cleaned with in piranha solution and the amino-silanised in a 3% APTES solution. The APTES that binds to the substrate serves as an anchorage point for the UV cured PEG-DA network. During the plasma treatment the $-O_3$ that is being bombarded 'knocks-out' the APTES that had binded to the glass substrates, meaning that the PEG-DA network does not have anchorage points anymore, allowing the delamination of the cell repellent coatings. For this reason the plasma treatment is not an adequate process to increase the wettability of the PEG ink on the substrate.

Figure 47 shows a schematic of the effect of ozone plasma treatment on amino-silanised glass cover slips.

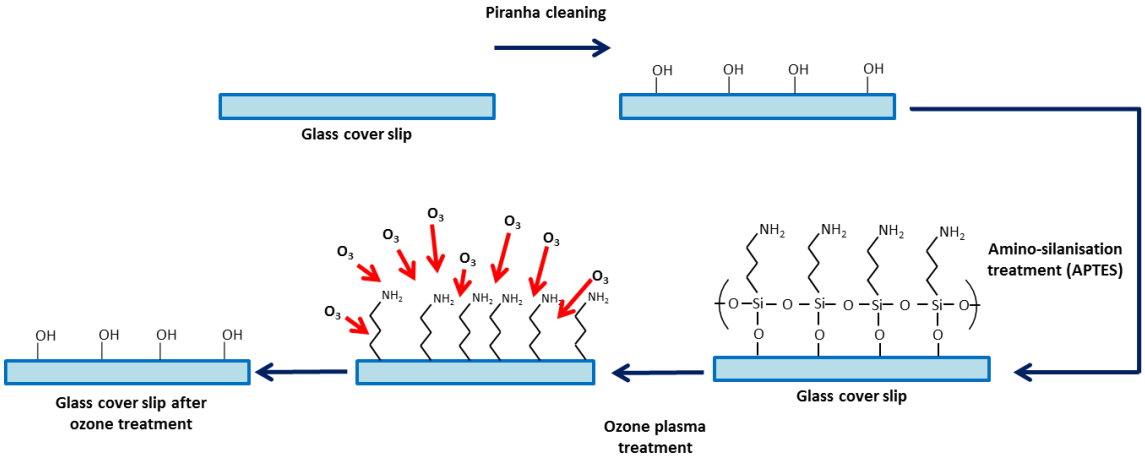

Figure 47 Schematic showing the effect of ozone plasma treatment of amino-silanised glass

4.5.2. Ink modification to increase wettability

In order to reduce the contact angle of the PEG ink with the substrate 3-(Trimethoxysilyl)propyl methacrylate 98% (TMSP-MA) is incorporated to the PEG ink. This ink modification eliminates the need of silanising the glass coverslips before the printing process.

The TMSP-MA mixed in the PEG ink binds with the –OH radicals left on the substrate after the piranha solution cleaning, allowing the PEG ink to adhere to the substrate and withstand the cell culture process. The TMSP-MA molecule (shown in Figure 48) uses the three $-OCH_3$ to bond to the substrate, leaving the $=CH_2$ with the double bond free to react with the PEG and photo-initiator.

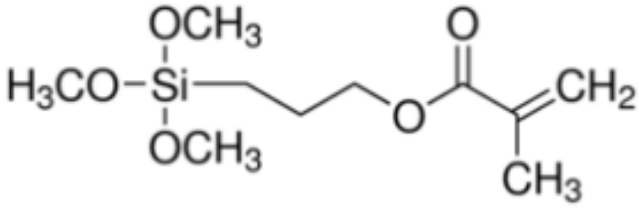

Figure 48 TMSP-MA molecule

The PEG-DA binds to this double bonded $=CH_2$, the photo-initiator breaks the double bond there and leaves a free radical, allowing the PEG to attach and remain adhered to the substrate. Figure 49 shows the silanisation of a piranha cleaned glass coverslip using TMSP-MA and the interaction of TMSP-MA with the UV cured PEG-DA network.

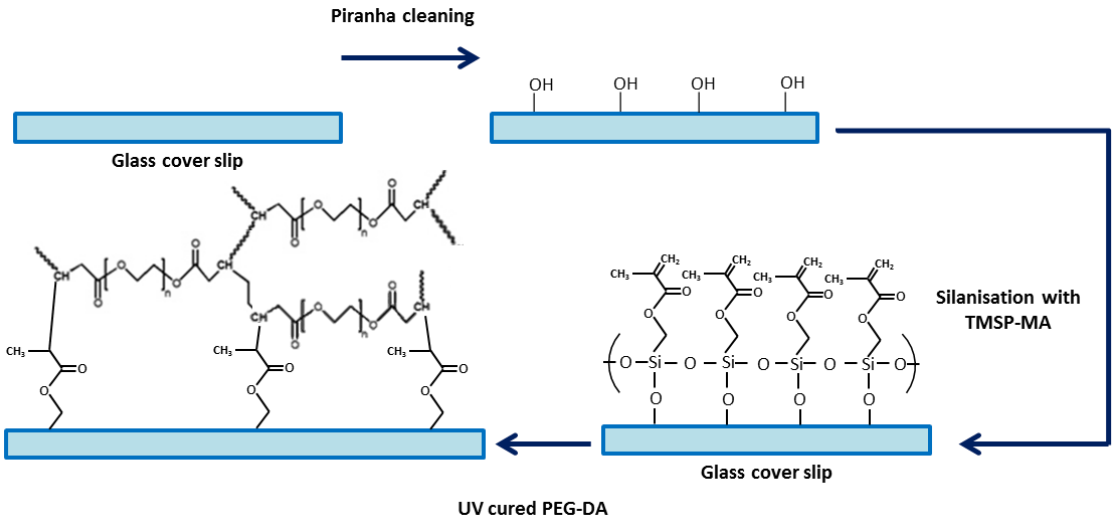

Figure 49 Schematic showing the silanisation of a glass substrate using TMSP-MA and its interaction with a UV cured PEG-DA network.

The PEG+TMSP-MA ink is prepared by adding 10% (v/v) of the TMSP-MA in the pre-defined PEG ink. Using the 10% v/v ratio decreases the viscosity of the ink (as shown in Figure 50) from 16.49 mPa · s to 14.56 mPa · s, decreasing as well the contact angle (shown in Figure 51) from 14.56° to 7.69° on a piranha cleaned glass cover slip. The decrease in the afore mentioned factors will increase the wettability of the PEG ink on the substrate.

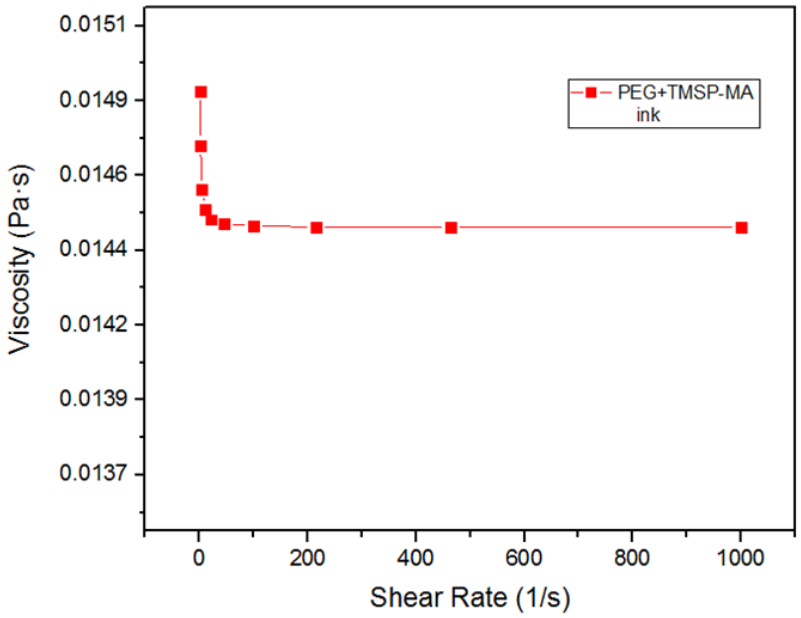

Figure 50 Viscosity of the PEG + TMSP-MA ink formulation.

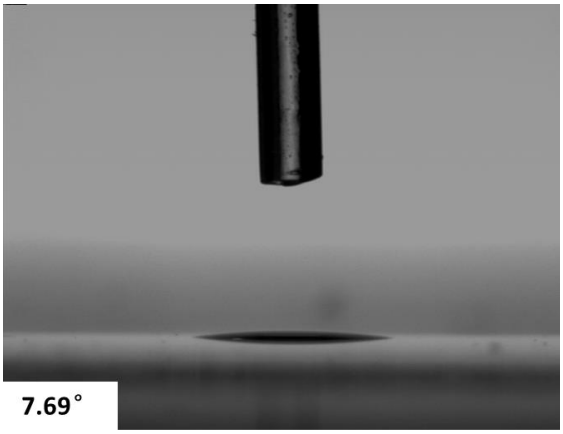

Figure 51 Contact angle of PEG + TMSP-MA ink formulation on a piranha cleaned glass cover slip.

The contact angle of the PEG+TMSP-MA ink is 7.69° when printed on piranha cleaned glass coverslips, in comparison to the 14.56° of the PEG ink on the silanised coverslip. Using the printing parameters that proved to produce continuous homogenous coatings for the PEG ink when printed on the silanised coverslips samples of the square in square pattern were produced. A printed and cured sample is presented in Figure 52.

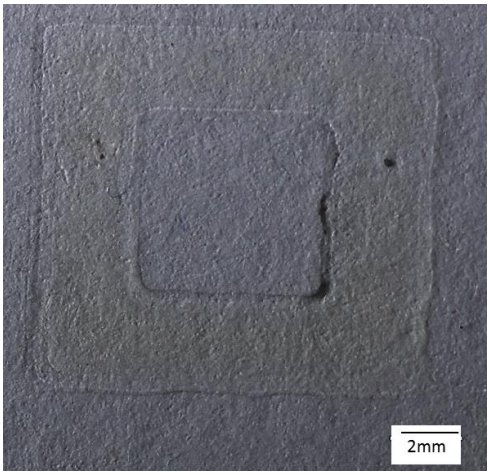

Figure 52 PEG + TMSP-MA printed sample on piranha solution cleaned substrate. Printed at 10mmps with 0.10mm step size

As shown in Figure 52, a printed sample with a continuous coating and a better quality is achieved using the PEG+TMSP-MA ink when printed on a piranha cleaned substrate using a printing velocity of 10mmps and a 0.10mm step size.

Different patterns are produced using the optimised parameters of step size and printing velocity. The word PEG printed using the PEG+TMSP-MA ink on the piranha cleaned substrates is presented in Figure 53.

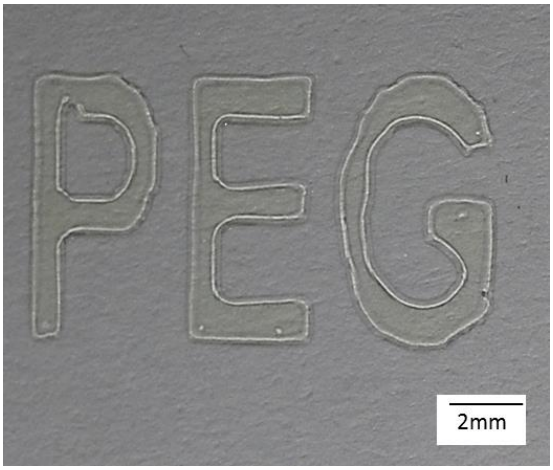

Figure 53 Word PEG printed using the PEG + TMSP-MA ink on a piranha cleaned glass coverslip.

4.5.3. Containment of cell populations

The printed samples are exposed to cell culture showing the cell repellence from the PEG and containing cell populations. Figure 54 shows cells growing on the area where the PEG+TMSP-MA ink was not printed while cells do not grow where the ink was printed. In Figure 54 C) it can be seen that the cell population started to be too large to be contained after 96 hours. The cell seeding density needs to be adjusted to allow the cells to be cultured for longer periods of time.

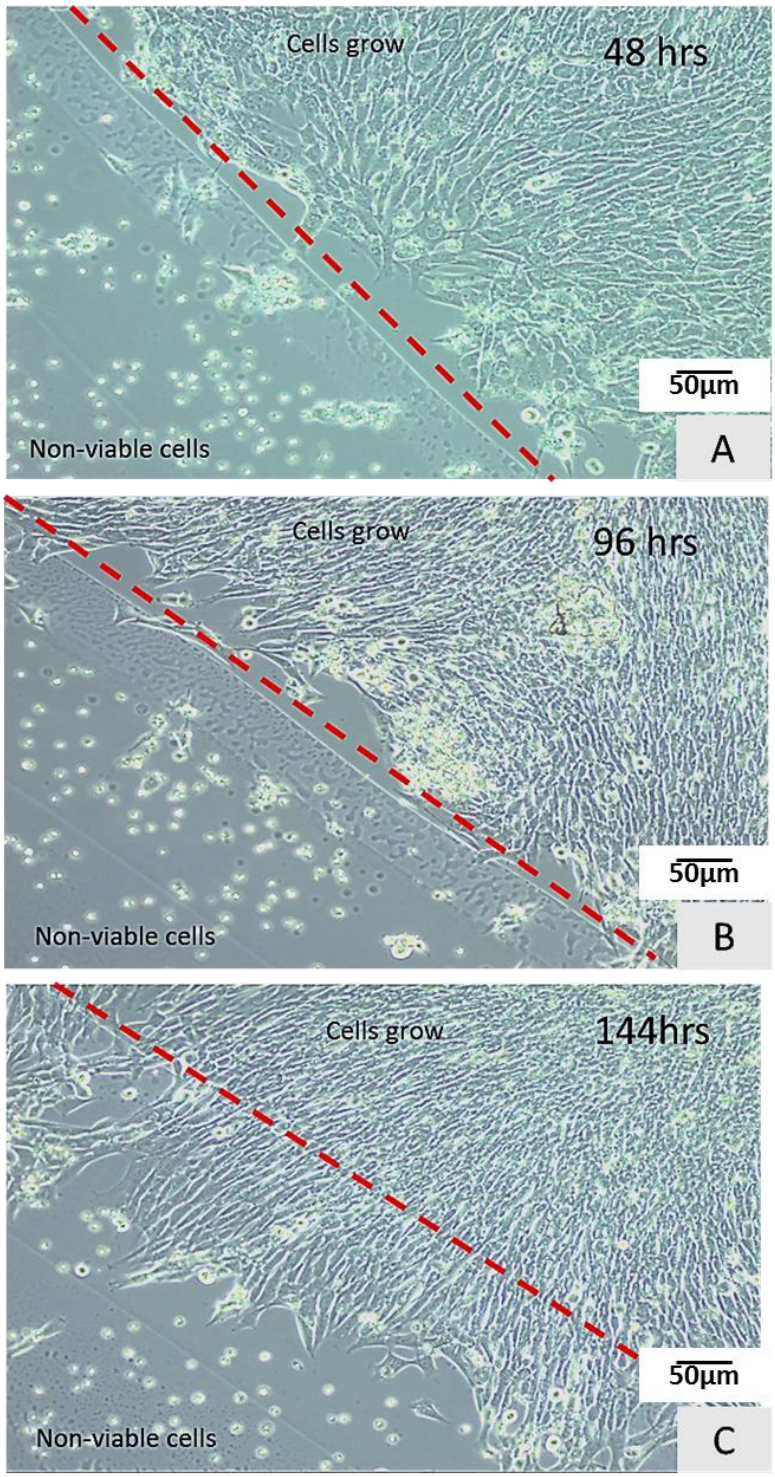

Figure 54 PEG + TMSP-MA ink printed samples seeded with 20,000 fibroblast cells after A) 48 hours B) 96 hours C) 144 hours

Figure 55 shows a printed sample with the square in square pattern where a cell population of fibroblasts has been successfully contained and where the PEG-DA + TMSP-MA ink successfully repel cell adhesion and proliferation.

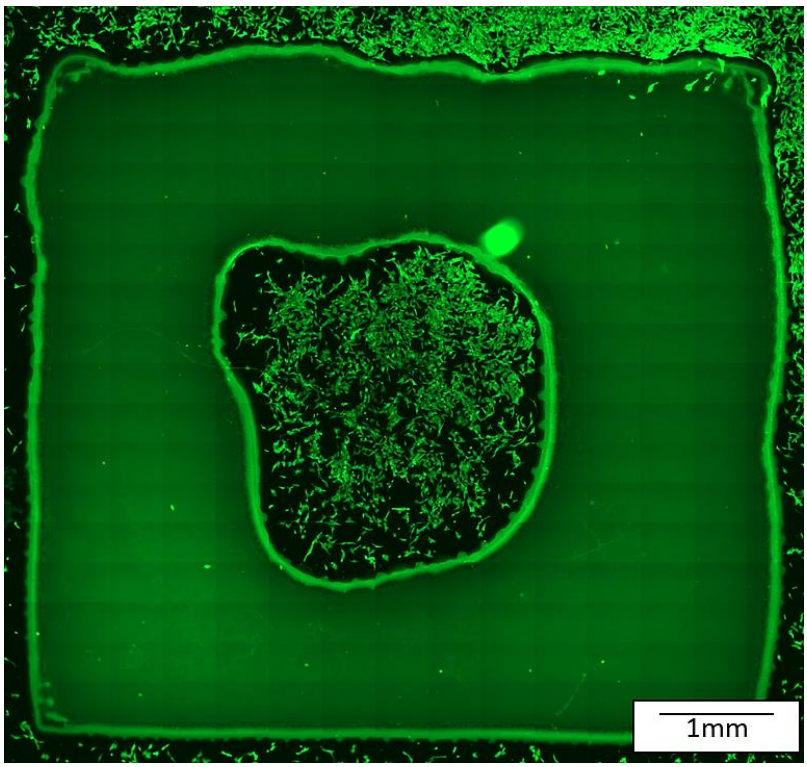

Figure 55 PEG-DA + TMSP-MA ink printed sample on piranha cleaned glass substrate seeded with 20,000 fibroblasts and cultured for 5 days. Cells have been stained with a FITC marker.

4.6. Summary

A PEG-DA based formulation has been optimised for the fabrication of continuous coatings in order to contain cell populations, by defining areas where cells cannot adhere and proliferate.

The viscosity, surface tension and density of the PEG-DA based formulations show that the selected formulations are suitable for inkjet printing. Printing experiments confirm that the PEG-DA based formulations are printable through a 0.08mm nozzle and that individual droplets of the PEG formulations can be produced. The initial aim of the work was to produce an ink formulation capable of repelling cells. This has been achieved and continuous cell repellent coatings manufactured.

The containment of L929 fibroblasts populations has been demonstrated by using the inkjet printed PEG-DA based formulation and the produced samples can withstand the cell culture environment. The containment of the cell populations is a result of the cell repellent capabilities of a PEG-DA based continuous UV cured coating.

Chapter 5

Amino-silanisation of glass via inkjet printing

Overview

The amino-silanisation of glass cover slips via inkjet printing is investigated in this chapter. A range of APTES in isopropanol formulations were developed and assessed in terms of their rheological properties for their suitability for inkjet printing. The APTES modified glass substrates via inkjet printing are then characterised in terms of their surface energy, surface chemistry and topography.

5.1. Background and rationale

The capacity of controlling cellular response and induce stem cell differentiation using surface modifications to the substrate has great academic and commercial benefits. The use of these surface modifications could lead to the fabrication of cell screening arrays with different chemistry that controls the phenotype of attached hMSC making an advance in the field of tissue engineering and lead to more efficient and personalised implants[1,12,83].

Experiments show that the direct contact of hMSCs with defined chemical groups that have been accurately arranged and physically defined as part of their immobilisation to a material substrate, can be used as the controlling tool to interact with cells in order to define their phenotype and function[1,2]. The control and definition is directly related to the cell adhesion which in turn controls specific cell signalling pathways and ultimate function[2]. Amino groups (–NH_2) groups directed stem cells to an osteogenic phenotype[1,2,12,81,83]. APTES has been widely used for surface modification of glass and silicon wafers to populate the substrates with the amino groups[127,195,196]. Having proved to populate substrates with –NH_2 groups and having been used for stem cell differentiation assays, APTES has been selected as the amino component for the silanisation of the 'cell active' areas of cell screening arrays.

5.2. APTES based silane formulations

An amino-silane compound is a monomeric silicon-based molecule with an amino (-NH_2) functional group. The general reaction of amino-silane coupling to an inorganic substrate is shown in Figure 56. It is necessary to have an –OH populated surface for the silanisation process to occur since is with these functional groups that the hydrolysable groups of the molecule can react to[197].

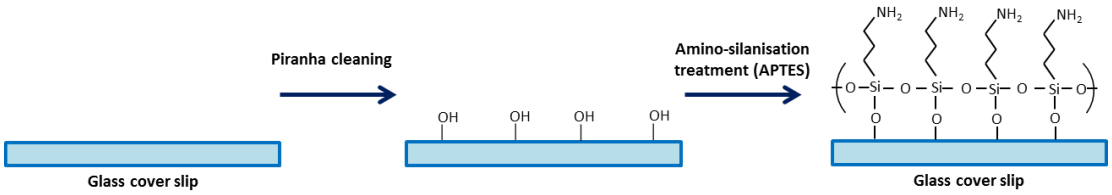

Figure 56 Amino-silanisation of a glass slide using APTES

A standard amino-silanisation process using APTES is described in the experimental chapter. This procedure is taken as a base for the definition of the APTES formulations to be developed for this chapter. The main component of the amino-silanisation solution is isopropanol, which is a common carrier for inkjet printing inks, and a percentage of APTES v/v is dissolved in the solution to define the density of APTES molecules to interact with the –OH populated glass substrate.

Different APTES in isopropanol formulations will be explored in this chapter for their inkjet printing and surface modification capabilities. The protocol followed for making the APTES formulations is described in the experimental chapter.

Silanes were chosen because when forming self-assembling monolayers (SAMs) if optimised, said monolayers are well defined and stable[198]. Stable uniform SAMs have been produced on glass coverslips[1,2,12] and silicon substrates[199] when the surfaces are hydroxylated by treatment in piranha solution and then the silane enriched surface is dried. These monolayer structures can be used to modify and customise the chemical and mechanical properties, for example a variety of SAMs with different functional groups have been used to control adhesion[200,201], it can be said that the SAMs are being used as an end to capture molecules like antibodies, proteins and cells to solid substrates[202,203]. Controlling the placement of silane-based SAMs of defined functional groups in specific locations of a substrate makes them valuable for said purposes.

The growth of APTES-based SAMs stands out from other silane systems because it involves an irreversible covalent crosslinking step. The crosslinking is paramount for achieving mechanically and chemically stable SAMs on a variety of substrates[204]. The use of a hydroxylated substrate, as carried out in this thesis, promotes a hydrolytic bond to the –OH surface groups that will immobilise the silane molecules[204,205] which will enhance the stability of the substrate's silanisation[204,206,207]. The kinetics of the hydrolytic bond in the self-assembly process can have important implications in the final film structure. This complicates the process since the hydrolysis rate is dependent on water content or humidity and temperature during the process[204].

Predictable structure and repeatable manufacture of SAMs are desirable for their applications. As mentioned before, the quality of the monolayer is sensitive to the conditions under which it is produced, the hydroxylation of the substrate, the humidity or amount of water present and the temperature[208]. Some commonly used fabrication methods[198,208–211] include the addition of water and the SAMs show variable properties and structures[212,213], for this reason the carrier defined for the

APTES inks will be 98% isopropanol to ensure the same presence of water in the solution, to try and reduce the variability in humidity during the silanisation process via inkjet printing.

Temperature of the process for the fabrication of silane SAMs on silica substrates plays an important role in the production of well organised monolayers as demonstrated in different studies[214,215], showing that SAMs produced under 30°C contained well-organised alkyl chains, while the monolayers produced in temperatures higher than 30°C showed a more chaotic assembly[214,215].

Water presence in the fabrication process has shown to be a paramount variable for the production of stable silane monolayers[201,204,216]. The Hoffman groups have explored the deposition process of silane when water is present and their results show that the monolayer growth produces island formation and a continuous disordered phase[217,218]. However, the silane molecules showed to later align and increase the monolayer coverage. The use of a dry process was explored by Wang et al[219] and they showed that using an anhydrous solution and deposition technique enhances the alignment and organisation of the SAMs. The monolayers produced with anhydrous processes showed to grow slowly but seemed to be more stable[219].

When SAMs are produced in temperatures lower than 30°C and in anhydrous solutions and environments, a topologically smooth, cluster-free and stable surface is formed[201]. However, the inkjet printing process used for depositing the APTES inks is not capable of ensuring an anhydrous environment. Silane SAMs produced with the presence of water in the process can present non-uniform nanoscale mechanical and topographical properties[220].

The control of humidity can prove difficult when the silane SAMs manufacturing process is transferred to an inkjet printing equipment like the MicroFab4 where there

is no humidity control and only the temperature of the substrate and nozzle can be controlled, but not the temperature of the printing chamber which can result in non-uniform modifications to the substrate and the possibility of not achieving monolayers in the process due to the crosslinking and polymerisation of the APTES molecules[201].

5.3. Inkjet printing of APTES formulation (-NH_2)

In order to have an inkjet printable formulation it is paramount that individual droplets can be jetted from the printing nozzle. Literature has shown that a dimensionless number defined as Z can predict if a formulation is printable in regards of its rheological properties and the diameter of the nozzle by which the formulation is to be jetted[187,190].

The rheological properties to be considered for the formulations are the viscosity, density, and surface tension of the potential ink formulation, as well as the diameter of the nozzle by which the ink will be jetted[155,188]. These properties are used to calculate the Ohnesorge number (Oh) that is a dimensionless number that relates the viscous forces to the inertial and surface tension forces[153,155,189].

The Ohnesorge number is calculated using Equation 3 where the viscosity of the ink is represented by μ; ρ represents the density and σ the surface tension. D represents the diameter of the nozzle to be used to jet the ink formulation.

Equation 3 Calculation of Ohnesorge number

$$\frac{\mu}{\sqrt{\rho\sigma D}} = Oh$$

The printability of an ink, represented by Z, is given by Equation 4, it is important to consider that for an ink to be printable the following relation needs to be met: $1 \leq Z \leq 14$[155,189,191].

Equation 4 Calculation for printability factor

$$Z = \frac{1}{Oh}$$

The different rheological properties and calculations for both the Ohnesorge number and the printability factor are presented in

Table 5.

Table 5 Rheological properties and Oh and Z calculation for the different APTES in isopropanol inks and isopropanol.

	Viscosity ($Ns/m^{2)}$	Density ($Kg/m^{3)}$	S. Tension (N/m)	Nozzle Dia (m)	Oh	Z
1% APTES	0.002438	810	0.02309	0.00008	0.0630	15.86
3% APTES	0.002447	812.1	0.0234	0.00008	0.0627	15.93
5% APTES	0.002447	814.3	0.02256	0.00008	0.0638	15.66
7% APTES	0.002445	817	0.02251	0.00008	0.0637	15.68
9% APTES	0.002456	822.3	0.02208	0.00008	0.0644	15.51
IPA	0.0021	790	0.0214	0.00008	0.0571	17.51

All of the different iterations of the APTES in isopropanol formulations show printability factors out of range, meaning that do not meet with the $1 \leq Z \leq 14$ requirement. Unexpectedly the isopropanol printability factor is also out of range when it is a common carrier for inkjet printable inks. Literature shows that inks that

are out of the printability range 1 ≤ Z ≤14 can still be inkjet printed at higher pressures[221].

Considering that the printability factor Z is not too far from range, a wave form for the APTES inks was defined. The wave-form is given by the voltage at which the piezoelectric element of the printer head will be exposed and a set of times (that can vary depending on the different formulations used as inks); the defined voltage is then applied to the piezoelectric component in the printer head for specific times, in the range of milliseconds (also defined for each formulation). The finished set of optimal voltages and times are shown in Table 6. The set voltage and time parameters will then define a wave-form presented in Figure 57.

Table 6 Voltage and time values set for the production of individual droplets when printing with a 80um printer-head nozzle

Rise time	7µs
Dwell time	10µs
Fall time	7µs
Echo time	20µs
Rise time	7µs
Dwell voltage	+25 V
Echo voltage	-25 V

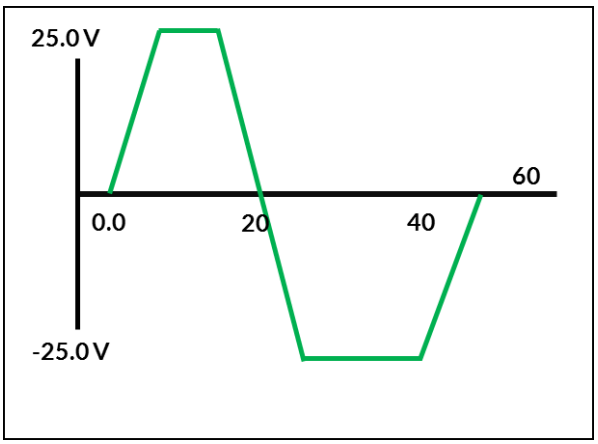

Figure 57 Wave form for individual droplets production of the APTES inks through an 80um nozzle

With the defined set of parameters and wave formula presented in Table 6 and Figure 57 it is possible to produce individual droplets of the APTES inks allowing them to be used for inkjet printing.

5.4. Track optimisation of APTES based formulation

In order to produce continuous stable printed lines and subsequent coatings, it is important to define an appropriate set of parameters that include; the step size (spacing between deposited droplets), printing velocity (velocity at which the substrate moves in relation to the printer head) and the frequency at which the droplets of ink are generated. The viscosity of the ink and its interaction with the substrate also plays an important role in the generation of stable continuous lines[155,190].

Printing track optimisation experiments were conducted varying the step size, which is the distance at which drops are deposited on the substrate. Step sizes ranging from 0.05mm to 0.20mm were employed at increases of 0.05mm and print velocities ranging from 0.05mm per second to 3.0mm per second were assessed in order to find the optimal printing parameters for the inks.

The visualisation of the printed tracks proved to be challenging due to the transparency of the inks and the glass substrate where the ink formulations are deposited. In order to visualise and image the printed tracks it was decided to add blue ink to the APTES in isopropanol formulations.

Samples were printed with the blue ink-APTES formulation but the produced tracks also proved to be difficult to visualise and image. It was decided to pursue a different visualisation method since the implications of adding the blue ink to how cells could react to it and not knowing if it is toxic for the cells.

Congo red is an organic compound that is not toxic for cells so it was decided to include it in the APTES in isopropanol formulations to change the colour from transparent to red. Congo red is soluble in organic solvents so it should dissolve in the APTES in isopropanol formulations[222].

Samples were printed using the Congo red-APTES formulation dissolving 1% w/v of the Congo red in the APTES in isopropanol formulation. However the printing nozzle was blocked when printing with this formulation. The 80um printer-head nozzle got clogged with the formulation not allowing producing individual droplets for inkjet printing. A different Congo red-APTES formulation was prepared by dissolving 0.5% w/v of the Congo red in the APTES in isopropanol formulation. With this 0.5% Congo red-APTES formulation the printer head nozzle was also blocked during the jetting of the formulation not allowing producing inkjet printed tracks.

The mechanics behind the blocking/clogging of the printer head can be simple. The printer head acts like an ink reservoir with a very tiny opening, the nozzle. During the printing process, the printer forces out tiny droplets, in the order of picolitres. The APTES inks are designed to dry fast using the isopropanol as a solvent, to avoid the APTES ink to over extend in the substrate out of the desired areas.

Due to the fast drying nature of the APTES ink, when exposed to the air the ink can dry up and block the nozzle. When no Congo red dye is present, the APTES does not generate a drastic blockage of the printer head since it tends to form monolayers, in some cases when humidity is high APTES polymerisation can appear and block the nozzle, however this issue was resolved by not adding water in the APTES inks and the water molecules present in the isopropanol did not trigger this fast polymerisation. In the other hand, the presence of the Congo red particles in the ink started clogging the printer head nozzle due to the evaporation of the isopropanol when contact in the air. After each blockage the printer head was cleaned with organic solvents (isopropanol and ethanol) since they dissolve the Congo red and the printer head was checked in the printer to confirm jetting and discard the possibility of physical damage. However after reintroducing the Congo red dyed ink, blockages continued to happen making the use of Congo red dye not feasible for the printing of the APTES inks.

Since the inclusion of coloured inks and Congo Red dye proved inefficient and not feasible for imaging printed tracks of the APTES formulations, a different approach was decided in order to confirm the substrate modification when inkjet printing APTES inks; this approach was that of printing larger areas in order to visualise a continuous surface area where the ink formulations are deposited. After confirming a

continuous surface modification, characterisation tools are to be used to confirm the presence of APTES in the oriented substrate.

5.5. Visualisation of printed APTES based formulation patterns

The visualisation of printed tracks of the inkjet printed APTES in isopropanol formulation has proven to be challenging due to its transparent nature and the limitation it imposes not being able to add colourants and other additives for its visualisation as discussed in section 5.4.

It was decided to print patterns instead of tracks for the optimisation of the printing process for it has the potential of being easier to visualise due to the change in surface energy of the glass coverslips. By having larger areas of the glass cover slips modified, inkjet printing a shape like a square with the APTES in isopropanol ink formulation would produce a defined area with different surface characteristics, allowing the use of surface characterisation techniques other than a simple visual inspection.

A series of 5mm x 5mm squares were printed using different velocities and step sizes for the optimisation of the printing process of the APTES inks. Printing experiments were conducted varying the step size, which is the distance at which drops are deposited on the substrate. Step sizes ranging from 0.05mm to 0.20mm were used at increases of 0.05mm and print velocities ranging from 0.05mm per second to 13.0mm per second were assessed in order to find the optimal printing parameters for the ink to be deposited and produce a continuous coverage of the 5mm x 5mm printed square

with the 3% APTES ink. The 3% APTES ink was selected due to the potential for stem cell differentiation it has as described in the literature[1,2,12].

The prints using a 0.05mm step size and printed at 1.5mmps showed coverage of the defined square and it kept its resolution. When printing at higher velocities the pattern began to lose definition and the 3% APTES ink spread over the defined area for the 5mm x 5mm square.

Figure 58 shows an inkjet printed patter in the shape of "NH_2" that was produced using the inkjet printing parameters defined as optimal by the printing optimisation process (0.05mm step size and 1.5mmps velocity). The DSLR picture had to be taken at an unconventional angle in order to image the defined pattern.

These printing parameters have proven to produce a continuous coverage of the defined area and maintain resolution of the printed patterns, for these reasons they are to be used in the inkjet printing of APTES inks moving forward with the research.

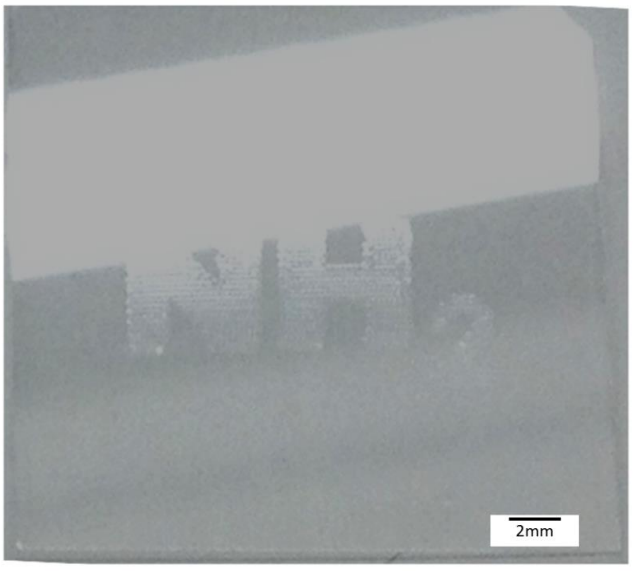

Figure 58 NH_2 inkjet printed pattern with a 3% APTES in isopropanol ink using a 0.05mm step size at a 1.5mmps velocity

5.6. Characterisation of APTES modified surfaces via inkjet printing

Chapter 4 focuses on the optimisation of an inkjet printable cell repellent coating where the function of the different experiments is based on whether the cells adhere and proliferate onto the modified substrate. If the cells do adhere to the produced samples, then the coating formulation is not fit for purpose and if the cells do not adhere nor proliferate on the coating formulation then it is fit for purpose.

The PEG-DA UV cured formulation can be visualised by DSLR imaging and its functionality can be assessed with optical and fluorescent microscopy in terms of cell adhesion on the produced coatings. With the APTES in isopropanol inks explored in this chapter the same procedure cannot be used to analyse the printed samples as discussed in Section 5.5.

In order to ensure that the desired surface modification has been achieved it is necessary to characterise the inkjet printed surface. The characterisation of a surface refers to the process achieved by different techniques to measure the chemical and mechanical properties of a surface.

Since the visualisation of the printed samples has proved to be a challenge it is important to define a procedure by which it can be confirmed that the APTES in the formulation is being deposited and adhered to the piranha cleaned glass cover slips.

This section of the research focuses on the characterisation of APTES inkjet printed samples to ensure that the desired surface modification of the samples has been achieved.

Three different processes are explored to assess both the surface modification, chemical composition and surface topography and roughness of the APTES inkjet printed samples. For the experiments described in the following subsections a range of five different APTES inks is used where the formulation consists of 1%, 3%, 5%, 7% and 9% of APTES in an isopropanol carrier.

5.6.1. Contact angle on APTES modified surfaces via inkjet printing

The contact angle is the angle of a drop of liquid when it is deposited on a substrate. It defines the wettability of the substrate by the liquid[223,224]. The contact angle of a liquid can be controlled by the modification of the substrate's surface energy. If there is change of surface energy of the substrate it will be reflected on a change of the contact angle of a drop of liquid when in contact with said surface.

Chemical composition and topography of a substrate are factors that impact surface energy, hence the contact angle. If a material is being modified in the micro or nano scale it can be difficult to visualise said modification but by measuring the contact angle of water or a liquid onto the modified surfaces; it can be observed if a modification has been made, by comparing the contact angle of water on the modified surfaces against the contact angle of water on an unmodified or control sample.

A series of 5mm x 5mm square patterns were inkjet printed on a piranha cleaned glass slide using the five iterations of silane formulations (1%, 3%, 5%, 7% and 9% APTES in an isopropanol carrier) in order to visualise if a modification was made to the piranha cleaned glass cover slip by measuring the contact angle of water on the

printed samples, and comparing them to the contact angle of water on a piranha cleaned glass cover slip.

Figure 59 present the different contact angle of water on the silane modified glass cover slips and on a piranha cleaned glass cover slip.

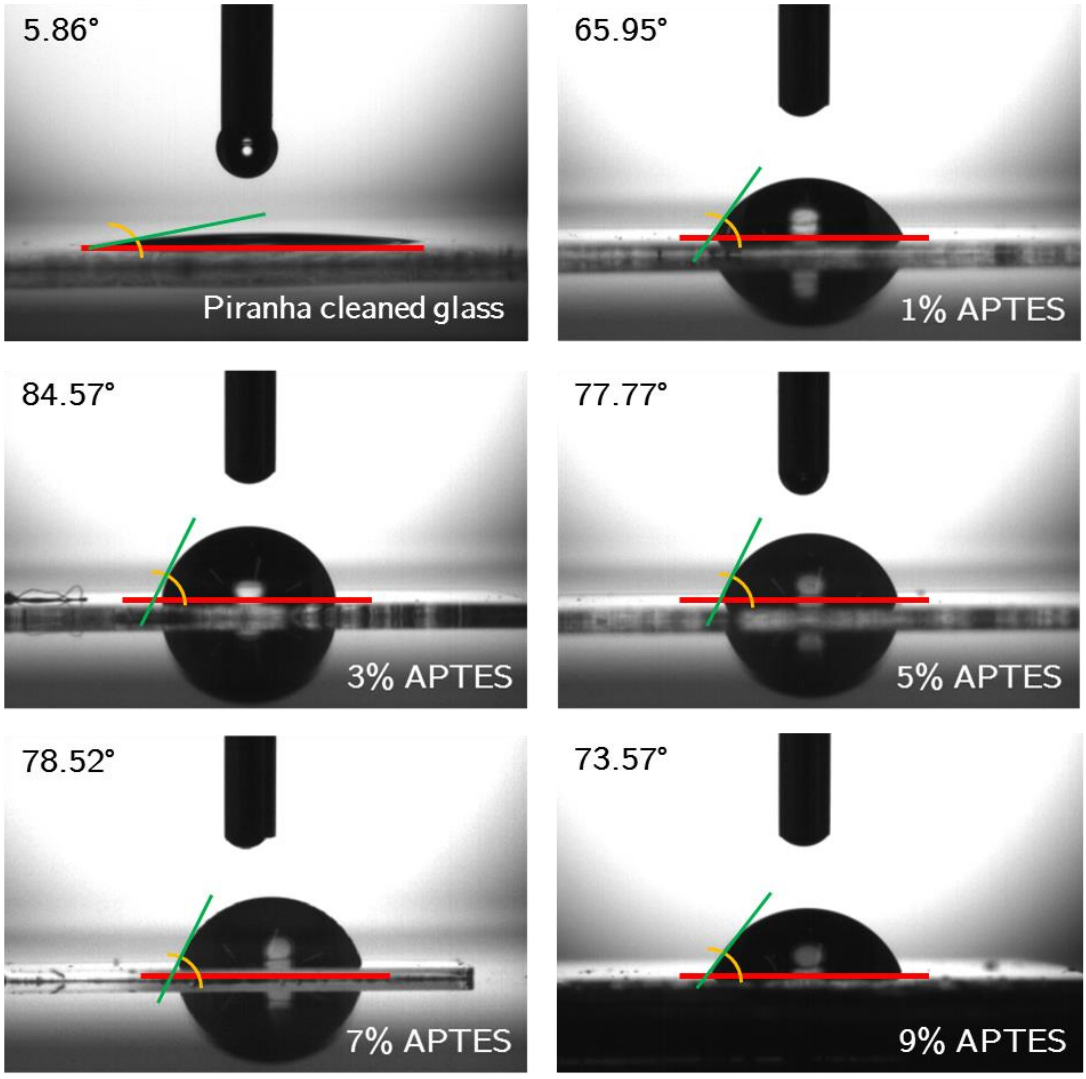

Figure 59 Contact angle of water on a control glass cover slip and on silane modified via inkjet printing glass cover slips

The use of contact angle measurements can be used as a visualisation method for the silane modification via inkjet printing of glass. The increase of the water contact angle when compared to the piranha cleaned glass cover slips confirms that a modification has been made to the surface of the piranha cleaned substrate.

APTES has shown in different studies to make substrates hydrophobic[127]. The hydrophobicity of a surface is measured via the contact angle, the larger the contact angle is, the more hydrophobic (or less hydrophilic) a substrate is. The contact angles measured on the inkjet printed samples confirm an increase in the hydrophobicity of the piranha cleaned glass cover slips. This can be attributed to the presence of APTES in the surface of the samples.

With the contact angle results shown in Figure 59 it is confirmed that a modification has been made to the glass substrate but even though the literature show that APTES and other silane molecules increase the contact angle surfaces[127,134], it still has to be confirmed that the amino groups of the APTES molecule are present on the modified substrate surface.

5.6.2. Fourier-transform infra-red spectra of APTES modified surface via inkjet printing

Fourier-transform infrared spectroscopy (FTIR) is a technology used to get a spectrum of transmission or absorption of a sample. FTIR measures the light absorption of a sample at different wavelengths. The light absorption causes the molecules and functional groups to vibrate at specific wavelengths of light. The vibrations are recorded and presented in the form of peaks in a spectrum allowing the

characterisation of a surface[225,226]. By understanding which peaks at specific wavelengths correspond to different functional groups, it can be known the chemical conformation of the substrate's surface.

A series of 5mm x 5mm square patterns were inkjet printed on a piranha cleaned glass slide using the five iterations of silane formulations (1%, 3%, 5%, 7% and 9% APTES in an isopropanol carrier) in order to characterise them by FTIR to confirm that the APTES molecules are present in the substrate's surface.

Figure 60 shows the APTES molecule where it can be observed the presence of not only $–NH_2$ groups but also that of $–CH_2$, $–CH_3$, silicon and oxygen.

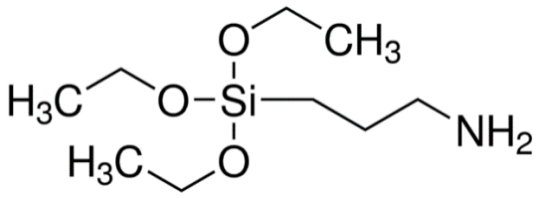

Figure 60 APTES molecule

By identifying the functional groups of the APTES molecule it can be investigated in the literature where the peaks for the vibration of each functional group are expected to appear in the FTIR spectra.

It is important to consider that FTIR is not a quantitative analysis, so the intensity of the peaks is not proportional to the amount of functional groups present in the surface being analysed[225,226]. A surface with a higher population of amino groups does not necessary show higher or lower peaks in the spectra than a sample with a lower population of the same functional group[225].

Figure 61 shows the FTIR spectra of a glass cover slip where only a sharp peak appears between 1500 cm-1 and 600 cm-1; this peak is considered the footprint of the material and it matches the range where the glass footprint is expected to appear[225]. The glass footprint is expected to be present in all of the FTIR spectra of the silane modified glass coverslips.

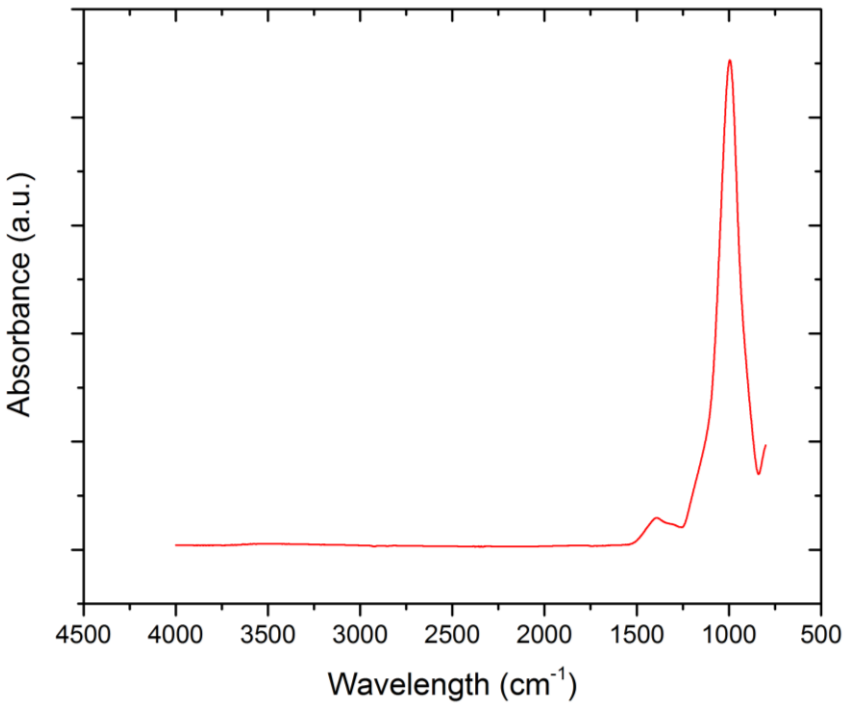

Figure 61 FTIR spectra of a glass cover slip

For the APTES modified glass cover slips the first $-NH_2$ peak is expected 3550cm^{-1} and 3200 cm^{-1} and it is expected to be a broad peak[225]. Broad peaks are not as apparent as strong or sharp peaks; they can be identified more like a slope in the spectra. The next peaks to appear in the FTIR spectra are to be between 3000 cm^{-1} and 2850 cm^{-1} and are expected to be sharp peaks. The peaks present in this area correspond to $-CH_3$ and $-CH_2$ groups, which are part of the APTES molecule[225].

Another $-NH_2$ peak is expected to appear between 1650 cm^{-1} and 1550 cm^{-1}. The identification of these peaks can be sometimes misinterpreted as part of the glass substrate footprint due to its proximity to the expected glass/silicon footprint[225].

Figure 62 shows the spectra of the different iterations of inkjet printed APTES modified glass cover slips where the areas where peaks are expected for $-NH_2$ groups and $-CH_3$ $-CH_2$ groups are expected to appear.

As seen in Figure 62 the initial broad peak or slope appears as expected in the defined area for the $-NH_2$ functional group (3550 - 3200 cm^{-1}) and the same happens with the $-CH_3$ and $-CH_2$ functional groups (3000 - 2850 cm^{-1}). The third area (1650 – 1550 cm^{-1}), where peaks are expected to appear for the APTES molecule also show the presence of peaks but they are not as clear as the first two regions since they start merging with the glass footprint.

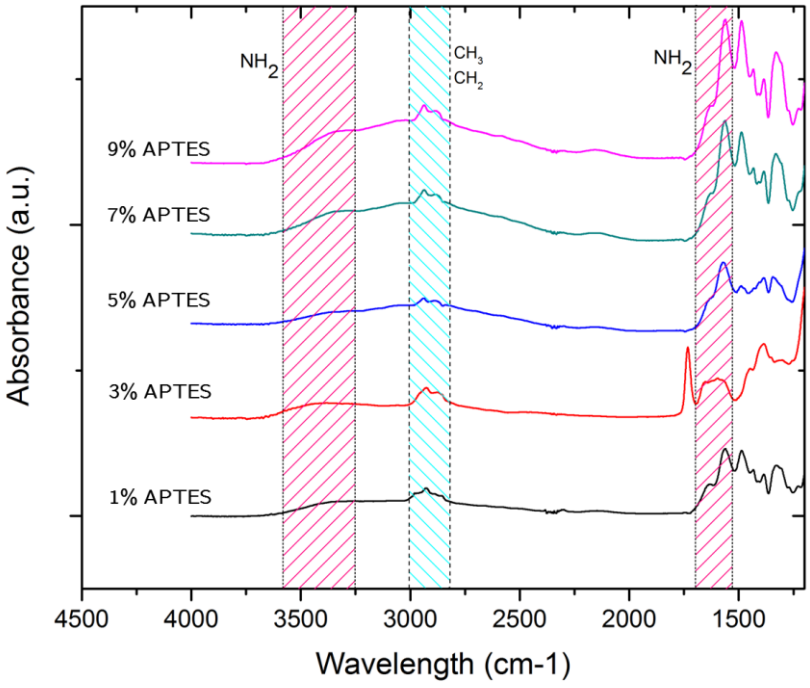

Figure 62 FTIR spectra of inkjet printed samples with different percentages of APTES in an isopropanol solution showing -NH_2 presence in modified glass slides

The FTIR spectra have confirmed the presence of the expected functional groups in the APTES molecule and the glass/silicon footprint. With this information it and the changes in contact angle as discussed in Section 5.4.1 it can be confirmed that the piranha cleaned glass cover slips have been amino-silanised with the use of inkjet printing.

5.6.3. Atomic force microscopy of APTES modified surface via inkjet printing

Atomic force microscopy is a high resolution type of scanning probe microscopy using a probe fitted in a piezoelectric element that registers the change in energy on the tip of the probe when in contact with the surface of a sample, allowing a scan resolution in the order of fraction of nanometres that can be presented in the form of a 3D image of the substrate's surface.

The contact angle measurements and FTIR analysis on the inkjet printed samples confirm that surface modifications have been made after depositing the different APTES in isopropanol inks. FTIR spectra show the presence of APTES specific functional groups deposited via inkjet printing, and the contact angle measurements show a change on the surface energy of the glass cover slips. With the use of AFM the change of topography and roughness can be analysed and compared between inkjet printed samples and a control glass slide.

A series of 5mm x 5mm square patterns were inkjet printed on piranha cleaned glass cover slips using the five iterations of silane formulation (1%, 3%, 5%, 7% and 9% APTES in an isopropanol carrier), to be characterised with the use of AFM. A

piranha cleaned glass cover slip was also analysed with AFM to use as a comparison point against the inkjet printed APTES modified samples. Changes in surface topography and surface roughness would confirm a surface modification by the inkjet printing of the APTES in isopropanol formulations.

AFM can be a powerful tool for surface characterisation, it allows visualising the change in topography and roughness of the substrate's surface of the inkjet printed APTES modified areas on the glass substrate. The AFM measurements show that each silane ink produce a different topography when printed on the piranha cleaned glass cover slips. The increase in roughness and the different surface topographies can be observed in Figure 63. Five AFM measurements were taken per sample, three different batches of samples were prepared using ink formulations prepared on the day of printing and printed in different days, and the presented roughness results are the average of all measurements.

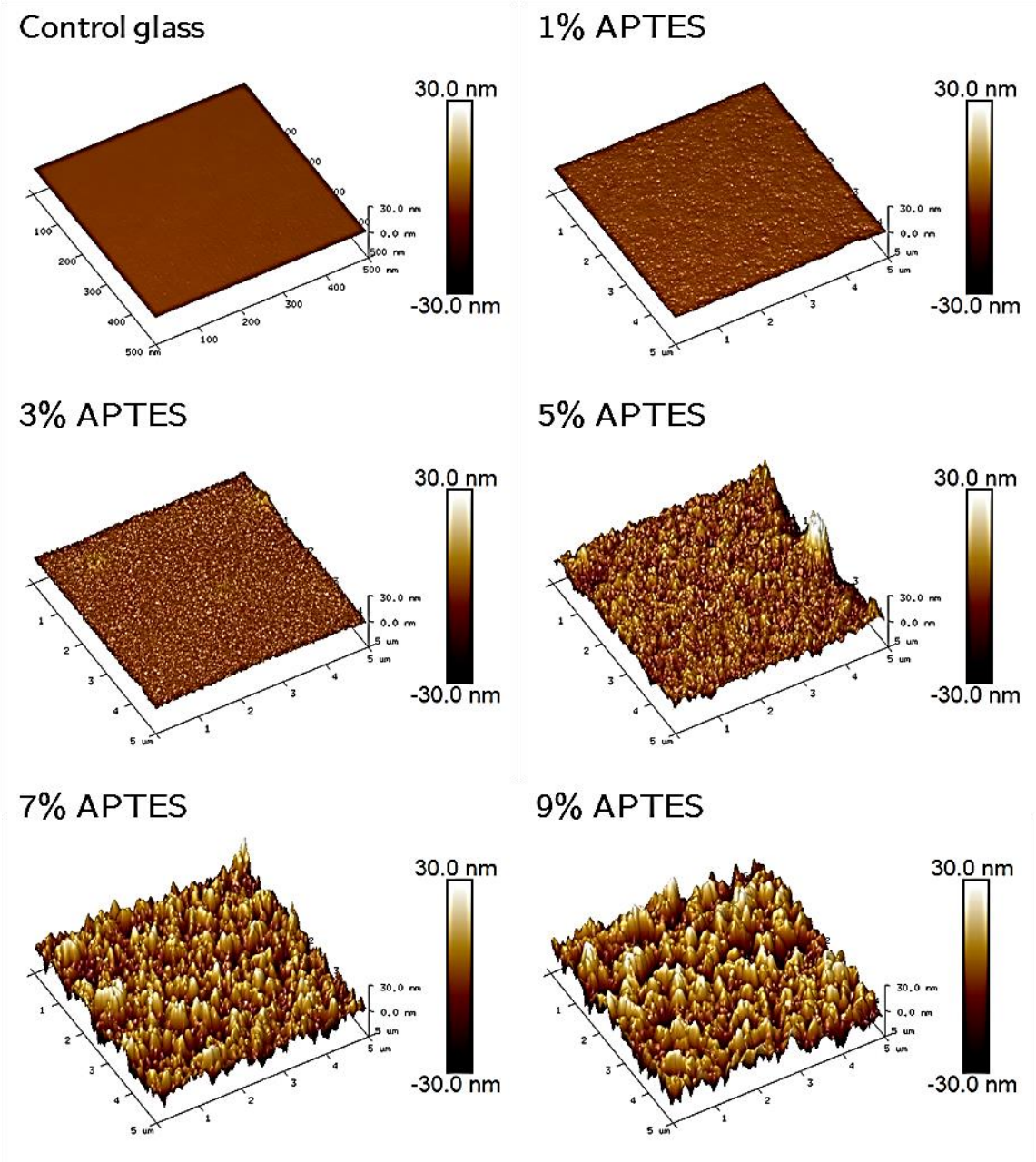

Figure 63 AFM measurements of a control glass cover slips and samples printed with the different iterations of silane inks showing the change in topography of a piranha cleaned glass cover slip.

Figure 64 shows the topography of a piranha cleaned glass slide. It can be observed that the surface is smooth and it can be confirmed by the roughness values presented, where the roughness of the glass cover slips is under 0.15nm. Literature presents Ra and Rq values of glass to be expected around 0.17nm and 0.22nm respectively[227].

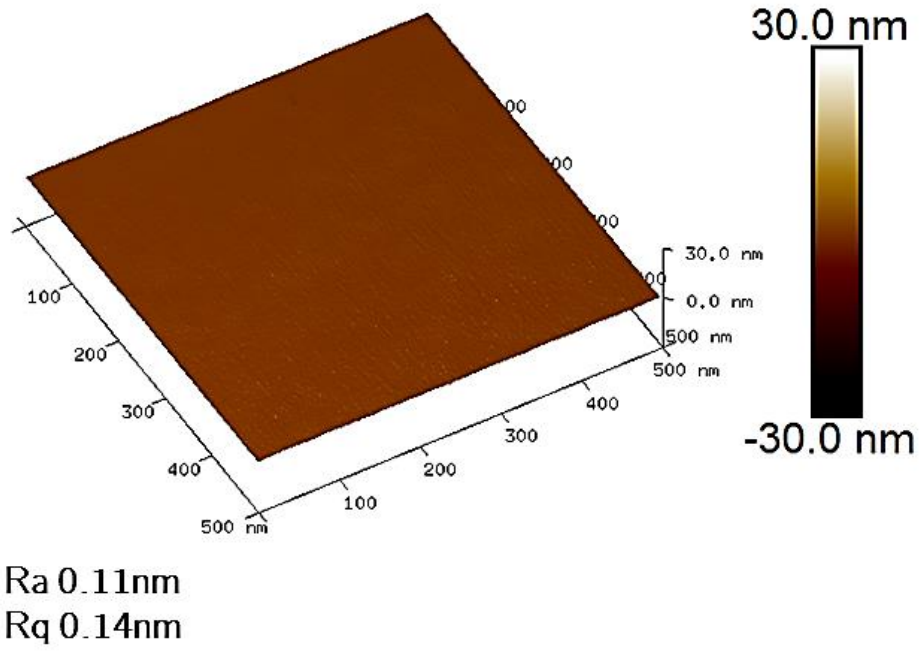

Figure 64 AFM image of the 3D topography of a piranha cleaned glass cover slip with roughness values

The values and topography presented in Figure 64 will be used as a comparison point for the results obtained when the inkjet printed samples are analysed using AFM.

Figure 65 shows the topography of a 1% APTES inkjet printing modified glass slide. A change in surface topography can be observed and confirmed by the increase of the roughness values of the analysed substrate. The roughness of the 1% APTES inkjet printing modified glass cover slip are Ra= 0.34nm and Rq= 0.43nm.

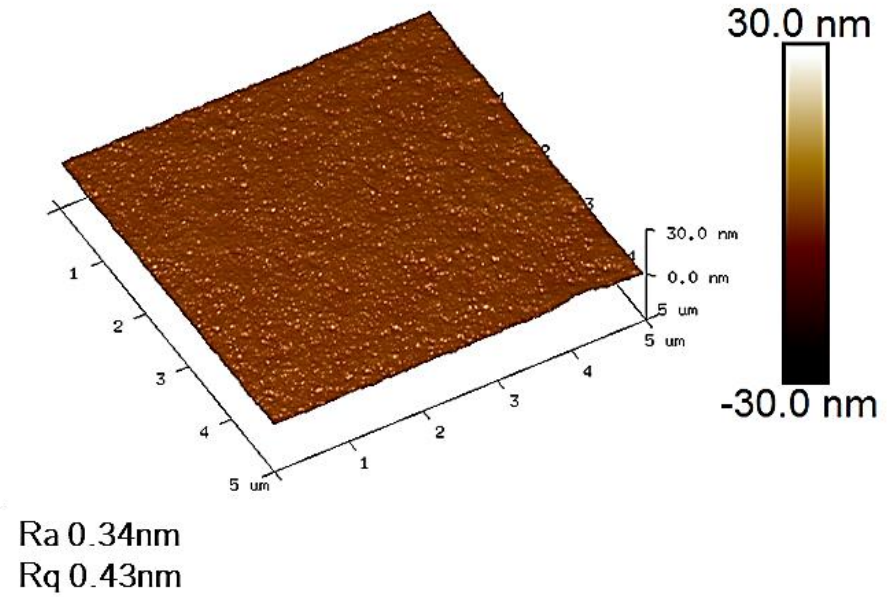

Figure 65 AFM image of the 3D topography of a 1% APTES inkjet printed modified glass cover slip with roughness values

Figure 66 shows the topography of a 3% APTES inkjet printing modified glass slide. A change in surface topography can be observed and confirmed by the increase of the roughness values of the analysed substrate. The roughness of the 3% APTES inkjet printing modified glass cover slip are Ra= 0.82nm and Rq= 1.15nm.

The surface topography and roughness of the 3% APTES modified glass cover slip via inkjet printing also show an increase when compared to the 1% APTES modified glass cover slip via inkjet printing.

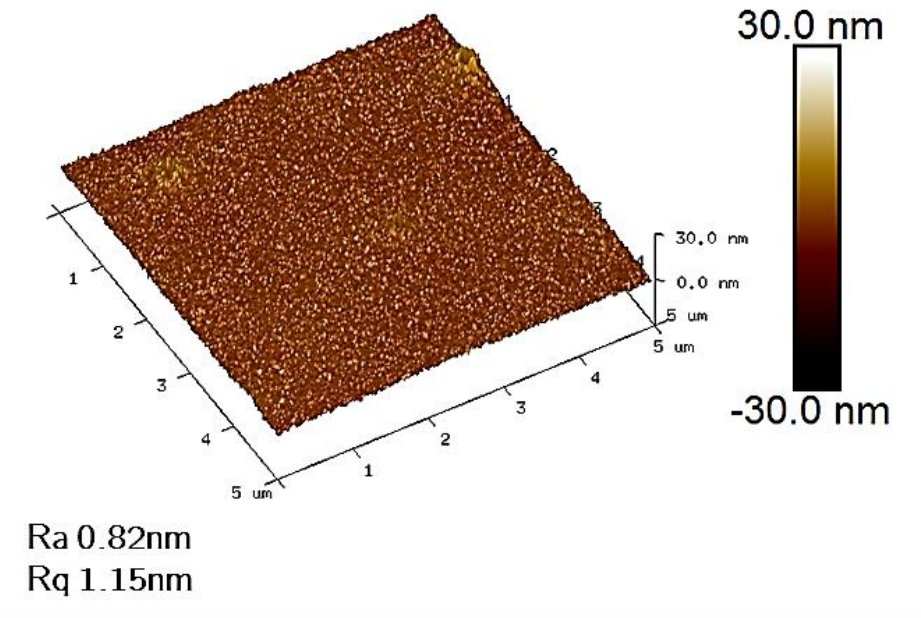

Figure 66 AFM image of the 3D topography of a 3% APTES inkjet printed modified glass cover slip with roughness values

Figure 67 shows the topography of a 5% APTES inkjet printing modified glass slide. A change in surface topography can be observed and confirmed by the increase of the roughness values of the analysed substrate. The roughness of the 5% APTES inkjet printing modified glass cover slip are Ra= 3.18nm and Rq= 4.46nm.

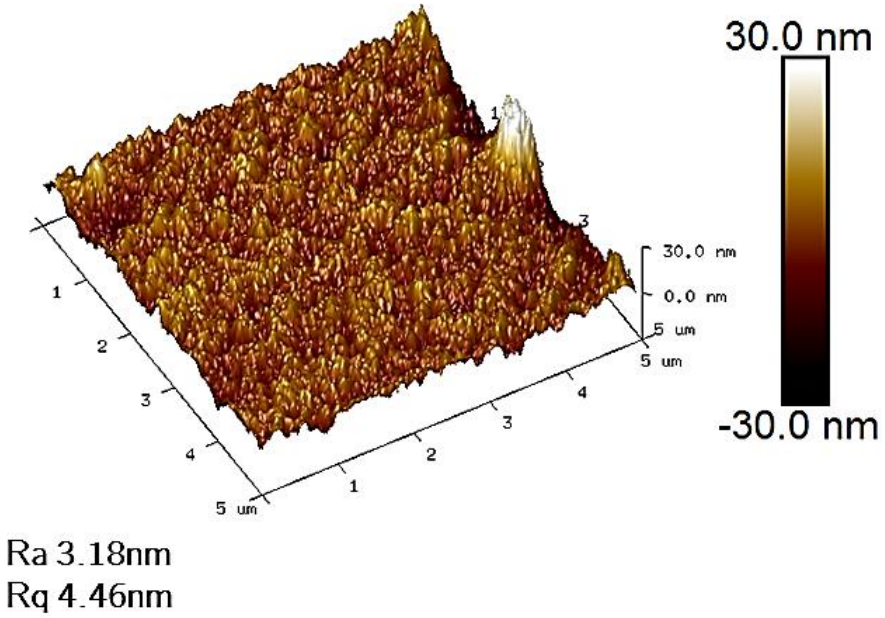

Figure 67 AFM image of the 3D topography of a 5% APTES inkjet printed modified glass cover slip with roughness values

The surface topography and roughness of the 5% APTES modified glass cover slip via inkjet printing also show an increase when compared to the 1% and 3% APTES modified glass cover slip via inkjet printing.

Figure 68 shows the topography of a 7% APTES inkjet printing modified glass slide. A change in surface topography can be observed and confirmed by the increase of the roughness values of the analysed substrate. The roughness of the 7% APTES inkjet printing modified glass cover slip are Ra= 6.07nm and Rq= 7.67nm.

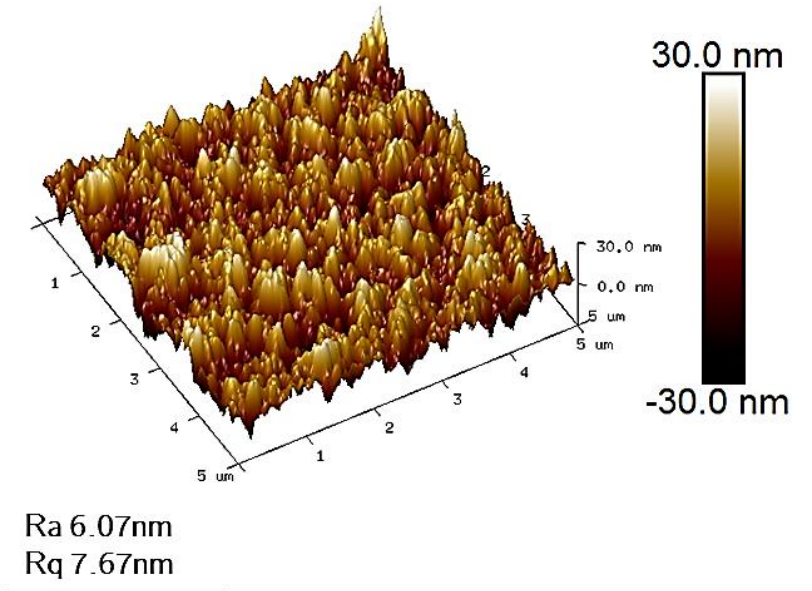

Figure 68 AFM image of the 3D topography of a 7% APTES inkjet printed modified glass cover slip with roughness values

An increase in surface roughness can be observed in the 7% APTES modified glass cove slip when compared to the 1%, 3% and 5% APTES modified glass cover slips.

Figure 69 shows the topography of a 9% APTES inkjet printing modified glass slide. A change in surface topography can be observed and confirmed by the increase of the roughness values of the analysed substrate. The roughness of the 9% APTES inkjet printing modified glass cover slip are Ra= 7.33nm and Rq= 9.33nm.

An increase in surface roughness can be observed in the 9% APTES modified glass cove slip when compared to the 1%, 3%, 5% and 7% APTES modified glass cover slips.

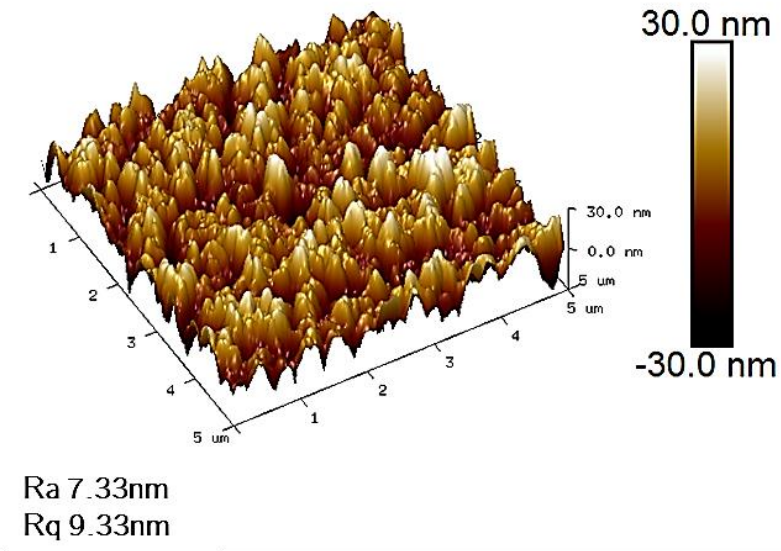

Figure 69 AFM image of the 3D topography of a 9% APTES inkjet printed modified glass cover slip with roughness values

With the AFM 3D images showing the topography and roughness values of the silane modified glass cover slips via inkjet printing of different percentages of APTES in an

isopropanol carrier it can be observed that the percentage of APTES in the ink has a direct correlation to the increase of roughness in the surface of the modified glass cover slip. Figure 70 shows the increase of the roughness of the control and APTES modified samples.

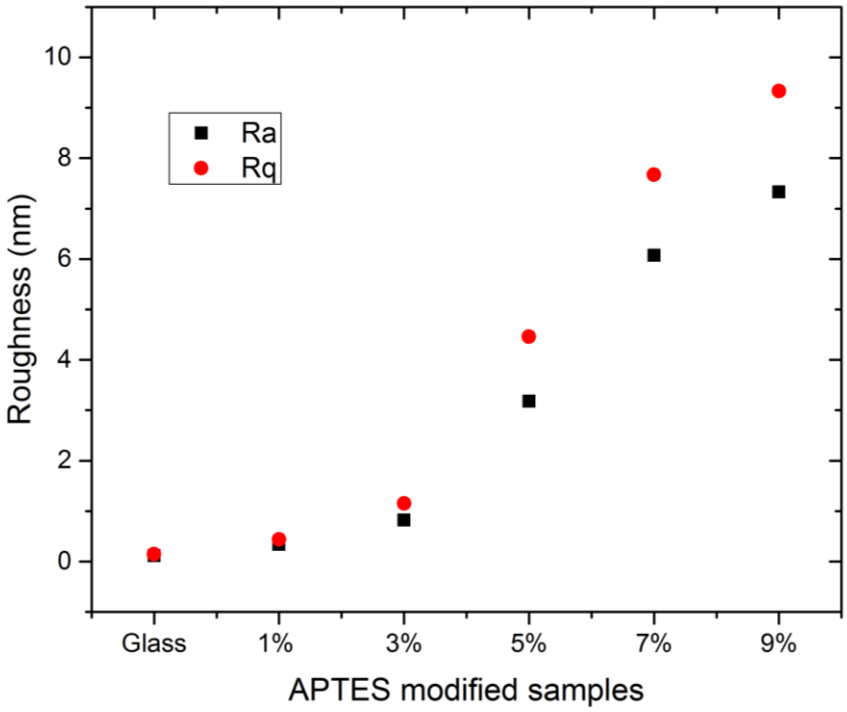

Figure 70 Graph showing Ra and Rq for control and APTES modified glass cover slips

In Chapter 6 the impact of the surface roughness and chemical modifications of the glass cover slip surface on cell viability are evaluated.

5.7. Summary

The rheological analysis of the different APTES formulations in isopropanol shows that they are suitable for inkjet printing. Printing experiments show that the formulations are jettable and can be controlled to print a variety of print features in order to selectively silanised specific areas of the glass substrate.

Different characterisation techniques were used in order to confirm the surface modification. The results show that the surface energy of the substrate was modified as shown by different contact angles of water on modified and non-modified substrates, as well as the change in chemical composition of the glass cover slips surface, as shown in the FTIR spectra; and the change in topography and surface roughness as reflected in the AFM measurements.

The research presented in this chapter demonstrates that the amino-silanisation of glass substrates can be achieved via inkjet printing, allowing to selectively modifying areas of the substrate's surface as required for the manufacturing of screening arrays.

Chapter 6

Cell screening arrays

Overview

The manufacturing process for the production of inkjet printed cell screening arrays is investigated in this chapter. The use of the cell repellent formulation developed in Chapter 4 is used to produce a design where cell populations can be contained to specific windows where the glass substrate has been amino-silanised via inkjet printing. The final inkjet printed cell screening arrays are assessed in terms of withstanding the cell culture environment for 28 days. hMSC are seeded in the cell active areas of the array in order to assess their response to the APTES inks developed in Chapter 5 in terms of cell viability and population density.

6.1. Background and rationale

A cell screening array is usually a two dimensional arrangement of biological samples or biomaterials (such as PEG and APTES), deposited in an arranged way on a substrate (usually glass slides or glass cover slips)[78,106,107,228,229] where then cells are seeded to analyse their interaction with the deposited materials[18,84,111,179,181,230,231]. Cell screening arrays can be used for the development of new biomaterials, drug testing and in vitro toxicology tests, as well as materials to drive stem cell differentiation[16,106,111,181,195,229].

In order to produce a cellular screening array the PEG-DA based formulations and silane based formulations must be able to be printed onto the same substrate allowing independent cell populations to interact with the modified areas of the substrate[107,110,112]. The screening arrays must withstand the cell culture environment for 28 days[232–235], allowing the cell populations to proliferate on the desired areas in order to analyse their response to the altered surface chemistry and topography of each individual modification.

The manufacturing process of an inkjet printed cell screening array using six different inks is explored in this chapter. The inks used for producing a cell screening array are a UV curable PEG-DA based ink that repels cells allowing cell populations containment as presented in Chapter 4, and five inks with different percentages of APTES in an isopropanol carrier that modify the surface chemistry and topography as presented in Chapter 5. The inks will be referred in this section as PEG-DA ink, 1% APTES, 3% APTES, 5%APTES, 7% APTES and 9% APTES depending on their formulation.

6.2. Inkjet printing of PEG and silane based formulations simultaneously

In Chapters 4 and 5 the UV curable PEG-DA based and silane in isopropanol inks (respectively) were printed and assessed individually after printing in terms of cell adhesion (UV curable PEG-DA ink formulation) and surface modification (silane in isopropanol formulations). Both types of inks are printed on a previously piranha cleaned glass substrate (as described in the experimental chapter), allowing both inks to modify the same substrate letting the manufacturing process to be simple by not requiring different cleaning or surface modification processes before the formulations are inkjet printed.

In order to print a cell screening array using the different inks, a printing order must be defined. It is important to mention that the PEG-DA ink needs to be UV cured, so the process order to be defined must include: the inkjet printing of the silane (APTES) inks, inkjet printing of the PEG-DA ink and the UV curing of the PEG-DA printed coatings.

The pattern to be printed for the process optimisation experiments is a square of the APTES ink surrounded by a PEG-DA square; as shown in Figure 71, where the grey area represents the PEG-DA printed formulation (cell repellent coating) and the blue patterned square represents the glass substrate modified via inkjet printing using silane in isopropanol formulations.

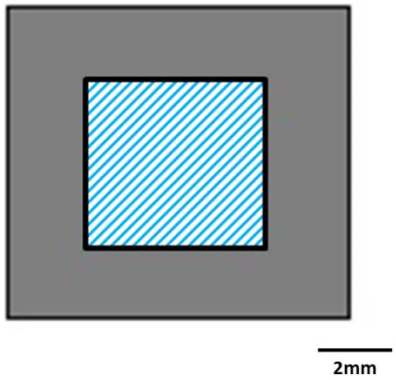

Figure 71 Square in square pattern for inkjet printing of PEG-DA ink (grey area) and silane ink (blue area)

6.1.1. Cell screening array printing order: Silane based inks, PEG based ink, UV curing

The APTES inks use isopropanol as a carrier which has a low evaporation point (80.37 °C) allowing the micro-droplets that are inkjet printed to evaporate at a fast rate thanks to the surface area to volume ratio of the jetted droplets. Due to the isopropanol evaporation at room temperature, reason it was decided that the first printing experiments of both PEG-DA inks and APTES inks would follow the order

of: APTES ink printing then the PEG-DA ink would be printed and the whole sample then exposed to UV light for the curing of the PEG-DA ink.

By printing the APTES ink first the selective silanisation of the piranha cleaned glass substrate happened before the PEG-DA ink was deposited. The wettability of the APTES-isopropanol solution modified the hydrophobicity of the surface resulting in the printing of a non-continuous coating of the PEG-DA coating as shown in Figure 72. Since the cell repellent coating (PEG-DA ink) is not continuous, a cell population cannot be contained to the desired location, for this reason its response analysis when growing in the APTES modified substrate cannot be achieved.

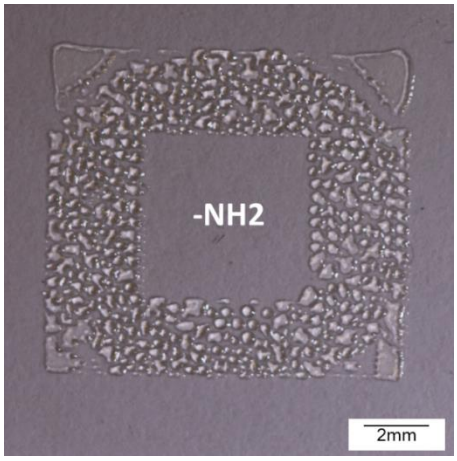

Figure 72 Sample of a UV cured square in square printed pattern where the PEG-DA ink was printed before the APTES ink and finally UV cured after both inks were inkjet printed.

The printed samples show a broken cell repellent coating making this manufacturing approach not suitable for the production of cell screening arrays.

6.1.2. Cell screening array printing order: PEG based ink, silane based inks, UV curing

Since the UV curing of the inkjet printed PEG-DA coating requires the sample to be removed from the printer it was decided to print samples in the following order: Inkjet printing of PEG-DA ink, inkjet printing of APTES ink and UV curing of the sample. By printing the PEG-DA ink first a non-cured PEG-DA continuous coating was printed followed by the APTES ink before removing the sample from the inkjet printed for UV curing.

As shown in Figure 73 the final UV cured samples does not present a continuous coating of the cell repellent coating. The PEG-DA coating formed a continuous coating in its non-cured state before the inkjet printing of the APTES ink in the inner square of the pattern. The isopropanol used as a carrier in the APTES ink interacted with the non-cured PEG-DA cell repellent coating and forced it to break due to the wettability of the isopropanol and its evaporation.

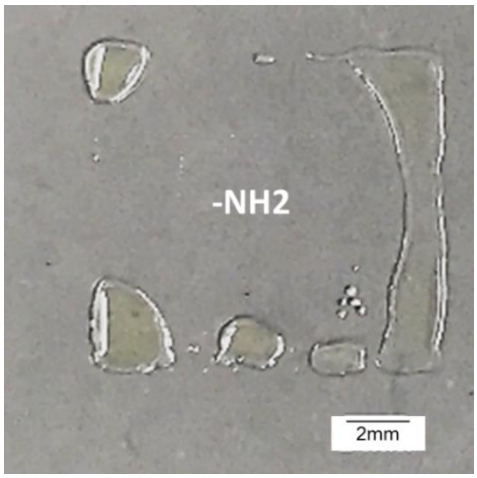

Figure 73 Sample of a UV cured square in square printed pattern where the APTES ink was printed before the PEG-DA ink and finally UV cured after both inks were inkjet printed.

The printed samples show a broken cell repellent coating making this manufacturing approach not suitable for the production of cell screening arrays.

6.1.3. Cell screening array printing order: PEG based ink, UV curing, silane based inks

According to the printing results of the PEG-DA based ink and the silane inks before UV curing the samples, it was decided to inkjet print the PEG-DA ink, cure it and then print the silane ink.

In order to have the APTES ink printed in the exact 'open window' of the PEG-DA printed square, a gage has been designed to sit on the printing platform to ensure that all samples will be positioned in the same location. The use of the gage allows depositing the inks in the correct coordinates every print.

The designed gage, shown in Figure 74, guarantees that the samples will be positioned on the same coordinates every print. The fixed positioning of the glass cover slip for printing allows the sample to be taken out of the printer after the PEG-DA is printed in order to be UV cured and then being re-positioned after UV curing of the PEG-DA coating, so the APTES inks can be printed in the required position.

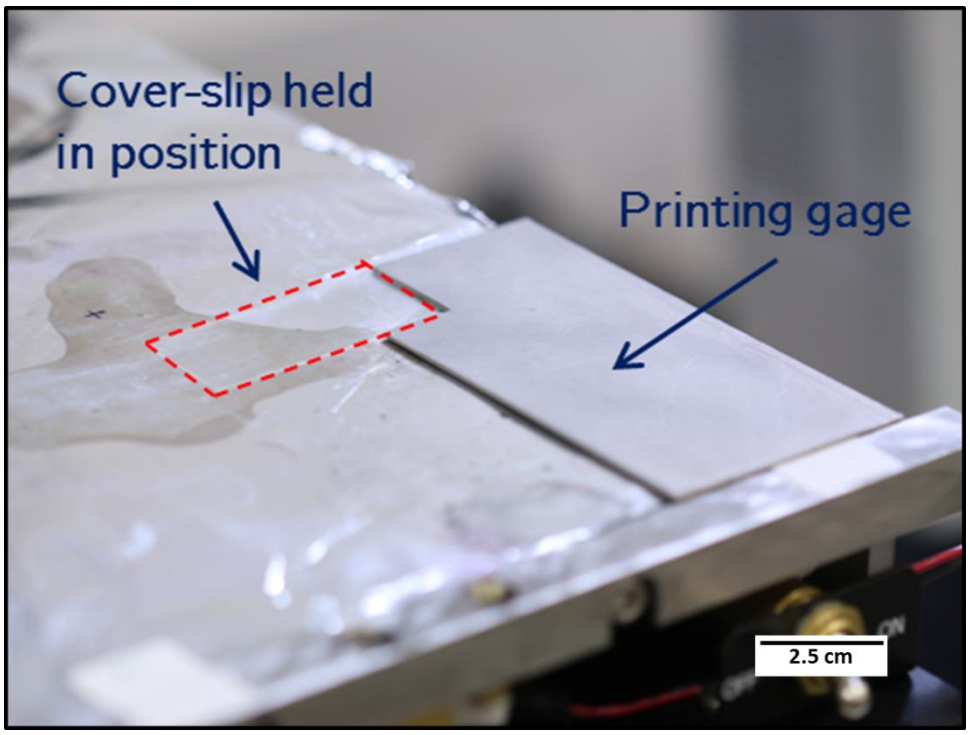

Figure 74 Printing gage positioned on the printer while holding a glass slide in position for printing.

After relocating the PEG-DA printed sample back in the inkjet printer the APTES ink is printed and the sample does not show any physical modification to the printed PEG-DA ink allowing having a continuous coating of the cell repellent coating and a silane modified area within this cell repellent square. This will allow containing a cell population to a specific silane modified area of the cover slip.

Figure 75 shows an inkjet printed sample of both PEG-DA and APTES inks where the PEG-DA ink has been printed initially then removed from the printer for UV curing and then relocated for the printing of the APTES ink.

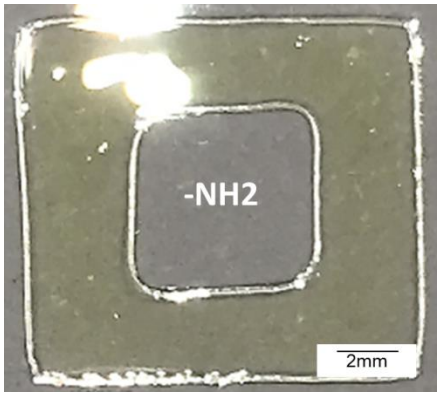

Figure 75 Sample of a UV cured square in square printed pattern where the PEG-DA ink was printed, then removed from the printer for UV curing and finally relocated in the inkjet printer where the APTES ink is printed in the 'open window'.

The samples printed following this procedure show a continuous PEG-DA cell repellent coating surrounding a silane modified area via inkjet printing for the containment and analysis of cell populations. For this reason, the PEG-DA printing → UV curing → silane ink printing is the approach used for the inkjet printing of the cell screening arrays.

6.3. Cell screening arrays design

In this section, different designs for the inkjet printing of the cell screening arrays are explored.

Before this section, all the printed samples of the PEG-DA ink and PEG-DA and APTES inks were printed in a square in square pattern as shown in Figure 71. In order to analyse various cell populations on a single sample it is necessary to be able to contain them on different locations using the cell repellent coating.

A set of patterns were developed and inkjet printed on the previously piranha cleaned glass slides. The presented patterns were designed to allow the containment of multiple cell populations.

An initial design of a screening array with 5 windows for silane modification via inkjet printing was developed, as shown in Figure 76. This design keeps the same window dimensions as well as the width of the PEG-DA coating that has proven to contain cell populations. Five windows of 5mm x 5mm are printed and arranged in a checker design where the areas for cell seeding are separated by a 2.5mm width PEG-DA cell repellent coating.

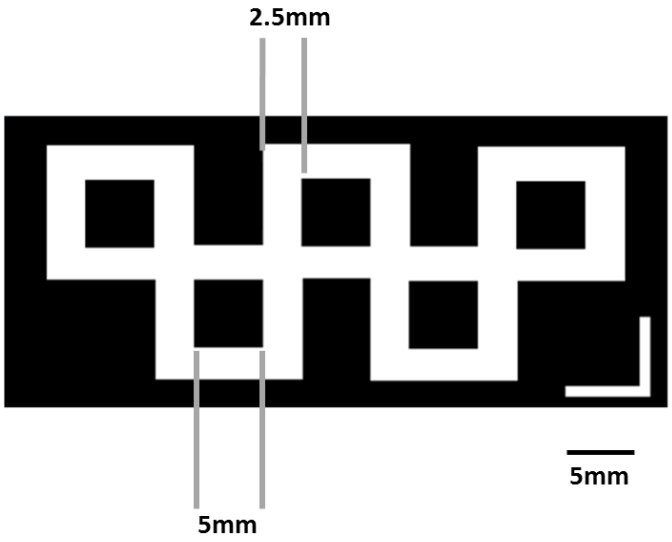

Figure 76 Design for a cell screening array with 5 windows for silane modification and cell population containment.

After the 5 windows cell screening array pattern was designed, the PEG-DA area of the array was printed and UV cured to confirm that a continuous coating of the cell repellent coating can be produced using this design, and that the increase of surface area of the PEG-DA and UV cured coating does not affect the fabrication of the areas where the silane modifications via inkjet printing are to be done.

The printed samples present a continuous cell repellent coating after one pass of printing, meaning that the pattern is only printed once on the piranha cleaned cover slip. Samples were printed with two passes (the designed pattern is printed twice, one on top of each other) and showed better defined features.

Figure 77 shows a two pass PEG-DA coating printed 5 windows pattern of the cell screening array, where a continuous coating of the cell repellent coating has been achieved allowing the containment of cell populations to the windows where the silane modifications are to be done.

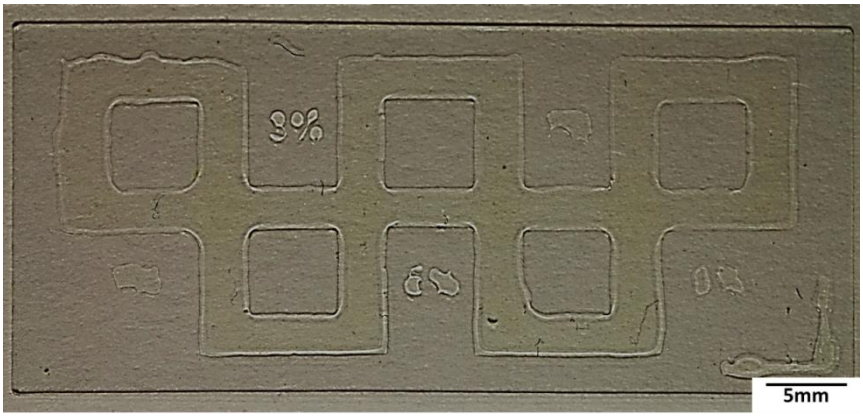

Figure 77 Inkjet printed PEG-DA sample using the 5 windows cell screening array design.

As mentioned in Section 6.1, six different ink formulations are to be evaluated in terms of the manufacturing of cell screening arrays and cell viability on printed areas. Five of these inks are different percentages of APTES in an isopropanol carrier that are to silanised the piranha cleaned glass substrate and the PEG-DA based ink that forms the cell repellent coating.

The 5 windows cell screening array allows the selective silanisation of five specific areas, each area to be silanised using a specific percentage of APTES in the isopropanol carrier ink. The 5 windows pattern did not consider the need of having a control cell population to serve as a comparative base for cell behaviour of the cellular populations growing on the amino-silanised windows.

For this reason a 6 windows screening array pattern was designed as shown in Figure 78. This design keeps the same window dimensions but reduces the width of the PEG-DA coating between cell populations in order to fit an extra window for the control cell population. Six windows of 5mm x 5mm are printed and arranged in a checker design where the areas for cell seeding are separated by a 1.25mm width PEG-DA cell repellent coating.

After the 6 windows cell screening array pattern was designed the PEG-DA area of the chip was printed and UV cured to confirm that a continuous coating of the cell repellent coating can be produced and that the width modification of PEG-DA and UV cured coating does not affect the fabrication of the areas where the silane modifications via inkjet printing are to be done.

The printed samples present the continuous cell repellent coating after one pass of printing, meaning that the pattern is only printed once on the piranha cleaned cover slip. Samples were printed with two passes (the designed patter is printed twice, one on top of each other) and showed better defined features.

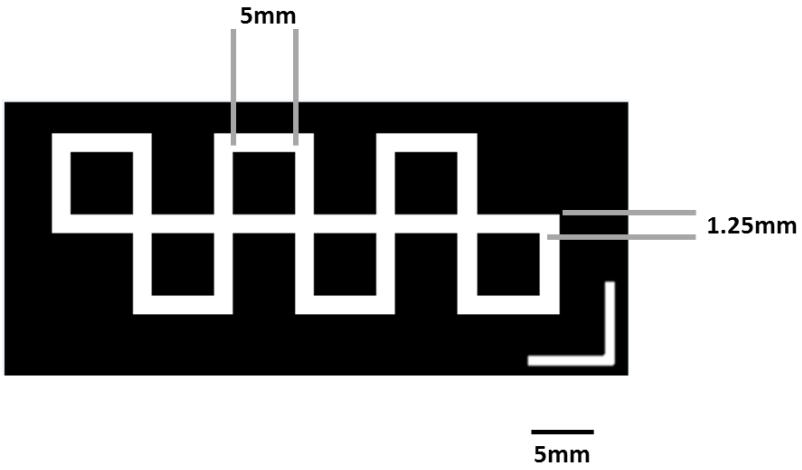

Figure 78 Design for a cell screening array with 6 windows for silane modification and cell population containment.

Figure 79 shows a two pass PEG-DA coating printed 6 windows pattern of the cell screening array, where a continuous coating of the cell repellent coating has been achieved allowing the isolation of the windows where the silane modifications are to be done and where cell populations are to be contained from one and other.

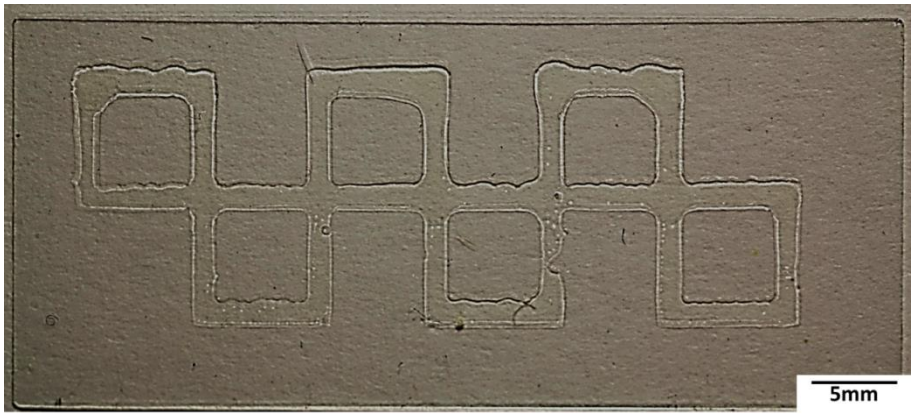

Figure 79 Inkjet printed PEG-DA sample using the 6 windows cell screening array design.

In order to assess the printing capabilities for higher throughput cell screening arrays a 40 windows screening array pattern was designed as shown in Figure 80. This design reduces the window for surface modification dimensions and reduces the width of the PEG-DA coating between cell populations in order to fit a larger amount of windows for the assessment of more cell populations. Forty windows of 2.5mm x 2.5mm are printed and arranged in a checker design where the areas for cell seeding are separated by a 1.25mm width PEG-DA cell repellent coating.

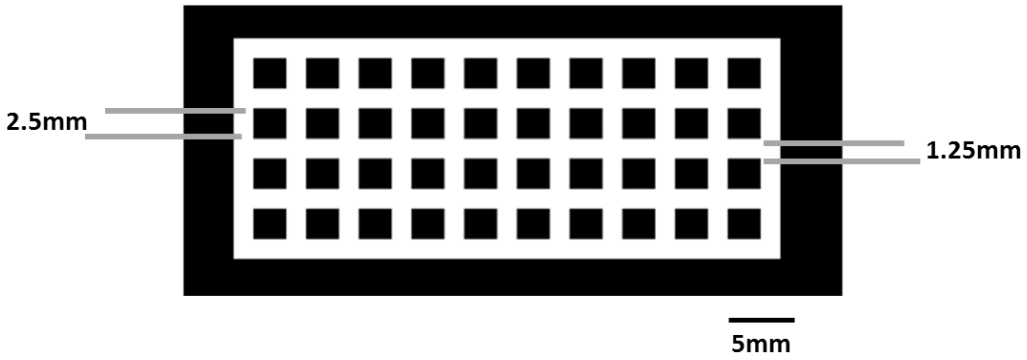

Figure 80 Design for a cell screening array with 40 windows for silane modification and cell population containment.

After the 40 windows cell screening array pattern was designed the PEG-DA area of the chip was printed and UV cured to confirm that a continuous coating of the cell repellent coating can be produced and that the width modification of PEG-DA and UV cured coating does not affect the fabrication of the areas where the silane modifications via inkjet printing are to be done.

Figure 81 shows a two pass PEG-DA coating printed 40 windows pattern of the cell screening array where a continuous coating of the cell repellent coating has been achieved allowing the isolation of the windows where the silane modifications are to be done and where cell populations are to be contained.

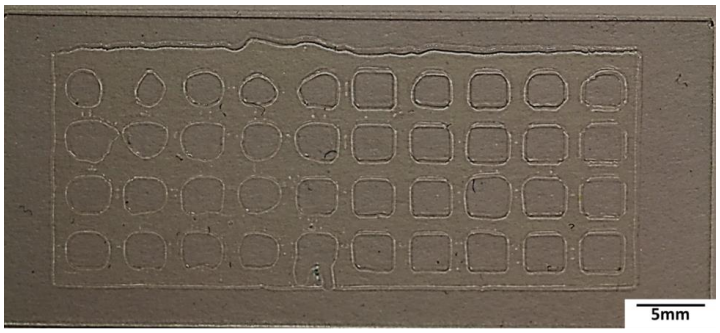

Figure 81 Inkjet printed PEG-DA sample using the 40 windows cell screening array design.

Due to the larger volume area of the printed PEG-DA cell repellent coating the internal flow of the ink when deposited on the substrate before curing deforms the designed pattern[189,190] so not all the forty inner windows maintain the squared shape but still are separated from one and other.

The reduction of size in the inner windows for the 40 windows screening array pattern also increases the difficulty of maintaining a viable cell population in a small area starting from the seeding process and then the cell culture for the required time.

The five windows pattern and six windows pattern have been selected as the designs to be used moving forward in this research since the PEG-DA coating prints of the cell repellent coating maintain a continuous coating that allows the containment of cell populations and also the 5mm x 5mm area of the windows to be silanised via inkjet printing allow the cell growth and proliferation for a cell population for an extended period of time.

6.4. Delamination of PEG coating under cell culture environment

Chapter 4 it describes how the PEG-DA UV curable inkjet printed formulation can be affected by the cell culture environment, in some cases causing the detachment or delamination of the cell repellent coating. For this reason the inkjet printed cell screening array patterns were exposed to the cell culture environment for 28 days in order to confirm that the printed PEG-DA UV curable coating can withstand this

environment without delaminating so the cell populations can be contained to their specific windows/areas for the duration of the cell response experiments.

The printed cell screening arrays were then exposed to the cell culture environment (incubation at 36 degrees Celsius and 5% CO_2). For this, the samples are washed with methanol to remove any excess PEG from the print. The samples are sterilised using 70% ethanol. Once sterile, the prints are submerged in cell culture media for 28 days to assess if the printed patterns can withstand the cell culture process without delamination.

Initial tests show delamination of the PEG-DA UV curable coating after 14 days in the cell culture environment as presented in Figure 82.

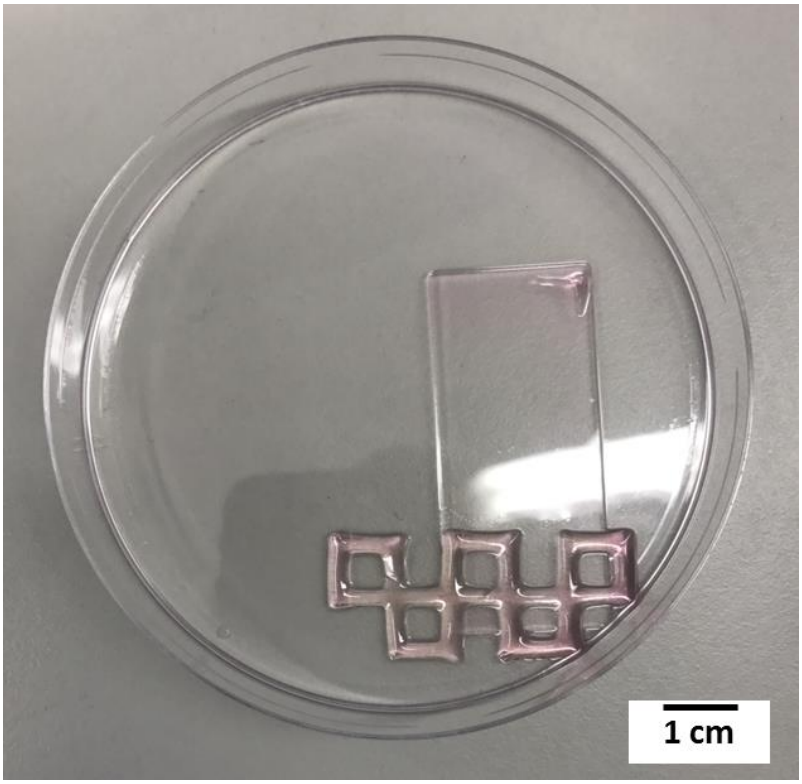

Figure 82 Delamination of PEG-DA UV curable coating in a 6 window cell screening array pattern after 14 days in cell culture environment.

The delamination of the cell repellent coating poses an important limitation to the project since it drives the duration of the experiments that can be carried out for cell response analysis. Stem cell differentiation studies require 28 days of cell culture to allow the cells to interact with their environment and start differentiating into different tissue cell types[232,233].

The physical forces of the cell culture media plus the biological effect of the cell culture media itself can be the cause of the 'peeling effect' or delamination showed by the inkjet printed samples.

Two main approaches were explored to avoid the delamination of the PEG-DA cell repellent coating before 28 days. The first is to reduce the thickness of the cell repellent coating so the effects of the 'pulling' forces of the cell culture media are reduced. The second approach is to re-assess the chemical binding of the PEG-DA UV curable coating to the piranha cleaned glass cover slips.

6.4.1. Cell repellent coating thickness reduction

In order to reduce the thickness of the coating the printed samples can be printed with only one pass (the pattern is to be printed only once on the piranha cleaned glass slide) reducing the volume of PEG-DA deposited on the substrate by half.

The thickness of a film can be calculated using

Equation 5, where m is the mass of the printed material, ρ is the density of the ink and A is the area of the printed pattern.

Equation 5 Formula for calculating film thickness.

$$th = \frac{m}{\rho A}$$

In order to calculate the mass of the printed material the piranha cleaned glass slides were weighted before and after curing. The mass differential between printed and non-printed glass slides is the mass of the printed material, in this case the PEG-DA UV curable ink.

Table 7 shows film thickness measurements of both 5 and 6 windows chip patterns printed with one and two passes to show the film thickness reduction from 2 pass to 1 pass prints of the PEG-DA UV curable cell repellent coating. The presented thickness was calculated using the mass of the printed sample after the UV curing of the cell repellent coating. Ten samples of each iteration were measured for the calculations of the film thickness, the average of the measurements are the presented values.

Table 7 PEG-DA UV cured film thickness calculation for 5 windows and 6 windows printed with 1 and 2 passes.

Printed pattern	Density of ink (g/mL)	Mass of printed material (gr)	Area of print (mm^2)	Thickness (mm)
5 window design (2 pass)	1.086	0.0098	403.75	0.020
5 window design (1 pass)	1.086	0.0055	403.75	0.012
6 window design (2 pass)	1.086	0.0053	225.65	0.022

6 window design (1 pass)	1.086	0.0025	225.65	0.010

The printed samples with the reduced thickness were exposed to the cell culture environment until any possible delamination started. The samples withstood 21 days in cell culture before the delamination of the PEG-DA UV curable film started. An improvement on the 14 days that the 2 pass printed samples withstand in the cell culture environment but still 7 days short to the aim of 28 days without delamination, showing that the reduction of the film thickness play an important role on the delamination effect.

6.4.2. Chemical binding improvement of cell repellent coating to glass substrate

According to literature, the silanisation of a substrate can be improved when the silanised sample is 'baked' in an oven for 4 hours at 100°C[205]. The silanisation process leaves water molecules from when the $-CH_3$ groups at the end of the silane molecule interact with the –OH groups present on the surface of the piranha cleaned glass cover slips[205]. Since the silanisation agent is dissolved in the PEG-DA UV curable formulation, when deposited and cured the surface area of the printed and cured coating can hold water molecules between the cell repellent coating and the substrate.

In order to avoid having water molecules trapped between the coating and the substrate the samples can be dried removing all traces of water by keeping them in an oven for 4 hours at 100°C. Samples of the 5 and 6 window patterns were printed with

one and two passes. The printed samples were then UV cured and baked in an oven for 4 hours at 100°C. The UV cured and baked samples were then exposed to the cell culture environment until any delamination started.

The samples printed with 2 passes withstood 24 days in cell culture before the delamination of the PEG-DA UV curable coating started. An improvement on the 14 days that the 2 pass printed samples without baking withstand in the cell culture environment but still short to the aim of 28 days without delamination. The samples printed with 1 passes withstood 35 days in cell culture before the delamination of the PEG-DA UV curable coating started surpassing the aim of 28 days allowing this methodology to be used for the production of the cell screening arrays to assess cell response to APTES modified surfaces. Five samples of each iteration of cell screening arrays were used in the described experiment. The day of delamination presented corresponds to that of the sample of each iteration the presented delamination first.

6.5. Cellular response on inkjet printed screening arrays

After the cell density optimisation for human mesenchymal stem cells (hMSC) it was defined that, in order to have a viable cell population after 28 days in culturing, 5,000 cells were to be seeded in the 5mm x 5mm APTES modified and control windows of the 6 windows cell screening array.

A series of 6 window cell screening arrays were printed using the printing parameters for the PEG-DA based ink and the APTES in isopropanol inks defined and discussed in Chapter 4 and Chapter 5 respectively. A total of 30,000 hMSC were seeded in the designated areas of the screening array for cell population proliferation. Six windows in total, the control glass and five different iterations of the APTES ink, each seeded with 5000 hMSC. The cell seeding protocol is described in the experimental chapter.

Figure 83 shows the AFM measurements and roughness values of a piranha cleaned glass coverslip and samples printed using the different iterations of APTES in isopropanol ink formulations (from 1% APTES to 9% APTES). This figure will be used to compare how the difference in roughness and topography caused by the silanisation via inkjet printing has an effect on cell viability and overall cell population density.

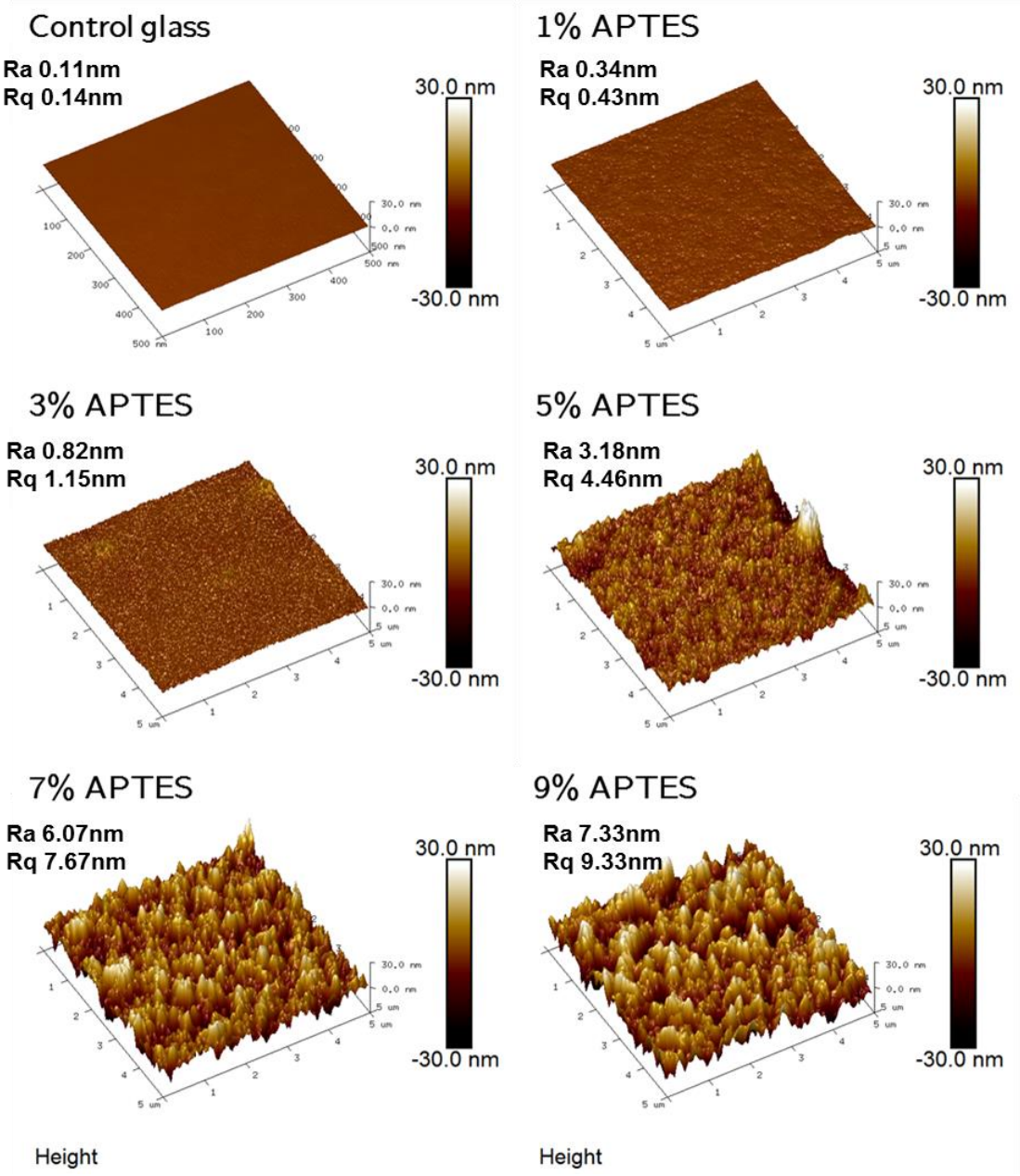

Figure 83 AFM measurements of a piranha cleaned control glass cover slips and samples printed with the different iterations of silane inks showing the change in topography and roughness values.

In Figure 84 the population of hMSC seeded on the control glass is presented. Images were taken over four different periods of time to see the change in behaviour of the cell population at different stages. The images presented in Figure 84 will serve as a comparison point for the images taken of the cells populations growing on the APTES modified windows of the screening array.

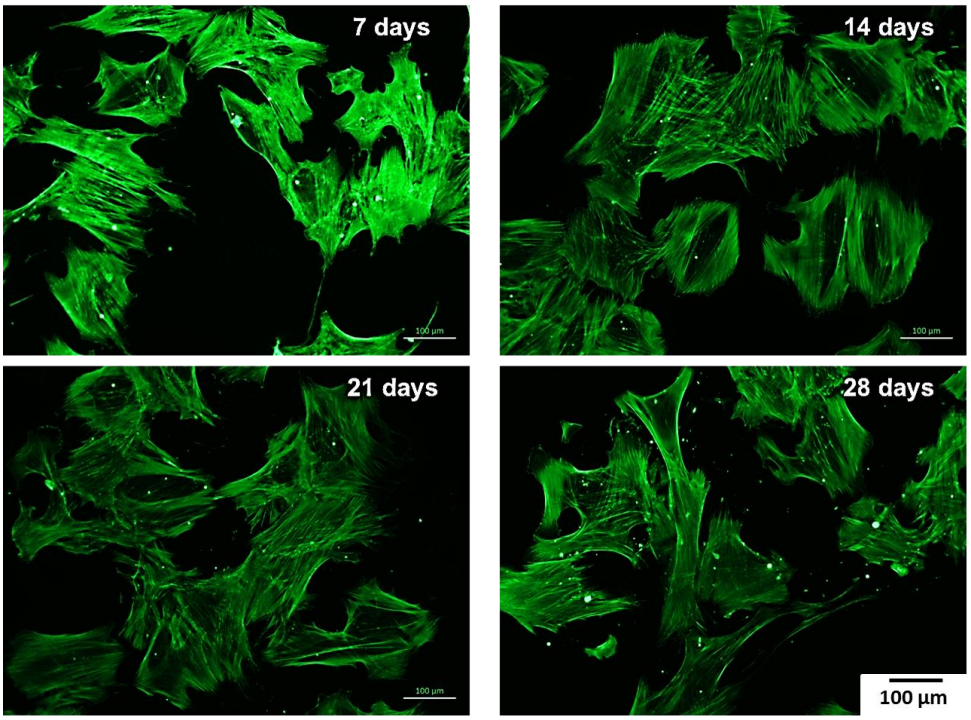

Figure 84 hMSC seeded on control window of the 6 windows screening array and cultured over different periods of time. 5,000 cells were seeded per window. Images taken by fluorescent microscopy after dying the cells with Oregon Green.

It is important to consider that the APTES modification of the glass cover slips is not only a chemical modification but also a physical modification. By inkjet printing the 1% APTES formulation the surface roughness and topography was modified when compared to that of a control un-modified glass sample as shown in Figure 83.

In Figure 85 the population of hMSC seeded on the 1% APTES modified window of the 6 windows cell screening array is shown. Images were taken over four different periods of time to see the change in behaviour of the cell population at different stages. It can be observed that the seeded cells have adhered to the 1% APTES modified glass substrate. Over the observed periods of time the cell population shows to be growing and spreading over the modified area.

The shape of the cells presented in Figure 85 is very close to that of the cells growing on the control window but the cells growing on the 1% APTES modified window show more spreading of the cell. This change of shape can be seen via the stress fibres of the cells that have been dyed with Oregon Green. The surface roughness of the 1% APTES modified sample shows to be adequate for cell adhesion and proliferation.

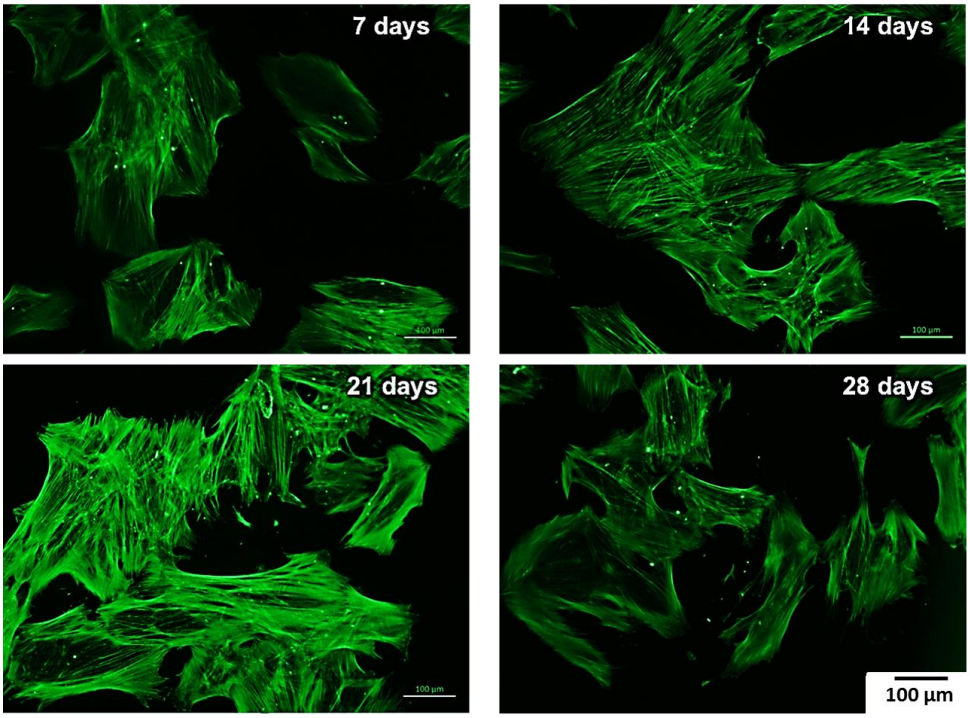

Figure 85 hMSC seeded on the 1% APTES modified window of the 6 windows screening array and cultured over different periods of time. 5,000 cells were seeded per window. Images taken by fluorescent microscopy after dying the cells with Oregon Green.

By inkjet printing the 3% APTES formulation the surface roughness and topography was modified when compared to that of a control un-modified glass sample as shown in Figure 83. In Figure 86 the population of hMSC seeded on the 3% APTES modified window of the 6 windows cell screening array is shown. Images were taken over four different periods of time to see the change in behaviour of the cell population at different stages. It can be observed that the seeded cells have adhered to the 3% APTES modified glass substrate. Cells show to be growing and spreading on the silane modified area and show that the 3% APTES modified environment is positive for growing a cell population. Over the observed periods of time the cell population shows to be growing and spreading over the modified area. The surface roughness of the 3% APTES modified sample shows to be adequate for cell adhesion and proliferation.

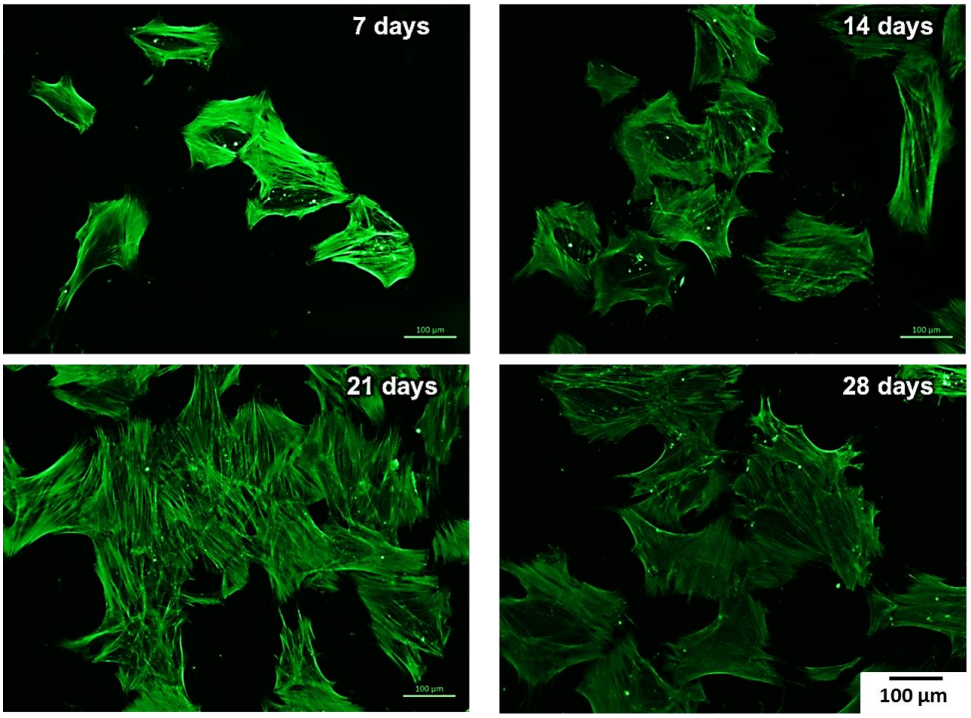

Figure 86 hMSC seeded on the 3% APTES modified window of the 6 windows screening array and cultured over different periods of time. 5,000 cells were seeded per window. Images taken by fluorescent microscopy after dying the cells with Oregon Green.

By inkjet printing the 5% APTES formulation the surface roughness and topography was modified when compared to that of a control un-modified glass sample as shown in Figure 83. In Figure 87 the population of hMSC seeded on the 5% APTES modified window of the 6 windows cell screening array is shown. Images were taken over four different periods of time to see the change in behaviour of the cell population at different stages. It can be observed that the seeded cells have adhered to the 5% APTES modified glass substrate. Cells show to be growing and spreading but an apparent change in shape and spread of cell population can be observed.

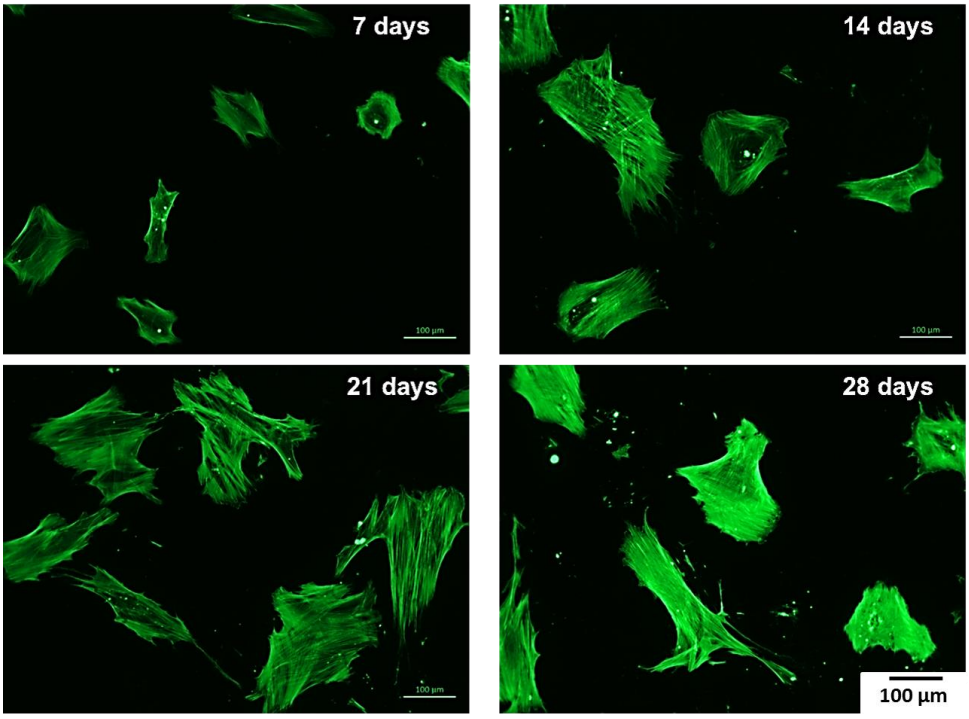

Figure 87 hMSC seeded on the 5% APTES modified window of the 6 windows screening array and cultured over different periods of time. 5,000 cells were seeded per window. Images taken by fluorescent microscopy after dying the cells with Oregon Green.

When compared to the control samples in Figure 84 it can be seen that the individual cells do not spread as cells in the control sample do. hMSC in the 5% APTES modified window show a more compact shape. This change in morphology and cell

population density can be attributed to the increased roughness of the sample after the 5% APTES modification.

By inkjet printing the 7% APTES formulation the surface roughness and topography was modified when compared to that of a control un-modified glass sample as shown in Figure 83. In Figure 88 the population of hMSC seeded on the 7% APTES modified window of the 6 windows cell screening array is shown. Images were taken over four different periods of time to see the change in behaviour of the cell population at different stages. It can be observed that the seeded cells have adhered to the 7% APTES modified glass substrate. Cells show to be growing and spreading but an apparent change in shape and spread of cell population can be observed specially in the initial 7 days and the end of 28 days.

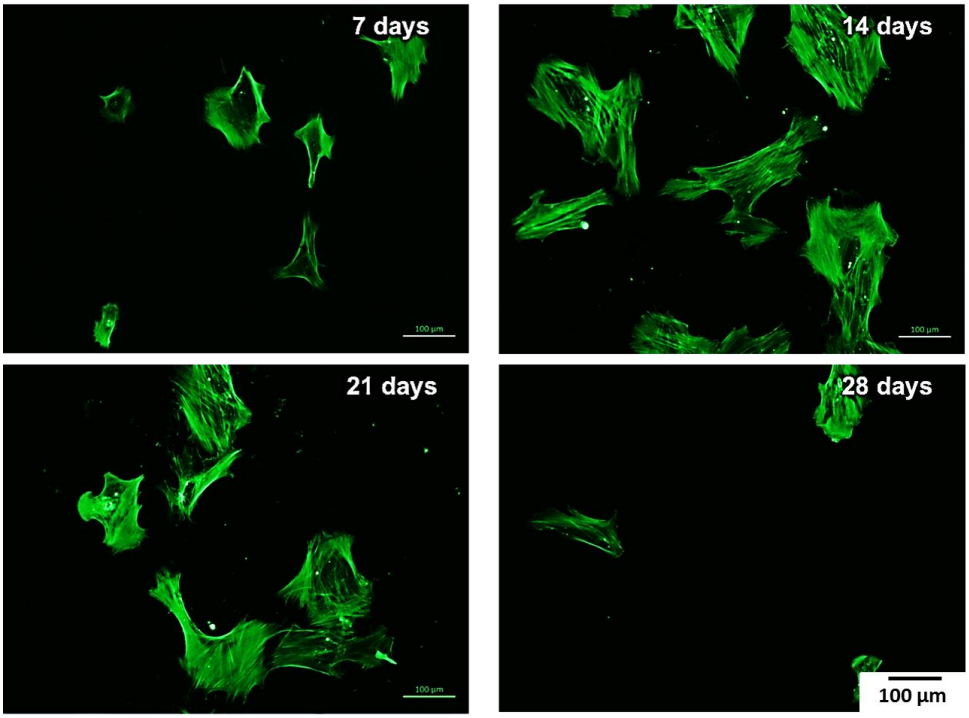

Figure 88 hMSC seeded on the 7% APTES modified window of the 6 windows screening array and cultured over different periods of time. 5,000 cells were seeded per window. Images taken by fluorescent microscopy after dying the cells with Oregon Green.

When compared to the control samples in Figure 84 it can be seen that the individual cells do not spread as cells in the control sample do. hMSC in the 7% APTES modified window show a more compact shape. This change in morphology and cell population density can be attributed to the increased roughness of the sample after the 7% APTES modification.

By inkjet printing the 9% APTES formulation the surface roughness and topography was modified when compared to that of a control un-modified glass sample as shown in Figure 83. In Figure 89 the population of hMSC seeded on the 9% APTES modified window of the 6 windows cell screening array is shown. Images were taken over four different periods of time to see the change in behaviour of the cell population at different stages. It can be observed that the seeded cells have adhered to the 9% APTES modified glass substrate. Cells do not show to be growing or spreading and a very noticeable change in shape and spread of cell population can be observed throughout the 28 days.

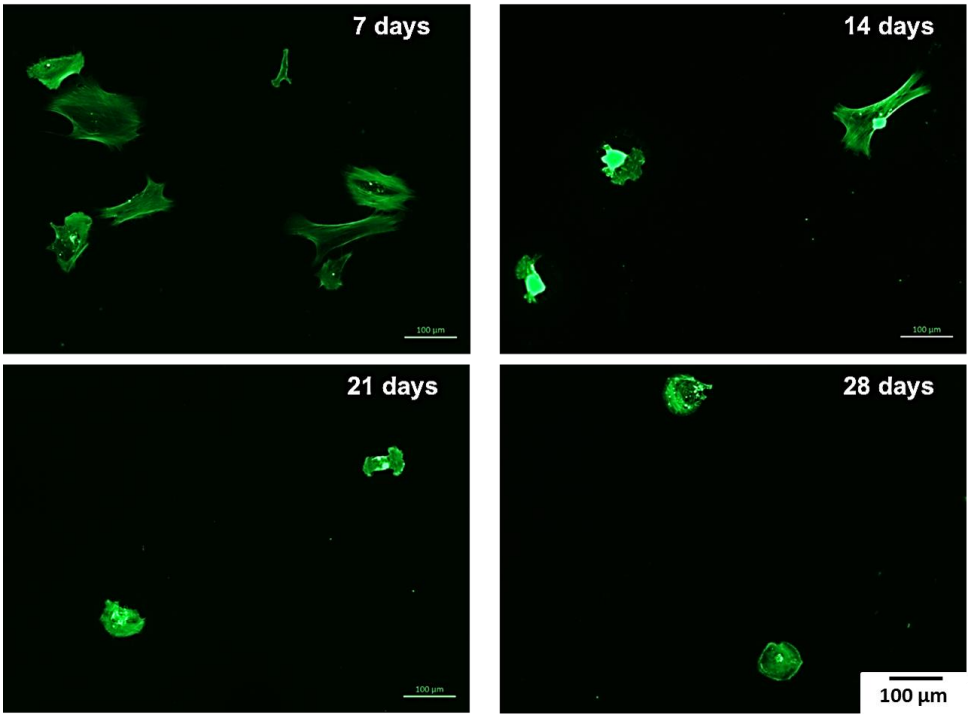

Figure 89 hMSC seeded on the 9% APTES modified window of the 6 windows screening array and cultured over different periods of time. 5,000 cells were seeded per window. Images taken by fluorescent microscopy after dying the cells with Oregon Green.

When compared to the control samples in Figure 84 it can be seen that the individual cells do not spread as cells in the control sample do. hMSC in the 9% APTES modified window show a more compact shape, almost circular. This change in morphology and cell population density can be attributed to the increased roughness of the sample after the 9% APTES modification.

The cell behaviour results observed in this chapter prove that an inkjet printed cell screening array for analysing cellular response of different materials in a single 'chip' can be achieved by using a PEG-DA based cell repellent coating and APTES modification of a glass cover slip.

Cells show to adhere and grow on all iterations of the APTES modified windows of the screening array. However cells demonstrate to prefer the windows where lower APTES concentrations were printed and it can be related to the roughness of the substrate surface where they were seeded as seen in Figure 90.

Studies have shown that surface topography plays an important role in the viability of cells on a substrate[78,181,236,237]. It has been demonstrated by Ranella et al[236] that the increase in roughness of a substrate has a direct impact on cell viability. Wettability also plays an important role on cell adhesion. When super-hydrophobicity levels are achieved on a substrate due to its topography, cell viability decreases[236–238]. Surface roughness and chemical composition have proven to be factors that drive cell viability, and have the potential (when optimised) to drive stem cell differentiation[34,232,234,236–240]. The results presented in this chapter confirm that the increase in surface roughness has a direct impact on the decrease of cell viability. It has also been demonstrated that the increase in surface roughness is directly linked to the increase of APTES being deposited via inkjet printing.

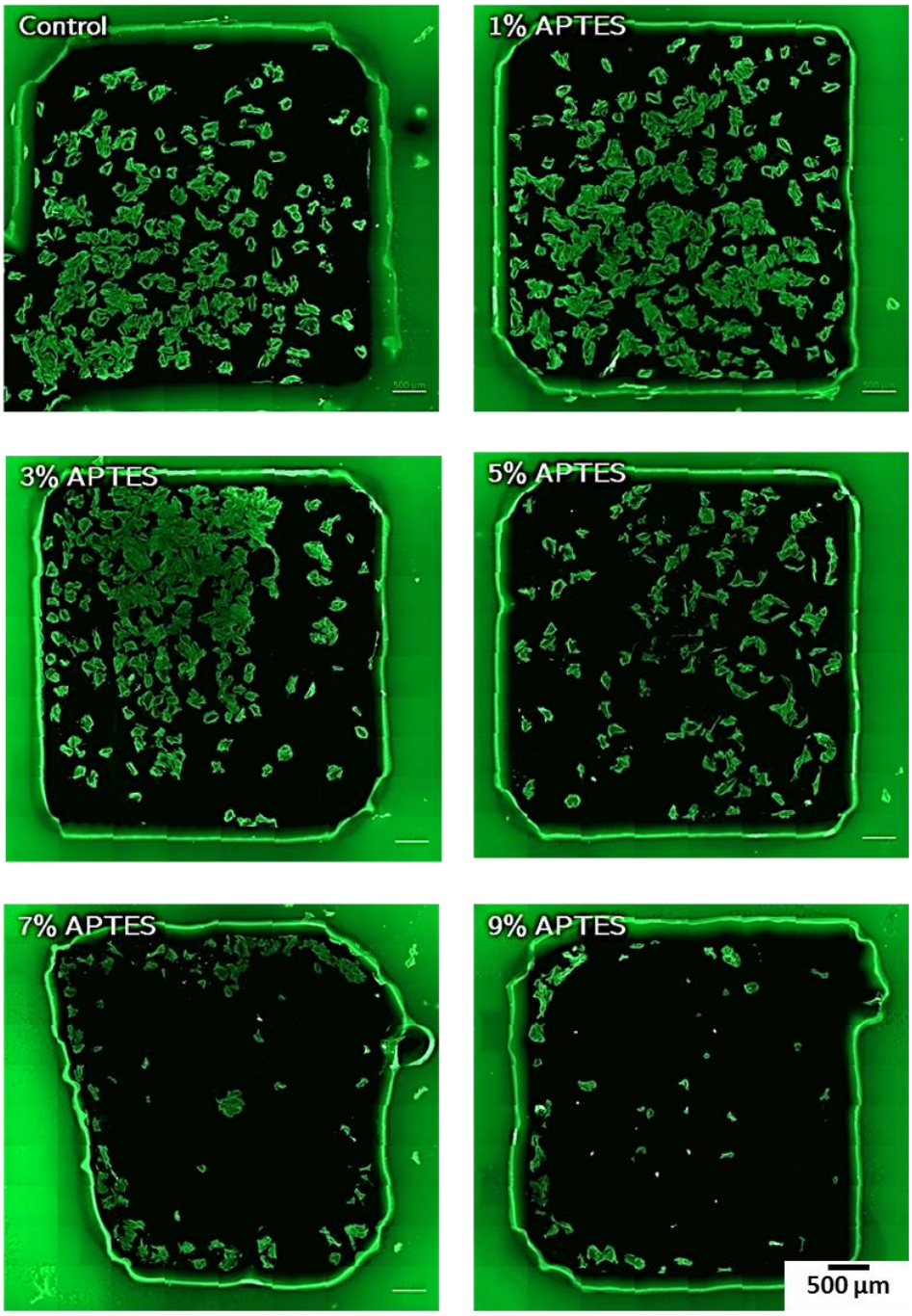

Figure 90 PEG-DA cell repellent coating areas showing containment of hMSC populations seeded on a control (unmodified) glass cover slip and areas modified with the different APTES ink formulations. 5000 cells seeded per window and cultured for 28 days. Images taken by fluorescent microscopy after dying the cells with Oregon Green.

6.6. Summary

In this chapter it has been demonstrated that cell screening arrays can be manufactured using the inkjet printing technology. The cell screening arrays consist of a cell repellent coating used to contain cell populations and 'cell active' inks (APTES in isopropanol carrier inks) used to selectively modify the substrate where the cell populations grow.

A manufacturing process has been optimised for cell repellent and cell active inks, where the cell repellent coating has to be UV cured and the final print with both the cell repellent coating and cell active coating is dried in an oven to improve the silanisation process.

The cell screening arrays manufactured via inkjet printing have proven to successfully contain human mesenchymal stem cell (hMSC) populations to the APTES modified substrates. The 'cell active' modified windows within the cell screening arrays, show a difference in cell density and cellular morphology after 28 days in cell culture, confirming that the APTES chemistry is not toxic to the cells and showing that there is a direct correlation between surface roughness and cell population density. Because the manufactured screening arrays have proven to withstand at least 28 days in cell culture, it means that the arrays are applicable for starting to analyse stem cells for differentiation by the use of immunochemistry.

Chapter 7

Conclusions and future work

7.1. Introduction

In summary, inkjet printing of a PEG based ink for the manufacturing of cell repellent coatings and inkjet printing of isopropanol containing APTES inks for surface modification of glass have been investigated, for the manufacturing of cell screening arrays. A novel method of immobilising PEG on a glass substrate has been developed, in order to produce continuous cell repellent coatings via inkjet printing that can withstand cell culture environment conditions for at least 28 days. The main purpose of printing the cell repellent coatings is being able to contain cell populations to specific locations, so cell screening arrays can be manufactured.

7.2. Conclusions

In Chapter 4 inkjet printing of a PEG based cell repellent coatings was investigated. Three different approaches for immobilising PEG on a glass substrate were explored: a physical approach (dip coating on water soluble PEG flakes), chemical binding of PEG on a glass slide (a PEG molecule with a silane ending) and UV curable PEG approach. The physical and chemical binding processes proved to be unstable, therefore not suitable for repelling cell adhesion since the produced coatings allow cell adhesion and proliferation. However, the UV curable approach of immobilising PEG on the glass substrate (via spin coating) proved to avoid cell adherence due to its stable high density of PEG and continuous coverage of the surface.

Rheological analyses were carried out on the UV curable PEG formulation in order to confirm the potential of translating it to inkjet printing. Printing experiments confirm that the UV curable PEG formulation can be printed through a 0.08mm printer head, although continuous UV curable PEG coatings could not be manufactured.

In order to produce continuous cell repellent coatings via inkjet printing, a novel ink was developed. The new ink improves the wettability of the formulation when deposited on the substrate and allows the PEG to be chemically bound with the glass substrate. Continuous stable cell repellent UV curable PEG coatings were produced using the novel formulation, and the cell repellent coatings proved to be able to contain cell populations to specific areas.

Chapter 5 explored the surface modification of a glass substrate by depositing APTES in different solutions on glass. Amino-silanisation using APTES has shown to have an effect on hMSC differentiation, for this reason APTES was selected. Isopropanol was

used as the carrier solution for the APTES inks since it has been used for inkjet printing of other materials. Five ink formulations were developed for surface modification of glass: 1% APTES in isopropanol (v/v), 3% APTES in isopropanol (v/v), 5% APTES in isopropanol (v/v), 7% APTES in isopropanol (v/v) and 9% APTES in isopropanol (v/v).

The visualisation of the APTES inks after printing proved to be difficult since they are transparent. The inclusion of dyes and an after printing analysis of the APTES formulations were investigated but were unable to show the prints. However, surface characterisation techniques were utilised in order to confirm that the APTES present in the formulation had modified the glass substrate. The changes in contact angle of water on the modified show that there has been a change in the surface energy that can be attributed to the deposited ink formulations on the substrate. The use of FTIR confirms that there has been a chemical modification by showing the presence of $-NH_2$ on the glass substrate. The change in topography and surface roughness has also been confirmed by the use of AFM. With the information collected from the surface characterisation techniques it is confirmed that the glass substrate has been amino-silanised with APTES via inkjet printing, an amino-silanisation process never used before.

In Chapter 6, the manufacturing of cell screening arrays with the ink formulations developed in Chapter 4 and Chapter 5 was explored. The cell screening arrays consist of areas that have been amino-silanised, using different concentrations of APTES, surrounded by a cell repellent coating (UV curable PEG based formulation). Cell populations can then be contained to specific amino-silanised areas so their behaviour on the different iterations of APTES modified areas can be studied.

Different designs of cell screening arrays were developed but it was decided to use a 6 windows screening array, so the five different APTES in isopropanol inks could be assessed (in terms of cell response) while still having an unmodified window to be used as a control sample. The cell repellent coating developed in Chapter 4 proved to be able to contain hMSC cell populations to specific locations.

In order to manufacture cell screening arrays that can be used to assess stem cell differentiation it was paramount to make sure the printed screening arrays could withstand the cell culture environment for at least 28 days (the time period needed for stem cell differentiation analysis via immunochemistry). The produced cell screening arrays proved to withstand the cell culture environment conditions for the desired time frame.

Finally, hMSC were seeded on the inkjet printed cell screening arrays and the cell populations contained to different surface chemistries/topographies were compared to each other and the control sample after 28 days in cell culture. The main result shown by the cell screening arrays is that there was an hMSC cell population density decrease directly linked to the increase of APTES deposited on the glass substrate. A change in cell morphology can also be observed in the windows that have a higher presence of APTES in the surface, further optimisation of the APTES inks will define the optimal surface modifications via inkjet printing using APTES inks to drive stem cell differentiation.

7.3. Future work

The investigation carried out in this thesis has raised further questions, which are beyond the scope of the project here presented. The following areas are considered to continue the research for the manufacturing of cell screening arrays via inkjet printing:

- APTES ink concentration optimisation for stem cell differentiation:

With the current research, it has been proven that a glass substrate can be amino-silanised with APTES via inkjet printing. A wider range of APTES concentrations can then be investigated to assess which concentration is optimal for driving stem cell differentiation towards bone tissue formation.

- Further optimisation of cell culture process for stem cell differentiation analysis:

In order to assess stem cell differentiation by the use of immunochemistry, it is paramount to have a dense cell population. With immunochemistry different dyes are used as markers for specific proteins and cell fibres that can show changes in the cells. At the moment the stem cell populations contained by the UV curable PEG based coating are not dense enough to carry out these analyses.

- Manufacturing of other cell active inks:

The use of APTES for modifying the glass substrate allows leaving $-NH_2$ groups on the surface for cells to interact with them. Different chemistries for ink formulations could be developed to selectively modify the cell active areas of the cell screening arrays. Formulations with varying concentrations of –OH groups to be deposited on the substrate can be optimised to drive stem cell differentiation towards cartilage cells. Formulations with varying concentrations of $-CH_3$ groups to be deposited on the glass substrate can be optimised to maintain and enhance the stem cell phenotype.

- Manufacturing of 3D scaffolds with specific surface chemistries:

With the potential information gathered from the cell screening arrays, an optimum concentration of the different surface chemistries will show stem cell differentiation which will allow to manufacture 3D scaffolds with specific surface chemistries in order to promote stem cell differentiation, allowing the manufacturing of tailor made living bone and cartilage implants.

References

1. Curran JM, Chen R, Hunt JA. Controlling the phenotype and function of mesenchymal stem cells in vitro by adhesion to silane-modified clean glass surfaces. Biomaterials. 2005;26(34):7057–67.

2. Curran JM, Pu F, Chen R, Hunt JA. The use of dynamic surface chemistries to control msc isolation and function. Biomaterials. 2011;32(21):4753–60.

3. Arai K, Iwanaga S, Toda H, Genci C, Nishiyama Y, Nakamura M. Three-dimensional inkjet biofabrication based on designed images. Biofabrication. 2011;3(3).

4. Yamaguchi S, Ueno A, Akiyama Y, Morishima K. Cell patterning through inkjet printing of one cell per droplet. Biofabrication. 2012;4(4).

5. Boland T, Tao X, Damon BJ, Manley B, Kesari P, Jalota S, et al. Drop-on-demand printing of cells and materials for designer tissue constructs. Mater Sci Eng C. 2007;27(3):372–6.

6. Gross A, Schöndube J, Niekrawitz S, Streule W, Riegger L, Zengerle R, et al. Single-Cell Printer: Automated, On Demand, and Label Free. J Lab Autom. 2013;18(6):504–18.

7. Roth EA, Xu T, Das M, Gregory C, Hickman JJ, Boland T. Inkjet printing for

high-throughput cell patterning. Biomaterials. 2004;25(17):3707–15.

8. Mironov V, Trusk T, Kasyanov V, Little S, Swaja R, Markwald R. Biofabrication: A 21st century manufacturing paradigm. Biofabrication. 2009;1(2).

9. Sirringhaus H, Shimoda T. Inkjet Printing of Functional Materials. MRS Bull. 2003;28(11):802–6.

10. Creagh LT, McDonald M. Design and Performance of Inkjet Print Heads for Non-Graphic-Arts Applications. MRS Bull. 2003;28(11):807–11.

11. Khan MS, Fon D, Li X, Tian J, Forsythe J, Garnier G, et al. Biosurface engineering through ink jet printing. Colloids Surfaces B Biointerfaces. 2010;75(2):441–7.

12. Curran JM, Chen R, Hunt JA. The guidance of human mesenchymal stem cell differentiation in vitro by controlled modifications to the cell substrate. Biomaterials. 2006;27(27):4783–93.

13. Ferris CJ, Gilmore KG, Wallace GG, In Het Panhuis M. Biofabrication: An overview of the approaches used for printing of living cells. Appl Microbiol Biotechnol. 2013;97(10):4243–58.

14. Jakab K, Norotte C, Marga F, Murphy K, Vunjak-Novakovic G, Forgacs G. Tissue engineering by self-assembly and bio-printing of living cells. Biofabrication. 2010;2(2).

15. Deravi L, Wright D, Sumerel J. Printing bioinks with technologically relevant applications. Chem Ink jet Inks [Internet]. 2009;269–82. Available from: http://f3.tiera.ru/2/Ch_Chemistry/Magdassi S. (ed.) The Chemistry of Inkjet

Inks (WS, 2010)(ISBN 9812818219)(339s)_Ch_.pdf#page=265

16. Mrksich M, Whitesides GM. Patterning self-assembled monolayers using microcontact printing: A new technology for biosensors? Trends Biotechnol. 1995;13(6):228–35.

17. Snyder PW, Johannes MS, Vogen BN, Clark RL, Toone EJ. Biocatalytic microcontact printing. J Org Chem. 2007;72(19):7459–61.

18. NAKANISHI J, TAKARADA T, YAMAGUCHI K, MAEDA M. Recent Advances in Cell Micropatterning Techniques for Bioanalytical and Biomedical Sciences. Anal Sci [Internet]. 2008;24(1):67–72. Available from: http://joi.jlc.jst.go.jp/JST.JSTAGE/analsci/24.67?from=CrossRef

19. Xia Y, Rogers JA, Paul KE, Whitesides GM. Unconventional Methods for Fabricating and Patterning Nanostructures. Chem Rev [Internet]. 1999;99(7):1823–48. Available from: http://pubs.acs.org/doi/abs/10.1021/cr980002q

20. Hudd A. Inkjet Printing Technologies. Chem inkjet inks [Internet]. 2010;3–18. Available from: http://www.oki.com/en/otr/downloads/otr-161-10.pdf%5Cnhttp://books.google.com/books?hl=en&lr=&id=Rl1CsTwRrfYC&oi=fnd&pg=PA1&dq=Part+I:+Basic+concepts&ots=qSuzTdExY8&sig=0hoMyXOAgsJuoqFEcf6uf85AS2c

21. Park JU, Hardy M, Kang SJ, Barton K, Adair K, Mukhopadhyay DK, et al. High-resolution electrohydrodynamic jet printing. Nat Mater. 2007;6(10):782–9.

22. Deravi LF, Gerdon AE, Cliffel DE, Wright DW, Sumerel JL. Output analysis of materials inkjet printer. Appl Phys Lett. 2007;91(11):7–10.

23. Kingshott P, Griesser HJ. Surfaces that resist bioadhesion. Curr Opin Solid State Mater Sci. 1999;4:403–12.

24. Krishnan S, Weinman CJ, Ober CK. Advances in polymers for anti-biofouling surfaces. J Mater Chem. 2008;18(29):3405–13.

25. Magin CM, Cooper SP, Brennan AB. Non-toxic antifouling strategies. Mater Today [Internet]. 2010;13(4):36–44. Available from: http://dx.doi.org/10.1016/S1369-7021(10)70058-4

26. Chambers LD, Stokes KR, Walsh FC, Wood RJK. Modern approaches to marine antifouling coatings. Surf Coatings Technol [Internet]. 2006;201(6):3642–52. Available from: http://dx.doi.org/10.1016/j.surfcoat.2006.08.129

27. Werner C, Maitz MF, Sperling C. Current strategies towards hemocompatible coatings. J Mater Chem [Internet]. 2007;17(32):3376. Available from: http://xlink.rsc.org/?DOI=b703416b

28. Wisniewski N, Reichert M. Methods for reducing biosensor membrane biofouling. Colloids Surfaces B Biointerfaces. 2000;18(3–4):197–219.

29. Revzin A, Tompkins RG, Toner M. Surface engineering with poly(ethylene glycol) photolithography to create high-density cell arrays on glass. Langmuir. 2003;19(23):9855–62.

30. Ratner BD. New ideas in biomaterials science—a path to engineered biomaterials. J Biomed Mater Res [Internet]. 1993 Jul;27(7):837–50. Available from: http://doi.wiley.com/10.1002/jbm.820270702

31. Rasi Ghaemi S, Harding F, Delalat B, Vasani R, Voelcker NH. Surface

engineering for long-term culturing of mesenchymal stem cell microarrays. Biomacromolecules. 2013;14(8):2675–83.

32. Bilbaut T, Gachon AM, Dastugue B. Deposits on soft contact lenses. Electrophoresis and scanning electron microscopic examinations. Exp Eye Res. 1986;43(2):153–65.

33. ANDRADE JD, HLADY V. Plasma Protein Adsorption: The Big Twelve. Ann N Y Acad Sci [Internet]. 1987 Dec;516(1 Blood in Cont):158–72. Available from: http://doi.wiley.com/10.1111/j.1749-6632.1987.tb33038.x

34. Ayala R, Zhang C, Yang D, Hwang Y, Aung A, Shroff SS, et al. Engineering the cell-material interface for controlling stem cell adhesion, migration, and differentiation. Biomaterials [Internet]. 2011;32(15):3700–11. Available from: http://dx.doi.org/10.1016/j.biomaterials.2011.02.004

35. Lang AW, Motta P, Hidalgo P, Westcott M. Bristled shark skin: A microgeometry for boundary layer control? Bioinspiration and Biomimetics. 2008;3(4).

36. Scardino A, De Nys R, Ison O, O'Connor W, Steinberg P. Microtopography and antifouling properties of the shell surface of the bivalve molluscs Mytilus galloprovincialis and Pinctada imbricata. Biofouling. 2003;19(SUPPL.):221–30.

37. Bers AV, Wahl M. The Influence of Natural Surface Microtopographies on Fouling. Biofouling [Internet]. 2004 Feb;20(1):43–51. Available from: http://www.tandfonline.com/doi/abs/10.1080/08927010410001655533

38. Hamming LM, Phillip B. Fouling Resistant Biomimetic Poly(Ethylene Glycol) Based Grafted Polymer Coatings. Mater Matters [Internet]. 2008;3(3):52.

Available from: https://www.sigmaaldrich.com/content/dam/sigma-aldrich/articles/material-matters/pdf/fouling-resistant0.pdf

39. Chen S, Li L, Zhao C, Zheng J. Surface hydration: Principles and applications toward low-fouling/nonfouling biomaterials. Polymer (Guildf) [Internet]. 2010;51(23):5283–93. Available from: http://dx.doi.org/10.1016/j.polymer.2010.08.022

40. Tse CCW, Ng SS, Stringer J, MacNeil S, Haycock JW, Smith PJ. Utilising Inkjet Printed Paraffin Wax for Cell Patterning Applications. Int J Bioprinting [Internet]. 2016;2(0). Available from: http://ijb.whioce.com/index.php/int-j-bioprinting/article/view/02001

41. Carman ML, Estes TG, Feinberg AW, Schumacher JF, Wilkerson W, Wilson LH, et al. Engineered antifouling microtopographies – correlating wettability with cell attachment. Biofouling [Internet]. 2006 Jan;22(1):11–21. Available from: http://www.tandfonline.com/doi/abs/10.1080/08927010500484854

42. Kooten TG Van, Recum AF Von. Cell Adhesion to Textured Silicone Surfaces: The Influence of Time of Adhesion and Texture on Focal Contact and Fibronectin Fibril Formation. Tissue Eng [Internet]. 1999 Jun;5(3):223–40. Available from: https://www.liebertpub.com/doi/10.1089/ten.1999.5.223

43. Chung KK, Schumacher JF, Sampson EM, Burne RA, Antonelli PJ, Brennan AB. Impact of engineered surface microtopography on biofilm formation of Staphylococcus aureus. Biointerphases [Internet]. 2007 Jun;2(2):89–94. Available from: http://avs.scitation.org/doi/10.1116/1.2751405

44. Baier RE. Surface behaviour of biomaterials: The theta surface for biocompatibility. J Mater Sci Mater Med. 2006;17(11):1057–62.

45. Chang Y, Liao SC, Higuchi A, Ruaan RC, Chu CW, Chen WY. A highly stable nonbiofouling surface with well-packed grafted zwitterionic polysulfobetaine for plasma protein repulsion. Langmuir. 2008;24(10):5453–8.

46. Owens NF, Gingell D, Rutter PR. Inhibition of cell adhesion by a synthetic polymer adsorbed to glass shown under defined hydrodynamic stress. J Cell Sci. 1987;87 (Pt 5)(1978):667–75.

47. Alcantar N a, Aydil ES, Israelachvili JN. Polyethylene glycol – coated biocompatible surfaces. J Biomed Mater Res. 2000;51(August 1999):343–51.

48. Jeon S., Lee J., Andrade J., De Gennes P. Protein—surface interactions in the presence of polyethylene oxide. J Colloid Interface Sci [Internet]. 1991 Mar;142(1):149–58. Available from: http://linkinghub.elsevier.com/retrieve/pii/0021979791900438

49. Kjellander R, Florin E. Water structure and changes in thermal stability of the system poly(ethylene oxide)–water. J Chem Soc Faraday Trans 1 Phys Chem Condens Phases [Internet]. 1981;77(9):2053. Available from: http://xlink.rsc.org/?DOI=f19817702053

50. Morra M, Occhiello E, Garbassi F. Surface modification of blood contacting polymers by poly(ethyleneoxide). Clin Mater. 1993;14(3):255–65.

51. Harris JM, editor. Poly(Ethylene Glycol) Chemistry Biotechnical and Biomedical Applications. Springer; 1992.

52. Andrade JD, Hlady V, Lake S. Poly(ethylene oxide) and Protein Resistance. Adv Chem. 1996;(1):51–9.

53. LEE J, LEE H, ANDRADE J. Blood compatibility of polyethylene oxide

surfaces. Prog Polym Sci [Internet]. 1995;20(6):1043–79. Available from: http://linkinghub.elsevier.com/retrieve/pii/0079670095000114

54. Nagaoka S, Nakao A. Clinical application of antithrombogenic hydrogel with long poly (ethylene oxide) chains. Biomaterials. 1990;11(2):119–21.

55. Skardal A, Atala A. Biomaterials for Integration with 3-D Bioprinting. Ann Biomed Eng. 2015;43(3):730–46.

56. Southan A, Hoch E, Schönhaar V, Borchers K, Schuh C, Müller M, et al. Side chain thiol-functionalized poly(ethylene glycol) by post-polymerization modification of hydroxyl groups: Synthesis, crosslinking and inkjet printing. Polym Chem. 2014;5(18):5350–9.

57. Choi D, Lee W, Park J, Koh W. Preparation of poly(ethylene glycol) hydrogels with different network structures for the application of enzyme immobilization. Biomed Mater Eng. 2008;18(6):345–56.

58. Inzana JA, Olvera D, Fuller SM, Kelly JP, Graeve OA, Schwarz EM, et al. 3D printing of composite calcium phosphate and collagen scaffolds for bone regeneration. Biomaterials [Internet]. 2014;35(13):4026–34. Available from: http://dx.doi.org/10.1016/j.biomaterials.2014.01.064

59. Farbod K. glycol-based hydrogels for soft and hard tissue Royal Institute of Technology UV and spontaneously cured polyethylene glycol-based hydrogels for soft and hard tissue scaffolds Kambiz Farbod Supervisor : Michael Malkoch. 2016;(June 2011).

60. Tenner MG, Kuipers EW, Kleyn AW, Stolte S. Steric effects in molecular adsorption. J Chem Phys [Internet]. 1988 Nov 15;89(10):6552–3. Available

from: http://aip.scitation.org/doi/10.1063/1.455376

61. Atha DH, Ingham KC. Mechanism of precipitation of proteins by polyethylene glycols. Analysis in terms of excluded volume. J Biol Chem [Internet]. 1981 Dec 10;256(23):12108–17. Available from: http://www.ncbi.nlm.nih.gov/pubmed/7298647

62. Mu Q, Hu T, Yu J. Molecular Insight into the Steric Shielding Effect of PEG on the Conjugated Staphylokinase: Biochemical Characterization and Molecular Dynamics Simulation. Verma C, editor. PLoS One [Internet]. 2013 Jul 18;8(7):e68559. Available from: https://dx.plos.org/10.1371/journal.pone.0068559

63. D'souza AA, Shegokar R. Polyethylene glycol (PEG): a versatile polymer for pharmaceutical applications. Expert Opin Drug Deliv [Internet]. 2016 Sep 17;13(9):1257–75. Available from: https://www.tandfonline.com/doi/full/10.1080/17425247.2016.1182485

64. Sheth SR, Leckband D. Measurements of attractive forces between proteins and end-grafted poly(ethylene glycol) chains. Appl Biol Sci. 1997;94(August):8399–404.

65. Churaev NV, Sergeeva IP, Sobolev VD. Hydrodynamic Thickness and Deformation of Adsorbed Layers of Polyethylene Oxides. J Colloid Interface Sci [Internet]. 1995 Feb;169(2):300–5. Available from: http://linkinghub.elsevier.com/retrieve/pii/S0021979785710375

66. Bailon P, Berthold W. Polyethylene glycol-conjugated pharmaceutical proteins. Pharm Sci Technolo Today [Internet]. 1998 Nov;1(8):352–6. Available from: https://linkinghub.elsevier.com/retrieve/pii/S1461534798000868

67. Milla P, Dosio F, Cattel L. PEGylation of proteins and liposomes: a powerful and flexible strategy to improve the drug delivery. Curr Drug Metab [Internet]. 2012 Jan;13(1):105–19. Available from: http://www.ncbi.nlm.nih.gov/pubmed/21892917

68. Fishburn CS. The Pharmacology of PEGylation: Balancing PD with PK to Generate Novel Therapeutics. J Pharm Sci [Internet]. 2008 Oct;97(10):4167–83. Available from: https://linkinghub.elsevier.com/retrieve/pii/S0022354916327484

69. Zheng J, Lei N, He Q, Hu W, Jin J-G, Meng Y, et al. PEGylation is effective in reducing immunogenicity, immunotoxicity, and hepatotoxicity of α momorcharin in vivo. Immunopharmacol Immunotoxicol [Internet]. 2012 Oct 23;34(5):866–73. Available from: http://www.tandfonline.com/doi/full/10.3109/08923973.2012.666979

70. Wattendorf U, Merkle HP. PEGylation as a tool for the biomedical engineering of surface modified microparticles. J Pharm Sci [Internet]. 2008 Nov;97(11):4655–69. Available from: https://linkinghub.elsevier.com/retrieve/pii/S0022354916327642

71. Tsutsumi Y, Onda M, Nagata S, Lee B, Kreitman RJ, Pastan I. Site-specific chemical modification with polyethylene glycol of recombinant immunotoxin anti-Tac(Fv)-PE38 (LMB-2) improves antitumor activity and reduces animal toxicity and immunogenicity. Proc Natl Acad Sci [Internet]. 2000 Jul 18;97(15):8548–53. Available from: http://www.pnas.org/cgi/doi/10.1073/pnas.140210597

72. Cazalis CS, Haller CA, Sease-Cargo L, Chaikof EL. C-Terminal Site-Specific

PEGylation of a Truncated Thrombomodulin Mutant with Retention of Full Bioactivity. Bioconjug Chem [Internet]. 2004 Sep;15(5):1005–9. Available from: https://pubs.acs.org/doi/10.1021/bc049903y

73. Manjula BN, Tsai A, Upadhya R, Perumalsamy K, Smith PK, Malavalli A, et al. Site-Specific PEGylation of Hemoglobin at Cys-93(β): Correlation between the Colligative Properties of the PEGylated Protein and the Length of the Conjugated PEG Chain. Bioconjug Chem [Internet]. 2003 Mar;14(2):464–72. Available from: https://pubs.acs.org/doi/10.1021/bc0200733

74. Yang C, Lu D, Liu Z. How PEGylation Enhances the Stability and Potency of Insulin: A Molecular Dynamics Simulation. Biochemistry [Internet]. 2011 Apr 5;50(13):2585–93. Available from: https://pubs.acs.org/doi/10.1021/bi101926u

75. Chakrabarty B, Ghoshal AK, Purkait MK. Effect of molecular weight of PEG on membrane morphology and transport properties. J Memb Sci. 2008;309(1–2):209–21.

76. Li Y, Dennis Tolley H, Lee ML. Monoliths from poly(ethylene glycol) diacrylate and dimethacrylate for capillary hydrophobic interaction chromatography of proteins. J Chromatogr A [Internet]. 2010;1217(30):4934–45. Available from: http://dx.doi.org/10.1016/j.chroma.2010.05.048

77. Prime KL, Whitesides GM. Adsorption of Proteins onto Surfaces Containing End-Attached Oligo(ethylene oxide): A Model System Using Self-Assembled Monolayers. J Am Chem Soc. 1993;115(23):10714–21.

78. Derda R, Musah S, Orner BP, Klim JR, Li N, Kiessling LL. High-throughput discovery of synthetic surfaces that support proliferation of pluripotent cells. J Am Chem Soc. 2010;132(4):1289–95.

79. Chandradoss SD, Haagsma AC, Lee YK, Hwang J-H, Nam J-M, Joo C. Surface Passivation for Single-molecule Protein Studies. J Vis Exp [Internet]. 2014;(86):4–11. Available from: http://www.jove.com/video/50549/surface-passivation-for-single-molecule-protein-studies

80. Saito T, Teraoka K, Ota K. Arrayed three-dimensional structures designed to induce and maintain a cell pattern by a topographical effect on cell behavior. Mater Sci Eng C [Internet]. 2015;49:256–61. Available from: http://dx.doi.org/10.1016/j.msec.2015.01.021

81. Curran JM, Stokes R, Irvine E, Graham D, Amro NA, Sanedrin RG, et al. Introducing dip pen nanolithography as a tool for controlling stem cell behaviour: Unlocking the potential of the next generation of smart materials in regenerative medicine. Lab Chip. 2010;10(13):1662–70.

82. Delivopoulos E, Ouberai MM, Coffey PD, Swann MJ, Shakesheff KM, Welland ME. Serum protein layers on parylene-C and silicon oxide: Effect on cell adhesion. Colloids Surfaces B Biointerfaces [Internet]. 2015;126:169–77. Available from: http://dx.doi.org/10.1016/j.colsurfb.2014.12.020

83. Curran JM, Chen R, Stokes R, Irvine E, Graham D, Gubbins E, et al. Nanoscale definition of substrate materials to direct human adult stem cells towards tissue specific populations. J Mater Sci Mater Med. 2010;21(3):1021–9.

84. Celiz AD, Smith JGW, Patel AK, Hook AL, Rajamohan D, George VT, et al. Discovery of a Novel Polymer for Human Pluripotent Stem Cell Expansion and Multilineage Differentiation. Adv Mater [Internet]. 2015;27(27):4006–12. Available from: http://doi.wiley.com/10.1002/adma.201501351

85. Poudel I, Menter DE, Lim JY. Directing cell function and fate via

micropatterning: Role of cell patterning size, shape, and interconnectivity. Biomed Eng Lett. 2012;2(1):38–45.

86. González-quijano AMGK. Micro and nanoengineering advances for the development and commercialization of Organ-on-chips. 2017;2(3):1–2.

87. Martinez-Rivas A, González-Quijano GK, Proa-Coronado S, Séverac C, Dague E. Methods of micropatterning and manipulation of cells for biomedical applications. Micromachines. 2017;8(12).

88. Ware BR, Berger DR, Khetani SR, Al WET. Prediction of Drug-Induced Liver Injury in Micropatterned Co-cultures Containing iPSC-Derived Human Hepatocytes. 2015;145(2):252–62.

89. Städler B, Falconnet D, Pfeiffer I, Höök F, Vörös J. Micropatterning of DNA-Tagged Vesicles. Langmuir [Internet]. 2004 Dec;20(26):11348–54. Available from: https://pubs.acs.org/doi/10.1021/la0482305

90. Estevam-Alves R, Ferreira P, Coatrini A, Oliveira O, Fontana C, Mendonca C. Femtosecond Laser Patterning of the Biopolymer Chitosan for Biofilm Formation. Int J Mol Sci [Internet]. 2016 Aug 19;17(8):1243. Available from: http://www.mdpi.com/1422-0067/17/8/1243

91. Credi C, De Marco C, Molena E, Pla Roca M, Samitier Martí J, Marques J, et al. Heparin micropatterning onto fouling-release perfluoropolyether-based polymers via photobiotin activation. Colloids Surfaces B Biointerfaces [Internet]. 2016 Oct;146:250–9. Available from: https://linkinghub.elsevier.com/retrieve/pii/S0927776516304520

92. Lee Y, Lee HJ, Son KJ, Koh W-G. Fabrication of hydrogel-micropatterned

nanofibers for highly sensitive microarray-based immunosensors having additional enzyme-based sensing capability. J Mater Chem [Internet]. 2011;21(12):4476. Available from: http://xlink.rsc.org/?DOI=c0jm03881d

93. Formosa C, Pillet F, Schiavone M, Duval RE, Ressier L, Dague E. Generation of living cell arrays for atomic force microscopy studies. Nat Protoc [Internet]. 2015 Jan 31;10(1):199–204. Available from: http://www.nature.com/articles/nprot.2015.004

94. IMAMURA Y, MUKOHARA T, SHIMONO Y, FUNAKOSHI Y, CHAYAHARA N, TOYODA M, et al. Comparison of 2D- and 3D-culture models as drug-testing platforms in breast cancer. Oncol Rep [Internet]. 2015 Apr;33(4):1837–43. Available from: https://www.spandidos-publications.com/10.3892/or.2015.3767

95. Wang N, Ingber DE. Control of cytoskeletal mechanics by extracellular matrix, cell shape, and mechanical tension. Biophys J [Internet]. 1994 Jun;66(6):2181–9. Available from: https://linkinghub.elsevier.com/retrieve/pii/S0006349594810148

96. D'Arcangelo E, McGuigan AP. Micropatterning strategies to engineer controlled cell and tissue architecture in vitro. Biotechniques. 2015;58(1):13–23.

97. Poudel I, Menter DE, Lim JY, Martinez-Rivas A, González-Quijano GK, Proa-Coronado S, et al. Micropatterning strategies to engineer controlled cell and tissue architecture in vitro. Biotechniques. 2017;8(1):13–23.

98. Azioune A, Storch M, Bornens M, Théry M, Piel M. Simple and rapid process for single cell micro-patterning. Lab Chip [Internet]. 2009;9(11):1640. Available from: http://xlink.rsc.org/?DOI=b821581m

99. Chen CS, Mrksich M, Huang S, Whitesides GM, Ingber DE. Micropatterned Surfaces for Control of Cell Shape, Position, and Function. Biotechnol Prog [Internet]. 1998 Jun 5;14(3):356–63. Available from: http://doi.wiley.com/10.1021/bp980031m

100. Huang S, Brangwynne CP, Parker KK, Ingber DE. Symmetry-breaking in mammalian cell cohort migration during tissue pattern formation: Role of random-walk persistence. Cell Motil Cytoskeleton. 2005;61(4):201–13.

101. Badie N, Satterwhite L, Bursac N. A Method to Replicate the Microstructure of Heart Tissue In Vitro Using DTMRI-Based Cell Micropatterning. Ann Biomed Eng [Internet]. 2009 Dec 6;37(12):2510–21. Available from: http://link.springer.com/10.1007/s10439-009-9815-x

102. C. Paz A. Micropatterning Co-cultures of Epithelial Cells on Filter Insert Substrates. J Epithel Biol Pharmacol [Internet]. 2012 Jan 24;5(1):77–85. Available from: http://benthamopen.com/ABSTRACT/JEBP-5-77

103. Wan LQ, Ronaldson K, Guirguis M, Vunjak-Novakovic G. Micropatterning of cells reveals chiral morphogenesis. Stem Cell Res Ther [Internet]. 2013;4(2):24. Available from: http://stemcellres.com/content/4/2/24

104. Wan LQ, Ronaldson K, Park M, Taylor G, Zhang Y, Gimble JM, et al. Micropatterned mammalian cells exhibit phenotype-specific left-right asymmetry. Proc Natl Acad Sci [Internet]. 2011 Jul 26;108(30):12295–300. Available from: http://www.pnas.org/cgi/doi/10.1073/pnas.1103834108

105. Desai RA, Gopal SB, Chen S, Chen CS. Contact inhibition of locomotion probabilities drive solitary versus collective cell migration. J R Soc Interface [Internet]. 2013 Sep 18;10(88):20130717–20130717. Available from:

http://rsif.royalsocietypublishing.org/cgi/doi/10.1098/rsif.2013.0717

106. Barbulovic-Nad I, Lucente M, Sun Y, Zhang M, Wheeler AR, Bussmann M. Bio-microarray fabrication techniques - A review. Crit Rev Biotechnol. 2006;26(4):237–59.

107. Miller MB, Tang YW. Basic concepts of microarrays and potential applications in clinical microbiology. Clin Microbiol Rev. 2009;22(4):611–33.

108. Flaim CJ, Chien S, Bhatia SN. An extracellular matrix microarray for probing cellular differentiation. Nat Methods. 2005;2(2):119–25.

109. Singhvi R, al. et, Kumar A, Lopez GP, Stephanopoulos GN, Wang DIC, et al. Engineering cell shape and function. Science (80-). 1994;264(5159):696.

110. Wu RZ, Bailey SN, Sabatini DM. Cell-biological applications of transfected-cell microarrays. Trends Cell Biol. 2002;12(10):485–8.

111. Barata D, Van Blitterswijk C, Habibovic P. High-throughput screening approaches and combinatorial development of biomaterials using microfluidics. Acta Biomater [Internet]. 2016;34:1–20. Available from: http://dx.doi.org/10.1016/j.actbio.2015.09.009

112. Choudhuri S. Microarrays in biology and medicine. J Biochem Mol Toxicol. 2004;18(4):171–9.

113. Huntt AJ, Liberkot CA, Walbat DM, Rogers CT. Patterning of functional antibodies and other proteins by photolithography of silane monolayers. October. 1996;93(October):12287–91.

114. Joos T, Bachmann J. Protein microarrays: potentials and limitations. Front

Biosci (Landmark Ed [Internet]. 2009 Jan 1;14(14):4376–85. Available from: http://www.ncbi.nlm.nih.gov/pubmed/19273356

115. Takagi F, Kurosawa R, Sawaki D, Kamisuki S, Takai M, Ishihara K, et al. Pico liter dispenser with 128 independent nozzles for high throughput biochip fabrication. In: 17th IEEE International Conference on Micro Electro Mechanical Systems Maastricht MEMS 2004 Technical Digest [Internet]. IEEE; 2004. p. 276–9. Available from: http://www.ncbi.nlm.nih.gov/pubmed/19273356

116. Wang XH, Istepanian RSH, Song YH. Microarray image de-noising using stationary wavelet transform. Proc IEEE/EMBS Reg 8 Int Conf Inf Technol Appl Biomed ITAB. 2003;2003–Janua(4):15–8.

117. Rose D. Microfluidic Technologies and Instrumentation for Printing DNA Microarrays. In: Microarray Biochip Technology [Internet]. 2000. p. 19–38. Available from: https://medlineplus.gov/ency/article/003425.htm

118. Gin Fai Tsai J, Zugen Chen, Nelson S, Chang-Jin Kim. A silicon-micromachined pin for contact droplet printing. In: The Sixteenth Annual International Conference on Micro Electro Mechanical Systems, 2003 MEMS-03 Kyoto IEEE [Internet]. IEEE; p. 295–8. Available from: http://ieeexplore.ieee.org/document/1189744/

119. Weibel C. "The Spotting Accelerator™", Customizable Head Assembly for Advanced Microarraying. JALA J Assoc Lab Autom. 2002;7(3):89–94.

120. Martin BD, Gaber BP, Patterson CH, Turner DC. Direct protein microarray fabrication using a hydrogel `stamper'. Langmuir. 1998;14(15):3971–5.

121. Xia Y, Whitesides GM. Soft Lithography. Angew Chemie Int Ed [Internet]. 1998 Mar 16;37(5):550–75. Available from: http://doi.wiley.com/10.1002/%28SICI%291521-3773%2819980316%2937%3A5%3C550%3A%3AAID-ANIE550%3E3.0.CO%3B2-G

122. Lange SA, Benes V, Kern DP, Hörber JKH, Bernard A. Microcontact Printing of DNA Molecules. Anal Chem [Internet]. 2004 Mar;76(6):1641–7. Available from: http://pubs.acs.org/doi/abs/10.1021/ac035127w

123. Bernard A, Delamarche E, Schmid H, Michel B, Bosshard HR, Biebuyck H. Printing patterns of proteins. Langmuir. 1998;14(9):2225–9.

124. Renault JP, Bernard A, Bietsch A, Michel B, Bosshard HR, Delamarche E, et al. Fabricating arrays of single protein molecules on glass using microcontact printing. J Phys Chem B. 2003;107(3):703–11.

125. Ki-Bum Lee1, So-Jung Park1, Chad A. Mirkin1 *, Jennifer C. Smith2, Milan Mrksich2 *. Protein Nanoarrays Generated By Dip-Pen Nanolithography. Science (80-). 2002;295(5560):1702–5.

126. Piner RD, Zhu J, Xu F, Hong S. "Dip-Pen" Nanolithography. 1999;283(January):661–4.

127. Alang Ahmad SA, Wong LS, Ul-Haq E, Hobbs JK, Leggett GJ, Micklefield J. Protein micro- and nanopatterning using aminosilanes with protein-resistant photolabile protecting groups. J Am Chem Soc. 2011;133(8):2749–59.

128. Blawas AS, Reichert WM. Protein patterning. Biomaterials. 1998;19(7–9):595–609.

129. Lom B, Healy KE, Hockberger PE. A versatile technique for patterning biomolecules onto glass coverslips. J Neurosci Methods [Internet]. 1993 Dec;50(3):385–97. Available from: http://linkinghub.elsevier.com/retrieve/pii/016502709390044R

130. Pirrung MC, Huang C-Y. A General Method for the Spatially Defined Immobilization of Biomolecules on Glass Surfaces Using "Caged" Biotin. Bioconjug Chem [Internet]. 1996 Jan;7(3):317–21. Available from: http://pubs.acs.org/doi/abs/10.1021/bc960013v

131. Hengsakul M, Cass AEG. Protein Patterning with a Photoactivatable Derivative of Biotin. Bioconjug Chem [Internet]. 1996 Jan;7(2):249–54. Available from: http://pubs.acs.org/doi/abs/10.1021/bc960007z

132. Schena M, editor. Protein Microarryas. Jones & Bartlett Learning; 2005.

133. Ringeisen BR, Wu PK, Kim H, Pique A, Auyeung RYC, Young HD, et al. Picoliter-Scale Protein Microarrays by Laser Direct Write. Biotechnol Prog [Internet]. 2002 Oct 4;18(5):1126–9. Available from: http://doi.wiley.com/10.1021/bp015516g

134. Schwarz A, Rossier JS, Roulet E, Mermod N, Roberts MA, Girault HH. Micropatterning of Biomolecules on Polymer Substrates. Langmuir [Internet]. 1998 Sep;14(19):5526–31. Available from: http://dx.doi.org/10.1021/la980359p

135. Allain LR, Askari M, Stokes DL, Vo-Dinh T. Microarray sampling-platform fabrication using bubble-jet technology for a biochip system. Fresenius J Anal Chem [Internet]. 2001 Sep 12;371(2):146–50. Available from: http://link.springer.com/10.1007/s002160100962

136. Saunders RE, Derby B. Inkjet printing biomaterials for tissue engineering: bioprinting. Int Mater Rev [Internet]. 2014;59(8):430–48. Available from: http://www.tandfonline.com/doi/full/10.1179/1743280414Y.0000000040

137. Allain LR, Stratis-Cullum DN, Vo-Dinh T. Investigation of microfabrication of biological sample arrays using piezoelectric and bubble-jet printing technologies. Anal Chim Acta [Internet]. 2004 Aug;518(1–2):77–85. Available from: http://linkinghub.elsevier.com/retrieve/pii/S0003267004005835

138. Wijshoff H. The dynamics of the piezo inkjet printhead operation. Phys Rep. 2010;491(4–5):77–177.

139. Tate T. On the magnitude of a drop of liquid formed under different circumstances. London, Edinburgh, Dublin Philos Mag J Sci [Internet]. 1864 Mar 26;27(181):176–80. Available from: https://www.tandfonline.com/doi/full/10.1080/14786446408643645

140. Hue P. Le*, Le Technologies, Inc., Beaverton O. Progress and Trends in Ink-jet Printing Technology. J Imaging Sci Technol. 1998;42(1):49–62.

141. Hertz CH, Simonsson SI. Intensity modulation of ink-jet oscillographs. Med Biol Eng [Internet]. 1969 May;7(3):337–40. Available from: http://link.springer.com/10.1007/BF02474777

142. Buehner WL, Hill JD, Williams TH, Woods JW. Application of Ink Jet Technology to a Word Processing Output Printer. IBM J Res Dev [Internet]. 1977 Jan;21(1):2–9. Available from: http://ieeexplore.ieee.org/document/5391061/

143. Heinzl J, Hertz CH. Ink-Jet Printing. In 1985. p. 91–171. Available from:

https://linkinghub.elsevier.com/retrieve/pii/S006525390860877X

144. Fundamentals of Inkjet Printing [Internet]. 2016. Available from: http://doi.wiley.com/10.1002/9783527684724

145. Derby B. Bioprinting: Inkjet printing proteins and hybrid cell-containing materials and structures. J Mater Chem. 2008;18(47):5717–21.

146. Napadensky E. Inkjet 3D Printing. Chem Inkjet Inks [Internet]. 2009;255–67. Available from: http://www.worldscientific.com/doi/abs/10.1142/9789812818225_0013

147. Calvert P. Inkjet Printing for Materials and Devices. Chem Mater [Internet]. 2001 Oct;13(10):3299–305. Available from: http://pubs.acs.org/doi/abs/10.1021/cm0101632

148. Cooley P, Wallace D, Antohe B. Applicatons of Ink-Jet Printing Technology to BioMEMS and Microfluidic Systems. JALA J Assoc Lab Autom [Internet]. 2002 Oct 4;7(5):33–9. Available from: http://www.sciencedirect.com/science/article/B75DF-4BRJGBM-74/2/0debd8bfd84b653a2b6838d6238b29aa

149. Cummins G, Desmulliez MPY. Inkjet printing of conductive materials: a review. Circuit World [Internet]. 2012 Nov 16;38(4):193–213. Available from: https://www.emeraldinsight.com/doi/10.1108/03056121211280413

150. Magdassi S. Ink Requirements and Formulations Guidelines. In: The Chemistry of Inkjet Inks. 2010. p. 19–41.

151. Singh M, Haverinen HM, Dhagat P, Jabbour GE. Inkjet printing-process and its applications. Adv Mater. 2010;22(6):673–85.

152. Samuel J, Edwards P. Solvent-Based Inkjet Inks. Chem Inkjet Inks [Internet]. 2009;141–59. Available from: http://www.worldscientific.com/doi/abs/10.1142/9789812818225_0008

153. Derby B, Reis N. Inkjet Printing of Highly Loaded Particulate Suspensions. MRS Bull. 2003;28(11):815–8.

154. Pudas M, Hagberg J, Leppävuori S. Printing parameters and ink components affecting ultra-fine-line gravure-offset printing for electronics applications. J Eur Ceram Soc. 2004;24(10–11):2943–50.

155. Derby B. Inkjet Printing of Functional and Structural Materials: Fluid Property Requirements, Feature Stability, and Resolution. Annu Rev Mater Res [Internet]. 2010;40(1):395–414. Available from: http://www.annualreviews.org/doi/10.1146/annurev-matsci-070909-104502

156. Schmid C. Formulation and Properties of Waterborne Inkjet Inks. Chem Inkjet Inks [Internet]. 2009;123–40. Available from: http://www.worldscientific.com/doi/abs/10.1142/9789812818225_0007

157. Xu T, Binder KW, Albanna MZ, Dice D, Zhao W, Yoo JJ, et al. Hybrid printing of mechanically and biologically improved constructs for cartilage tissue engineering applications. Biofabrication. 2013;5(1).

158. Ben-moshe M. Unique Inkjet Ink Systems. Chem inkjet inks. 2010;203-.

159. Boehm RD, Gittard SD, Byrne JMH, Doraiswamy A, Wilker JJ, Dunaway TM, et al. Piezoelectric inkjet printing of medical adhesives and sealants. Vol. 62, Jom. 2010. p. 56–60.

160. Choi HW, Zhou T, Singh M, Jabbour GE. Recent developments and directions

in printed nanomaterials. Nanoscale [Internet]. 2015;7(8):3338–55. Available from: http://dx.doi.org/10.1039/c4nr03915g

161. Yang JC, Chien W, King M, Grosshandler WL. A simple piezoelectric droplet generator. Exp Fluids [Internet]. 1997 Nov 19;23(5):445–7. Available from: http://link.springer.com/10.1007/s003480050134

162. Schoeppler M. Diverging Ink Jet Technologies and Applications. In: NIP & Digital Fabrication Conference. 2006. p. 1–3.

163. Williams C. Ink-jet printers go beyond paper. Phys World [Internet]. 2006 Jan;19(1):24–9. Available from: http://stacks.iop.org/2058-7058/19/i=1/a=32?key=crossref.1141e47c5d492baa355f6d8607f1d055

164. Chen, Fu-Kang; Lu, Jhih-Ping; Su, Pei-Ju; Sung, Chao-Fu; Lee, Yuh-Zheng; Shiu, Jyh-Wen; Cheng, Kevin; Lin, Hong-Ye; Chang L-C. Mask-free Fabrication of Color Filter by an All Ink-Jet Printing Process. In: NIP & Digital Fabrication Conference. 2007. p. Pages 504-973., p. 852–854(3).

165. Dijksman JF, Duineveld PC, Hack MJJ, Pierik A, Rensen J, Rubingh J-E, et al. Precision ink jet printing of polymer light emitting displays. J Mater Chem [Internet]. 2007;17(6):511–22. Available from: http://xlink.rsc.org/?DOI=B609204G

166. Alamán J, Alicante R, Peña J, Sánchez-Somolinos C. Inkjet Printing of Functional Materials for Optical and Photonic Applications. Materials (Basel) [Internet]. 2016 Nov 10;9(11):910. Available from: http://www.mdpi.com/1996-1944/9/11/910

167. Hsiao W-K, Hoath SD, Martin GD, Hutchings IM. Ink Jet Printing for Direct

Mask Deposition in Printed Circuit Board Fabrication. J Imaging Sci Technol [Internet]. 2009;53(5):050304. Available from: http://www.ingentaconnect.com/content/ist/jist/2009/00000053/00000005/art00007

168. Ingo Reinhold, Werner Zapka, Wolfgang Voit, Frank Steinhäußer, Moritz Stürmer, Andreas Madjarov MV; XA, Järfälla S. Inkjet Printing of Phase-Change Materials With Xaar1001 Printheads. In: NIP26 International Conference on Digital Printing Technologies and Digital Fabrication. 2010. p. 319–22.

169. Cox WR, Chen T, Ussery D, Hayes DJ, Tatum JA, MacFarlane DL. Microjetted lenslet triplet fibers. Opt Commun [Internet]. 1996 Feb;123(4–6):492–6. Available from: https://linkinghub.elsevier.com/retrieve/pii/0030401895006141

170. Chen T, Cox WR, Lenhard D, Hayes DJ. Microjet printing of high-precision microlens array for packaging of fiber optic components. In: Eldada LA, Heyler RA, Rowlette, Sr. JR, editors. 2002. p. 136. Available from: http://proceedings.spiedigitallibrary.org/proceeding.aspx?doi=10.1117/12.469561

171. Bietsch A, Zhang J, Hegner M, Lang HP, Gerber C. Rapid functionalization of cantilever array sensors by inkjet printing. Nanotechnology [Internet]. 2004 Aug 1;15(8):873–80. Available from: http://stacks.iop.org/0957-4484/15/i=8/a=002?key=crossref.7b75dad8e31c560bec9a362a8a89fe82

172. Nakanishi T, Ohtsu I, Furuta M, Ando E, Nishimura O. Direct MS/MS Analysis of Proteins Blotted on Membranes by a Matrix-Assisted Laser

Desorption/Ionization-Quadrupole Ion Trap-Time-of-Flight Tandem Mass Spectrometer. J Proteome Res [Internet]. 2005 Jun;4(3):743–7. Available from: http://pubs.acs.org/doi/abs/10.1021/pr0497834

173. Koo H-S, Chen M, Pan P-C. LCD-based color filter films fabricated by a pigment-based colorant photo resist inks and printing technology. Thin Solid Films [Internet]. 2006 Nov;515(3):896–901. Available from: https://linkinghub.elsevier.com/retrieve/pii/S0040609006008698

174. Basaran OA. Small-scale free surface flows with breakup: Drop formation and emerging applications. AIChE J [Internet]. 2002 Sep;48(9):1842–8. Available from: http://doi.wiley.com/10.1002/aic.690480902

175. Chee M, Yang R, Hubbell E, Berno A, Huang XC, Stern D, et al. Accessing genetic information with high-density DNA arrays. Science [Internet]. 1996 Oct 25;274(5287):610–4. Available from: http://www.ncbi.nlm.nih.gov/pubmed/8849452

176. Kong F, Yuan L, Zheng YF, Chen W. Automatic Liquid Handling for Life Science. J Lab Autom [Internet]. 2012 Jun 6;17(3):169–85. Available from: http://journals.sagepub.com/doi/10.1177/2211068211435302

177. Derby B. Printing and prototyping of tissues and scaffolds. Science (80-). 2012;338(6109):921–6.

178. Ilkhanizadeh S, Teixeira AI, Hermanson O. Inkjet printing of macromolecules on hydrogels to steer neural stem cell differentiation. Biomaterials. 2007;28(27):3936–43.

179. Fujie T, Desii A, Ventrelli L, Mazzolai B, Mattoli V. Inkjet printing of protein

microarrays on freestanding polymeric nanofilms for spatio-selective cell culture environment. Biomed Microdevices. 2012;14(6):1069–76.

180. Hutchinson I. Raw Materials for UV Curable Inks. In: The Chemistry of Inkjet Inks [Internet]. 2010. p. 177–201. Available from: http://www.worldscientific.com/doi/abs/10.1142/9789812818225_0010

181. Patel AK, Tibbitt MW, Celiz AD, Davies MC, Langer R, Denning C, et al. High throughput screening for discovery of materials that control stem cell fate. Curr Opin Solid State Mater Sci [Internet]. 2016;20(4):202–11. Available from: http://dx.doi.org/10.1016/j.cossms.2016.02.002

182. Appel EA, Larson BL, Luly KM, Kim JD, Langer R. Non-cell-adhesive substrates for printing of arrayed biomaterials. Adv Healthc Mater. 2015;4(4):501–5.

183. Cui X, Boland T. Human microvasculature fabrication using thermal inkjet printing technology. Biomaterials [Internet]. 2009;30(31):6221–7. Available from: http://dx.doi.org/10.1016/j.biomaterials.2009.07.056

184. Shakhnovich A, Belmont J. FORMULATION AND MATERIALS FOR INKJET INKS Pigments for Inkjet Applications.

185. Edison SE. Formulating UV Curable Inkjet Inks. In: The Chemistry of Inkjet Inks. 2010.

186. Brand O, Fedder GK, Hierold C, Korvink JG, Tabata O. Inkjet-based Micromanufacturing. John Wiley & Sons; 2012.

187. Liu YF, Tsai MH, Pai YF, Hwang WS. Control of droplet formation by operating waveform for inks with various viscosities in piezoelectric inkjet

printing. Appl Phys A Mater Sci Process. 2013;111(2):509–16.

188. Jang D, Kim D, Moon J. Influence of fluid physical properties on ink-jet printability. Langmuir. 2009;25(5):2629–35.

189. Duineveld PC. The stability of ink-jet printed lines of liquid with zero receding contact angle on a homogeneous substrate. J Fluid Mech. 2003;477(477):175–200.

190. Stringer J, Derby B. Formation and stability of lines produced by inkjet printing. Langmuir. 2010;26(12):10365–72.

191. Dmitriev MN, Dmitriev NM. On determining the percolation Reynolds number and the characteristic linear dimension for ideal and fictitious porous media. Fluid Dyn. 2005;40(4):585–92.

192. Gao G, Yonezawa T, Hubbell K, Dai G, Cui X. Inkjet-bioprinted acrylated peptides and PEG hydrogel with human mesenchymal stem cells promote robust bone and cartilage formation with minimal printhead clogging. Biotechnol J. 2015;10(10):1568–77.

193. Qin X, Hu Q, Gao G, Guan S. Characterization of UV-curable poly(ethylene glycol) diacrylate based hydrogels. Chem Res Chinese Univ. 2015;31(6):1046–50.

194. Schiaffino S, Sonin AA. Molten droplet deposition and solidification at low Weber numbers. Phys Fluids. 1997;9(11):3172–87.

195. Amin YYI, Runager K, Simoes F, Celiz A, Taresco V, Rossi R, et al. Combinatorial Biomolecular Nanopatterning for High-Throughput Screening of Stem-Cell Behavior. Adv Mater. 2016;28(7):1472–6.

196. Ahmad SAA, Wong LS, Ul-Haq E, Hobbs JK, Leggett GJ, Micklefield J. Micrometer- and Nanometer-Scale Photopatterning Using 2-Nitrophenylpropyloxycarbonyl-Protected Aminosiloxane\rMonolayers. J Am Chem Soc. 2009;131(16):1513–22.

197. Dubey RC. Advanced Biotechnology. 1st ed. S. Chand; 2014.

198. Ulman A. An Introduction to Ultrathin Organic Films – From Langmuir–Blodgett to Self-Assembly. Academic Press, Inc; 1991.

199. Wang M, Liechti KM, Wang Q, White JM. Self-assembled silane monolayers: Fabrication with nanoscale uniformity. Langmuir. 2005;21(5):1848–57.

200. A. V. Zhuk, A. G. Evans, J.W. Hutchinson and GMW. The Adhesion Energy between Polymer Thin Films and Self-Assembled Monolayers. J Mater Res. 1998;13:3555–64.

201. Wang M, Liechti KM, Wang Q, White JM. Self-Assembled Silane Monolayers: Fabrication with Nanoscale Uniformity. Langmuir [Internet]. 2005 Mar;21(5):1848–57. Available from: https://pubs.acs.org/doi/10.1021/la048483y

202. Prime K, Whitesides G. Self-assembled organic monolayers: model systems for studying adsorption of proteins at surfaces. Science (80-) [Internet]. 1991 May 24;252(5009):1164–7. Available from: http://www.sciencemag.org/cgi/doi/10.1126/science.252.5009.1164

203. Liebmann-Vinson A, Lander LM, Foster MD, Brittain WJ, Vogler EA, Majkrzak CF, et al. A Neutron Reflectometry Study of Human Serum Albumin Adsorption in Situ. Langmuir [Internet]. 1996 Jan;12(9):2256–62. Available from: https://pubs.acs.org/doi/10.1021/la950642d

204. Schwartz DK. Mechanisms and kinetics of slef-assembled monolayer formation. Dict Genomics, Transcr Proteomics. 2001;107–37.

205. Hermanson GT. Bioconjugate Techniques. Second. Academic Press; 2008.

206. Bierbaum K, Grunze M, Baski AA, Chi LF, Schrepp W, Fuchs H. Growth of Self-Assembled n-Alkyltrichlorosilane Films on Si(100) Investigated by Atomic Force Microscopy. Langmuir [Internet]. 1995 Jun;11(6):2143–50. Available from: http://pubs.acs.org/doi/abs/10.1021/la00006a049

207. Zhao X, Yen A, Kopelman R. Anomalous Etching Kinetics of Self-Assembled Monolayers on Silica—Water Interfaces: Experiment and Modeling. J Phys Chem B [Internet]. 1997 Dec;101(49):10446–9. Available from: https://pubs.acs.org/doi/10.1021/jp972633e

208. Ulman A. Formation and Structure of Self-Assembled Monolayers. Chem Rev [Internet]. 1996 Jan;96(4):1533–54. Available from: https://pubs.acs.org/doi/10.1021/cr9502357

209. Sagiv J. Organized monolayers by adsorption. 1. Formation and structure of oleophobic mixed monolayers on solid surfaces. J Am Chem Soc [Internet]. 1980 Jan;102(1):92–8. Available from: http://pubs.acs.org/doi/abs/10.1021/ja00521a016

210. Maoz R, Sagiv J. On the formation and structure of self-assembling monolayers. I. A comparative atr-wettability study of Langmuir—Blodgett and adsorbed films on flat substrates and glass microbeads. J Colloid Interface Sci [Internet]. 1984 Aug;100(2):465–96. Available from: https://linkinghub.elsevier.com/retrieve/pii/0021979784904521

211. Kessel CR, Granick S. Formation and characterization of a highly ordered and well-anchored alkylsilane monolayer on mica by self-assembly. Langmuir. 1991;7(3):532–8.

212. Tripp CP, Hair ML. An infrared study of the reaction of octadecyltrichlorosilane with silica. Langmuir [Internet]. 1992 Apr;8(4):1120–6. Available from: http://pubs.acs.org/doi/abs/10.1021/la00040a018

213. Silberzan P, Leger L, Ausserre D, Benattar JJ. Silanation of silica surfaces. A new method of constructing pure or mixed monolayers. Langmuir [Internet]. 1991 Aug;7(8):1647–51. Available from: http://pubs.acs.org/doi/abs/10.1021/la00056a017

214. Brzoska JB, Shahidzadeh N, Rondelez F. Evidence of a transition temperature for the optimum deposition of grafted monolayer coatings. Nature [Internet]. 1992 Dec;360(6406):719–21. Available from: http://www.nature.com/articles/360719a0

215. Parikh AN, Allara DL, Azouz I Ben, Rondelez F. An Intrinsic Relationship between Molecular Structure in Self-Assembled n-Alkylsiloxane Monolayers and Deposition Temperature. J Phys Chem [Internet]. 1994 Aug;98(31):7577–90. Available from: http://pubs.acs.org/doi/abs/10.1021/j100082a031

216. Heise A, Stamm M, Rauscher M, Duschner H, Menzel H. Mixed silane self assembled monolayers and their in situ modification. Thin Solid Films. 1998;327–329(1–2):199–203.

217. Vallant T, Brunner H, Mayer U, Hoffmann H, Leitner T, Resch R, et al. Formation of Self-Assembled Octadecylsiloxane Monolayers on Mica and Silicon Surfaces Studied by Atomic Force Microscopy and Infrared Spectroscopy. J

Phys Chem B [Internet]. 1998 Sep;102(37):7190–7. Available from: https://pubs.acs.org/doi/10.1021/jp981282g

218. Singh A, Lee IS, Kim K, Myerson AS. Crystal growth on self-assembled monolayers. CrystEngComm [Internet]. 2011;13(1):24–32. Available from: http://xlink.rsc.org/?DOI=C0CE00030B

219. Wang Y, Lieberman M. Growth of Ultrasmooth Octadecyltrichlorosilane Self-Assembled Monolayers on SiO 2. Langmuir [Internet]. 2003 Feb;19(4):1159–67. Available from: https://pubs.acs.org/doi/10.1021/la020697x

220. Zhu X-Y, Mulder JA, Bergerson WF. Chemical Vapor Deposition of Organic Monolayers on Si(100) via Si−N Linkages. Langmuir [Internet]. 1999 Nov;15(23):8147–54. Available from: https://pubs.acs.org/doi/10.1021/la990728x

221. Zhang Y, Gregory DA, Smith PJ, Zhao X, Engineering B. Regenerated silk fibroin as an inkjet printable biomaterial. Print Fabr 2016. 2016;(Di):406–9.

222. Frid P, Anisimov S V., Popovic N. Congo red and protein aggregation in neurodegenerative diseases. Brain Res Rev. 2007;53(1):135–60.

223. Marmur A. Equilibrium Wetting Fundamentals. In: The Chemistry of Inkjet Inks. 2010. p. 43–54.

224. Quéré D. Wetting and Roughness. Annu Rev Mater Res [Internet]. 2008;38(1):71–99. Available from: http://www.annualreviews.org/doi/10.1146/annurev.matsci.38.060407.132434

225. Rodger CA. Spectroscopic methods in organic chemistry, fifth edition. [Internet]. Fourth. Vol. 9, Concepts in Magnetic Resonance. McGraw-Hill;

1997. 355-356 p. Available from:
http://doi.wiley.com/10.1002/%28SICI%291099-0534%281997%299%3A5%3C355%3A%3AAID-CMR5%3E3.0.CO%3B2-Y

226. Coates J. Interpretation of Infrared Spectra, A Practical Approach. In: Encyclopedia of Analytical Chemistry. Chichester, UK: John Wiley & Sons, Ltd; 2006. p. 1–23.

227. Carré A, Mittal KL, editors. Superhydrophobic Surfaces. Leiden - Boston; 2009.

228. Kilian KA, Moghe P V. High throughput strategies for the design, discovery, and analysis of biomaterials. Acta Biomater [Internet]. 2016;34:v–vi. Available from: http://dx.doi.org/10.1016/j.actbio.2016.03.019

229. Lee J, Abdeen AA, Zhang D, Kilian KA. Directing stem cell fate on hydrogel substrates by controlling cell geometry, matrix mechanics and adhesion ligand composition. Biomaterials [Internet]. 2013;34(33):8140–8. Available from: http://dx.doi.org/10.1016/j.biomaterials.2013.07.074

230. Wang PY, Clements LR, Thissend H, Tsaia WB, Voelckere NH. Screening rat mesenchymal stem cell attachment and differentiation on surface chemistries using plasma polymer gradients. Acta Biomater [Internet]. 2015;11(1):58–67. Available from: http://dx.doi.org/10.1016/j.actbio.2014.09.027

231. Du G, Fang Q, den Toonder JMJ. Microfluidics for cell-based high throughput screening platforms-A review. Anal Chim Acta [Internet]. 2016;903:36–50. Available from: http://dx.doi.org/10.1016/j.aca.2015.11.023

232. Faia-Torres AB, Guimond-Lischer S, Rottmar M, Charnley M, Goren T, Maniura-Weber K, et al. Differential regulation of osteogenic differentiation of

stem cells on surface roughness gradients. Biomaterials [Internet]. 2014;35(33):9023–32. Available from: http://dx.doi.org/10.1016/j.biomaterials.2014.07.015

233. Lindström S, Andersson-Svahn H. Overview of single-cell analyses: Microdevices and applications. Lab Chip. 2010;10(24):3363–72.

234. Faia-Torres AB, Charnley M, Goren T, Guimond-Lischer S, Rottmar M, Maniura-Weber K, et al. Osteogenic differentiation of human mesenchymal stem cells in the absence of osteogenic supplements: A surface-roughness gradient study. Acta Biomater [Internet]. 2015;28:64–75. Available from: http://dx.doi.org/10.1016/j.actbio.2015.09.028

235. Moeller HC, Mian MK, Shrivastava S, Chung BG, Khademhosseini A. A microwell array system for stem cell culture. Biomaterials. 2008;29(6):752–63.

236. Ranella A, Barberoglou M, Bakogianni S, Fotakis C, Stratakis E. Tuning cell adhesion by controlling the roughness and wettability of 3D micro/nano silicon structures. Acta Biomater [Internet]. 2010;6(7):2711–20. Available from: http://dx.doi.org/10.1016/j.actbio.2010.01.016

237. Shen X, Ma P, Hu Y, Xu G, Zhou J, Cai K. Mesenchymal stem cell growth behavior on micro / nano hierarchical surfaces of titanium substrates. Colloids Surfaces B Biointerfaces. 2015;127:221–32.

238. Gittens RA, Mclachlan T, Olivares-navarrete R, Cai Y, Berner S, Tannenbaum R, et al. The effects of combined micron- / submicron-scale surface roughness and nanoscale features on cell proliferation and differentiation. Biomaterials. 2011;32(13):3395–403.

239. Khang D, Choi J, Im YM, Kim YJ, Jang JH, Kang SS, et al. Role of subnano-, nano- and submicron-surface features on osteoblast differentiation of bone marrow mesenchymal stem cells. Biomaterials [Internet]. 2012;33(26):5997–6007. Available from: http://dx.doi.org/10.1016/j.biomaterials.2012.05.005

240. Bacakova L, Filova E, Parizek M, Ruml T, Svorcik V. Modulation of cell adhesion, proliferation and differentiation on materials designed for body implants. Biotechnol Adv [Internet]. 2011;29(6):739–67. Available from: http://dx.doi.org/10.1016/j.biotechadv.2011.06.004